

HUNGARIAN ACADEMY OF SCIENCES
CENTRE FOR ENERGY RESEARCH

29-33 KONKOLY-THEGE MIKLÓS ÚT

1121 BUDAPEST, HUNGARY

PROGRESS REPORT
ON RESEARCH ACTIVITIES
IN 2020

DEAR READER,

Welcome to the 2020 yearbook published by the MTA Centre for Energy Research (MTA EK), summarizing the scientific results of its three institutions and highlights in 2020. This booklet provides a summary of the research personals and equipment of departments and research groups working in the Centre.

The year 2020 was an unusual one in terms of awarded grants and new opportunities. The Centre and the whole Research network of MTA were working on the transition of reorganization into a new research network origination. According to the decision of the Hungarian Government the new network had to become independent from the Hungarian Academy of Sciences. The new organization was named after the great Hungarian physicist Loránd Eötvös. The Loránd Eötvös Research Network took over the research network from the MTA on the 1st of September 2019. Information on this new organization can be found at the URL: <http://www.elkh.org/>. The transition was relatively smooth, but gave very busy period to the involved leaders and personals of the Centre.

Three important, research works were selected for highlights this year.

The BNC researchers continued their work in various EU funded projects such as IPERION CH, E-RIHS, BrightnESS and CHANDA and all of them were ended this year. This year we had to work on the proposals to renew them for another period.

Ákos Horváth
Director General
horvath.akos@energia.mta.hu

CONTENTS

Dear Reader,.....	2
Contents.....	3
Mission Statement of MTA Centre for Energy Research.....	6
Scientific Advisory Board of the MTA Centre for Energy Research.....	6
Organization Structure of the MTA Centre for Energy Research (2020).....	7
Quality Management	8
Budapest Research Reactor	9
Environmental Protection Service.....	11
I. EU, NKFIH OR GOVERNMENT SUPPORTED RESEARCH ACTIVITIES	12
Development of ALLEGRO Gas-cooled Fast Reactor Demonstrator	13
Bending Test Simulation of VVER-440 Mockup.....	14
Activation Study of the ESS NMX Shutter Pit	15
Identification of Wintertime Combustion Process Related Aerosol Pollution in Budapest	16
Strategic Research Group for the Challenges of Renewable Energy Based Systems.....	18
Structure of Oxy-Halide Compositions for Use in Solid State Batteries.....	19
X-Ray Spectroscopic Characterization of Size-Fractionated Atmospheric Aerosol Particles.....	21
Chemical Evolution and Radionuclide Retention Studies for High-Level Radioactive Waste Disposal.....	23
Connecting Russian and European Measures for Large-scale Research Infrastructures – CREMLIN+	25
RadoNorm: Towards Effective Radiation Protection Based on Improved Scientific Evidence and Social Considerations – Focus on Radon and NORM	26
Progress on the EURAD SCF European Joint Programme	27
MELODI Virtual Workshop 2020 on the Effects of Spatial and Temporal Variation in Dose Delivery.....	28
II. RESEARCH AND DEVELOPMENT RELATED TO NUCLEAR POWER PLANTS	29
Activities of EK as Main Consultant of Paks NPP	30
Wall Thickness Measurement of E110 Slim Cladding Tube	32
Experiments for Fuel Rod Behaviour Modelling.....	34
Identification and Handling of Defective Fuel Rods	36
Development of Reconstitution Technology of Irradiated Specimens.....	37
Gamma-ray Measurement and Analysis of Spent Fuel Assemblies of Paks NPP (2020).....	38
Analysis of Dissolved and Particulate Corrosion Products Found in the Primary Coolant Circuit of the PAKS NPP	39
Renewing the Refuelling Neutron Monitoring and Reactivity Measurement Systems at Paks NPP.....	40
Studsvik Cladding Integrity Project.....	42
Review of SGTR and LOCA Available Experimental Data for the R2CA Project	43
Development of Accident Tolerant Nuclear Fuel Concepts	44
Optical Characterization of Stainless Steel Surfaces for Steam Generator Corrosion Studies.....	45
Utilization of Low-temperature Heat-sources for Energy Production.....	46
Simulation of an Unprotected Transient of ALLEGRO Using the Coupled KIKO3DMG/ ATHLET3.0 Code	47
Hot Duct Break Transient with Two- and Three-loop ALLEGRO Models.....	48
III. NUCLEAR SECURITY, DOSIMETRY AND SPACE RESEARCH.....	49
Logic Optimization for the RM-RADTEL Radiation Telescope	50

Development of Methods to Improve Precision of Environmental Radiation Measurements	52
Development of Guidelines for Determining the Internal Exposure of Workers	54
Inverse Exposure Rate Effect, its Potential Explanations, and their Implications on the Risk of Low Doses	56
Environmental Radiation Monitoring with Detectors in a New Generation Scalable Network – DoziNet 2.0	57
Metastatic Potential of HeLa-cells does not Increase Directly After Radiation Exposure	58
Simulation of Individual Radiosensitivity	59
New 3D Spectral Data Display Solution for the Whole Body Counter	60
Characterization of Radiation Exposure and its Biological Effects at Different Spatial Scales.....	61
Dosimetry Measurements in Pulsed Ionizing Radiation Fields Created by Gamma-Chopper	62
Effective Use of Dose Projection Tools in the Preparedness and Response to Nuclear and Radiological Emergencies: Part 1 ..	63
Neutron Irradiations for Radiation-hardness Testing of Electronic Sealing Systems	65
Budapest Neutron Monitor Station.....	66
IV. ENERGY AND ENVIRONMENTAL STUDIES.....	67
Catalytic Systems for Efficient Water Electrolysis.....	68
Methane Dry Reforming on In and CeO ₂ Promoted Ni/ Al ₂ O ₃ Catalysts.....	70
Preventing the Development of Antibiotic Resistance in Wastewater Matrices by High Energy Irradiation	71
Biogenic Carbon Content Determination of Catalytically Converted Biomass.....	72
Degradation of Propranolol in Dilute Aqueous Solution by High Energy Ionizing Radiation	73
Bimetallic Gold Catalysts in Aerobic Selective Oxidation of Alcohols.....	74
Evolution Models of the Power Grid Based on the Rate of System Development and Settlement Structures	75
Bivalent Radionuclide Adsorption on Clay Minerals.....	76
The Effect of Chemical Composition of Concrete on its Long-term Performance in an Irradiated Environment (V4-Korea RADCON)	77
Elimination of Oxacillin, its Degradation Products, their Toxicity and Antibacterial Activity by Using Ionizing Radiation ...	79
V. NUCLEAR ANALYSIS AND CHEMISTRY	Hiba! A könyvjelző nem létezik.
Neutron Scattering Studies on Porous Materials, Steels, Coordination Complexes, Extracellular Vesicles and Thin Films.....	81
Neutron Optics	84
Tungsten-carbide-rich Protective Coatings Produced by Noble-gas Irradiation Mixing	86
Applications of Nuclear Analytical Techniques.....	88
Development of Nuclear Analytical Techniques, Nuclear Data Measurements.....	91
Nanocomposites, Thin Iron Films and Nanoparticles Studied by Mössbauer Spectroscopy and Other Methods	92
Characterization of Nanoparticle Systems	93
Self-assembly and Reversible Reorganizations of Grana – Revealed by Small-angle Neutron Scattering.....	95
Neutron and X-ray Radiography and Tomography at BRR.....	96
Examining Technology and Provenance of Archaeological Ceramics.....	98
Non-destructive, Spatially-resolved Element Analysis of Structured Samples	99
Large Facility Analytical Studies of Polished and Ground Stone Artefacts	101
Investigation of Surface Reactivity on Steel/cement and Steel/clay Systems	103
VI. NUCLEAR FUSION RESEARCH.....	105
Participation in the Eurofusion Programme	106
Identity of the JET M-mode and the ASDEX Upgrade I-Phase Phenomena	107
Investigation of the Edge Plasma on the Wendelstein 7-X Stellarator.....	108
Installation and Commissioning of the EDICAM Video Diagnostic System at JT-60SA	109

Engineering Design Contributions to the DONES Project.....	110
Irradiation of Eurofer Material for EUROFUSION WPMAT Project.....	111
Participation in EUROFUSION WPMAT Project - Database and Material Property Handbook.....	112
Engineering Services for ITER's Lower-ports.....	113
Diffusion Bonding Experiments of 316L Specimens in a Gleeble 3800 Thermomechanical Simulator.....	114
ABBREVIATIONS.....	115

MISSION STATEMENT OF MTA CENTRE FOR ENERGY RESEARCH

- Research and development in the field of nuclear science and technology for facilitating the adoption and the safe use of nuclear technology in Hungary.
- To participate in international research effort aiming at the establishing a new generation of nuclear power plants and closing the fuel cycle.
- Maintaining and improving competence in nuclear science and technology, especially in the field of nuclear safety, security, health physics, nuclear and isotope chemistry.
- To guarantee the safe operation of Budapest Research Reactor (BRR), and to ensure the open access to the research facilities around the reactor operated by the Budapest Neutron Centre.
- Research activities to improve nuclear analytical and imaging methods and their applications for energy and materials science.
- Perform studies in the field of environmental physics related to energy generation, renewable energies, energy storage and their impact on public health, and on environmental safety.
- Research and development in the field of low carbon energy technologies and of energy saving in industrial technologies.
- Interdisciplinary research on complex functional materials and nanometer-scale structures, exploration of their physical, chemical, and biological principles, exploitation their operations in integrated micro- and nanosystems, and in the development of characterization techniques.
- Dissemination of the results in international programs, education and industrial research.

SCIENTIFIC ADVISORY BOARD OF THE MTA CENTRE FOR ENERGY RESEARCH

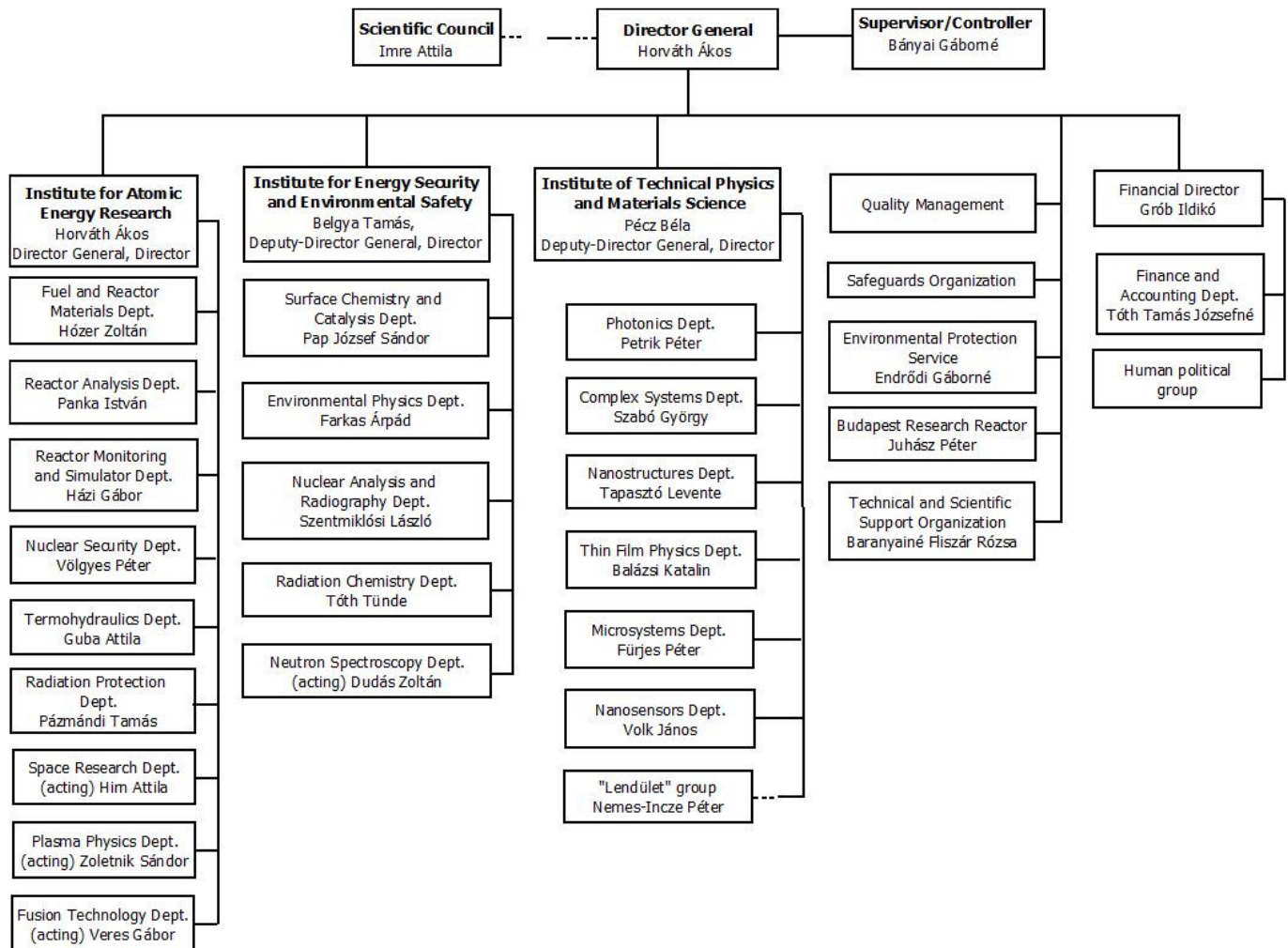
The Board consists of four Hungarian and two foreign leading scientists. The last meeting of the board took place in Budapest at MTE EK, on the 12th of June 2019. The results of year 2018 was presented and discussed.

In 2020, we didn't have a Board meeting because of the pandemic. Prof. Dr. László Keviczky the Chair resigned and we are searching for his replacement.

Members of the Board in 2020:

- Dr. Hervé Bernard, Deputy Chairman, Centre French Alternative Energies and Atomic Energy Commission (CEA)
- Dr. Maximilian Fleischer, Head of Department of Corporate Technology, Siemens AG
- Prof. Dr. Ádám Kiss, Eötvös Loránd University
- Dr. Zoltán Homonnay, Head of Laboratory of Nuclear Chemistry, Eötvös Loránd University
- Mr. István Hamvas, Director General, Paks Nuclear Power Plant
- Dr. József Rónaky, Scientific Advisor, Hungarian Atomic Energy Authority

ORGANIZATION STRUCTURE OF THE MTA CENTRE FOR ENERGY RESEARCH (2020)



QUALITY MANAGEMENT

In order to achieve the highest quality of research, development, design, condition monitoring and valuation, engineering, contracting and managing in design, production, implementation and inspection, the Research Centre’s quality management system has continuously been upgraded by the recommendations of ISO 9001 standard since 1994. Reviewing our QM system by integral audits and management reviews, evaluating improvement opportunities, maintaining project documentation, infrastructure, supporting communication, ensuring the competence of workers the management improves the Centre’s QM system. For the new organization structure, our Quality Policy has been renewed. Many new employees induced a need to upgrade our QM tuition practice. We organised the work and fire safety educations. Our QM system has been certified by Hungarian Standards Institution, IQNet, MVM Paks NPP and MVM Paks II NPP. The last one gives concrete certifications for special topics; up to now four of them were awarded, one of these documents is shown below.



Certifications by Hungarian Standards Institution, IQNet, and MVM Paks NPP and MVM Paks II NPP II

BUDAPEST RESEARCH REACTOR

One of the most important strategic large scale research facilities in Hungary is the Budapest Research Reactor (BRR). It serves the needs of an extensive and diverse scientific community by supporting R&D opportunities, helping innovation and providing a strong foundation for training and education.



Bird's eye view of the Budapest Research Reactor

The BRR is a VVR-type reactor that uses light water as moderator and cooling fluid. The power of the reactor is 10 MW provided from low enrichment uranium fuel, and its main purposes – as established during the feasibility/functionality study – are radioisotope production, production of thermal and cold neutron beams for research and applications in all areas, primarily development of new functional materials and neutron activation analysis.

The core is designed to have about 120 reactor-days per year, having time-spans of 10 days or 4 days in a week. We are committed to long-term safety and responsible operations, taking care of the wastes from the spent fuel coming from the reactor. Besides the temporary spent fuel storage pool, we also operate a long-term spent fuel storage building for the physical and environmental separation between the reactor and the spent fuel storage.

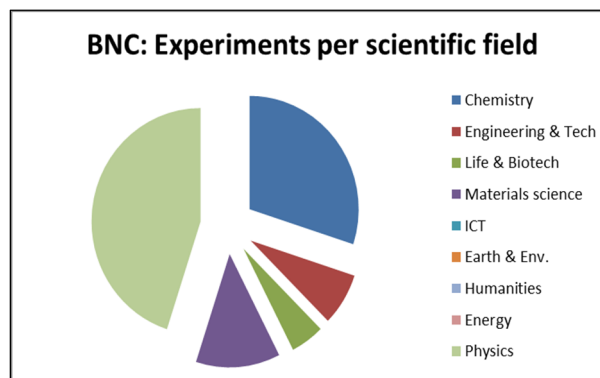


Top view of the research reactor



Layout of the BRR's facilities

The reactor hosts three kind of activities: the research activities utilizing neutron beams, production of radioisotopes for industrial and research purposes, and providing national and international training. We are proud of our innovative flagship research topics, which are carried out with a network of neutron beam stations, including beam-lines of thermal neutrons, experiments on powder and residual stress diffractometry, TOF neutron spectroscopy, radiography, biological irradiations and beam-lines of cold neutrons for experiments on small angle neutron scattering, reflectometry, prompt gamma activation analysis and nuclear data measurements. In accordance with recent worldwide trends, we are open to establishing new industrial relations, and supporting innovation. The BRR's experimental facilities are open for science based on excellence for researcher all over the world. We aim to increase our competence on special topics, to implement new technologies and develop new materials, to promote and exploit our R&D capacity at the national



and regional/international level. During the past years the BRR hosted several international schools on various technical and research topics, special trainings in the field of reactor physics, reactor operation, nuclear measurement techniques, and safety and environmental issues. Typical distribution of research topics is shown in the figure to the right.

The BRR is used by groups of different scientific communities from medical, environmental, material, archaeological, nuclear sciences and industry, as well as several Hungarian Universities. Neutron beams are uniquely suited to study the structure and dynamics of materials at the atomic level. The Budapest Neutron Centre (BNC) coordinates the scientific utilization of the research reactor. Some of main research topics currently are:

- neutron scattering, used to examine changes of sample properties under different conditions such as variations in vacuum or pressure, high and low temperature, and magnetic field, modelling real-world conditions.
- using prompt and delayed neutron activation analysis, it is possible to measure the concentration of elements in ppm and ppb levels even for small samples. Atoms of a sample become radioactive by exposure to neutrons from the reactor. They decay by gamma-rays characteristic for each element that can be detected by suitable detectors
- neutron activation is also used to produce different radioisotopes, widely used in industry and medicine. For example, Y-90 microspheres to treat liver cancer are produced by bombarding Y-89 with neutrons, which capture those. Production of radioisotopes for different applications such as medicine, sterilization and industrial use.
- testing reactor materials; materials are subjected to intense neutron irradiation which cause radiation damage of their crystalline structure. For instance, some steels become brittle. Thus, the so-called high-entropy alloys resist embrittlement are to be used in nuclear reactors.
- applied research using neutron beams to produce images of material interior. Examples are the visualization of porosities in materials or changes of density inside the sample. Dynamic neutron radiography of cooling system of refrigerator or visualization of fuel burn in engine system of a car and tomography of different materials and items.

The BNC provides researchers with 15 neutron instruments; 13 instruments are installed directly on the horizontal beam ports of the reactor or to the thermal and cold neutron guides, while the other 2 are placed at the vertical irradiation channels. The instruments are supported by a variety of sample environments and data analysis and visualization capabilities.

The BNC provides access to the international neutron user community through a peer-review system. Local scientists assist researchers and industrial users to find the appropriate neutron techniques that meet their research needs. The various neutron scattering instruments in BNC cater to a large number of users from Europe and has grown in strength and stature over the years.

BNC is a member of the League of advanced European Neutron Sources and CERIC-ERIC, and partner in recent EU Framework Programme projects (NMI3-II, CHANDA, IPERION CH, SINE2020, ESS-BrightnESS, E-RIHS, H2020 ARIAL).

BNC is strongly committed to the training of future professionals inland and all over the world in co-operation with the International Atomic Energy Agency. We cooperate with Hungarian universities (Budapest University of Technology and Economics, Eötvös Loránd University (ELTE), Pannon University, ...), BNC accommodates students for laboratory practice for studying nuclear-based techniques. A specialized course was developed for geology students of the ELTE to introduce nuclear analytical techniques into their education. BNC organizes the Central European Training School on Neutron Scattering annually, to train young scientists for neutron physics and to attract new users. The school provides insight into neutron scattering, element analysis and imaging techniques and their applications to study the structure and dynamics of condensed matter.

The Budapest Research Reactor is open to the public. Members of the local communities and high school and university students visit us regularly and learn more about the amazing nuclear science possibilities available at BRR.



Research staff of the Budapest Research Reactor facilities in the operator's room.

ENVIRONMENTAL PROTECTION SERVICE

During the use of nuclear energy, radioactive contamination of the air and the aquatic environment must be checked. As part of the Centre for Energy Research, this task is performed by the Environmental Protection Service for the entire area of the KFKI Campus.



Environment controlling gamma probe

Our Environmental Policy, developed on the basis of the relevant legislation, specifies the characteristics and frequency of the examinations for various sample types. These tests include monitoring of airborne gamma radiation, examinations of atmospheric fallout, and gamma spectrometry and total-beta activity of air aerosol particles. By the use of our own resources and tenders, we intend to develop our equipment and instrumentation in order to perform our tasks with high reliability.

During the year, a high-sensitivity ORTEC Model GEM C40 detector with an efficiency of 40% was purchased, and we also expanded the capacity of the spectrum analyser. Thus, with the expansion, we can currently operate four detectors in parallel, so we can perform up to date long-term tests. By purchasing an uninterruptible power supply, we were able to eliminate measurement restarts caused by short-term power outages.



ORTEC Model GEM C40 detector

In addition to checking the external environment, we also monitor the external and internal radiation exposure of employees exposed to radiation. Besides official TLD tests, the external radiation exposure is checked with RADOS type thermoluminescent dosimeters used by the Service under its own authority. The system has been continuously improved, so besides the reading device, they also have a heating furnace and an irradiation device.



TLD Oven

To determine the internal radiation exposure, we have a measuring system designed for whole-body examination. We constantly develop this system to get more accurate and detailed results. To minimize background radiation, we use specially designed ventilation equipment.

A detailed report of the work of the Service carried out in 2020 is available on the EK website.



Whole body measuring point

*Gáborné, Endródi
Head of Service
endrodi.gaborne@energia.mta.hu*



I. EU, NKFIH OR GOVERNMENT SUPPORTED RESEARCH ACTIVITIES



DEVELOPMENT OF ALLEGRO GAS-COOLED FAST REACTOR DEMONSTRATOR

János Gadó, András Keresztúri, Gusztáv Mayer

Objective

Gas-cooled fast reactor (GFR) technology was selected by the Generation IV International Forum (GIF) as a possible future development direction of GEN IV reactors. As part of this co-operative international endeavour, European and Japanese research institutes, universities and companies started to work on a 2400 MW thermal power reactor named GFR2400. This technology features fast-neutron spectrum and closed fuel cycle for efficient conversion of fertile uranium and management of actinides. The relatively high core coolant outlet temperature of around 800 °C ensures high thermal efficiency for this GFR system. Since there has never been built any gas-cooled fast reactor, parallel with this work a small power helium cooled demonstrator reactor named ALLEGRO is being developed. The primary goals of this currently 75 MWth power reactor are to demonstrate the helium cooled gas fast reactor technology and to test a new type of refractory carbide fuel in fast neutron spectrum and at high outlet coolant temperature. Because of the currently missing knowledge of the new refractory fuel behaviour, the first core of ALLEGRO is aimed to be developed by using MOX or UOX fuel with an outlet coolant temperature of about 520 °C; dedicated positions will be used for refractory fuel subassembly qualification, with helium outlet temperature of around 800°C. In a later step, when the new refractory fuel is validated, a fully refractory core is envisaged with a helium outlet coolant temperature of around 800 °C.

Methods

The recently launched Euratom SafeG project aims to improve the safety of the GFR technology. One of its tasks is dedicated to ALLEGRO core safety and core optimization. In order to achieve an optimized ALLEGRO core an iterative method is used between the thermal hydraulics and the neutronic calculations. As a first step, the selection of the most limiting transients is needed to be specified for the current ALLEGRO design. Based on previous categorization of initiating events for the Experimental Technology Demonstration Reactor (ETDR), a new list was proposed for the two-loop ALLEGRO design.

Euratom has recently launched also the Plutonium Management for More Agility (PUMMA) project for the investigation of the behaviour of fuel with high plutonium content and to study fuel recycling possibilities. Experiments made earlier will serve for the validation of fuel behaviour codes.

Results

The ongoing calculations suggest that the bypass transients may play a central role in safety analysis. The theoretical relation between the core design and the safety analyses, moreover the strategy of the core design depending on the safety margins were clarified in the preparatory phase of the project.

Remaining work

The final outcome of this task within the SafeG project will be an optimized MOX, UOX and refractory core. Iteration steps will be accomplished by using thermal hydraulics codes (CATHARE, ATHLET), Monte Carlo code (SERPENT), neutronic code (KIKO3DMG). Special attention should be paid for the analyses of the unprotected transients by using coupled codes.

The fast reactor fuel behaviour code FUROM-FBR developed by EK will be validated to experiments in the framework of the PUMMA project.

BENDING TEST SIMULATION OF VVER-440 MOCKUP

Levente Tatár

Objective

In the framework of the STYLE EU FP7 project a 1:5 scale replica of the VVER-440 main feedwater nozzle had been created. It was reused in the framework of the ATLAS EU Horizon2020 project. A bending arm has been welded to the replica of the nozzle and a suitable support structure has been created. After fatigue precracking of the replica a bending test was performed by an Instron universal testing machine at the Bay Zoltán Nonprofit Ltd. Force, displacements, as well as strain field (by ARAMIS optical system) have been recorded during the test [1]. This article presents a finite element model created to simulate the experiment.

Methods

The feedwater replica is bimetallic. A piece made from ferritic base metal (steel 15H2MFA) has austenitic cladding and buttering. Austenitic DMW (dissimilar metal welding) forms connection to the austenitic safe end. The bending arm is also austenitic. The support structure is ferritic. Finite element mesh for the feedwater nozzle replica, bending arm and supporting structure has been made by MSC Marc-Mentat. Due to symmetry, only half of the structure has been meshed. Material properties taken from literature were used for the support structure. Material properties for the ferritic part of the nozzle as well as the cladding, buttering and DMW were taken from the previous STYLE project. The real notch and fatigue precrack situated in the austenitic buttering layer was modelled by a discontinuity in the mesh. Gurson's damage model has been used. To simplify modelling incompatible mesh was used along with glued contacts.

Results

The simulation of the bending gave generally acceptable results until the onset of crack propagation (see Figure 1.). The force-displacement results are satisfactory for the beginning of the deformation process. The crack propagation is also simulated, however simulated crack propagation starts at considerably different forces and crosshead displacements than those observed experimentally. This behaviour is not uncommon for damage models as damage parameters usually need to be adjusted to obtain correct results.

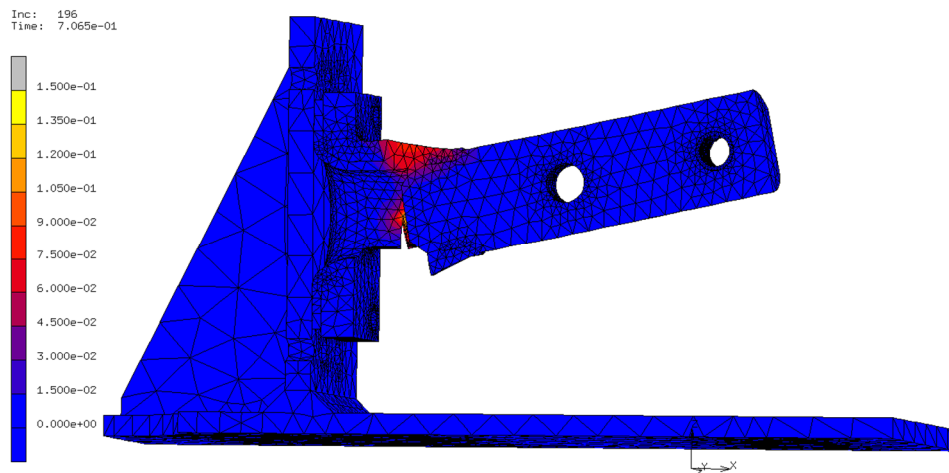


Figure 1: Deformed shape with total equivalent plastic strain

Remaining work

Even by using domain decomposition method, the runtime required for an analysis is unacceptably high. Thus, the necessary adjusting of the damage parameters cannot be done in due time. The usage of the glued contact leads to high overhead of the computations. On the other hand, the mesh in the vicinity of the crack tip is not fine enough. It has been observed that the hole facing the crack tip at the other side of the mock-up was also a starting point for a crack. Taking into account all these, a new model is being developed with the following properties:

- Only the mock-up and the bending arm is modelled without the support structure;
- Compatible mesh is used thorough the model;
- Symmetry is not used.

The new model should run in acceptable time, simulate crack emanating from the hole and have a fine enough mesh to correctly simulate damage in the vicinity of cracks.

Related publication

- [1] L. Tatár: *Medium Scale Experiment for VVER-440 Nozzle Mock-Up*, Centre for Energy Research Progress Report 2019, (2020)

ACTIVATION STUDY OF THE ESS NMX SHUTTER PIT

Dávid Hajdú, Péter Zagyvai

Objective

The aim of the study was to support the radiation protection planning of the Neutron Macromolecular Crystallography Diffractometer (NMX) shutter pit of the European Spallation Source (ESS). Though the original topic was the investigation of different iron and copper collimator concepts, this study became more important from the project's point of view, so a topic change has happened at the beginning of the research. This topic also comprises concrete, aluminium and boroglass activation calculations beside copper and iron.

Methods

Activation simulations were carried out using Monte Carlo N-Particle eXtended (MCNPX) and Cinder1.05 codes. Geometry of the shutter pit is plotted in Figure 1, in which the neutron source is on the left side. Five years of continuous neutron irradiation and one day of cooling were applied, representing a maintenance scenario. After cooling, gamma dose rates were tallied at the sealing of the shutter pit.

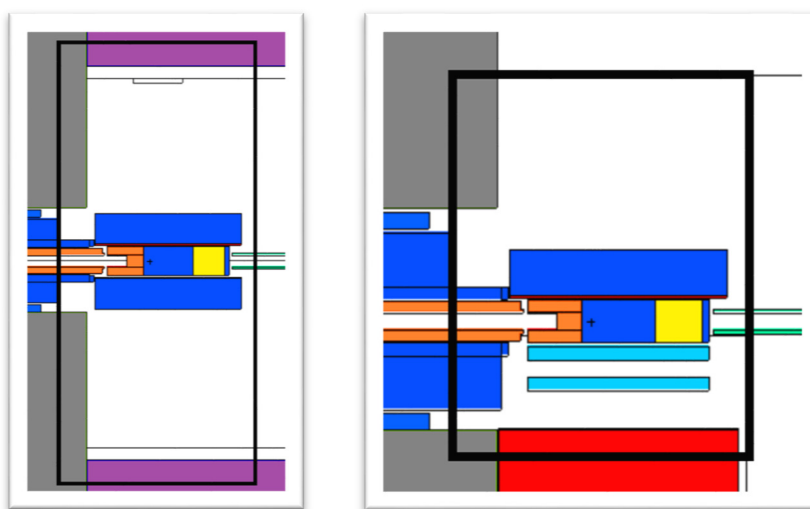


Figure 1: Top-view (left) and side-view (right) of the shutter pit

Black lines are the borders of the investigated area. Colours correspond to the materials: 1. grey - heavy concrete 2. purple - normal concrete 3. dark blue - steel 4. light blue - aluminium 5. orange - copper 6. yellow - polyethylene 7. red - Mirrobor

Results

The most important result is that the Mirrobor cover on the surface of the shutter effectively absorbed most of the neutrons. Due to this phenomenon the only considerable activation was the moderate activation of the first copper part of the shutter. Around 1.5-3 nSv/h dose rate can be attributed to this unit. This can be considered as the total dose rate from neutron activation products. In coppers ^{64}Cu is the most important activation product considering short-term consequences, the effect of trace elements is marginal.

As gamma radiation from decay of radioisotopes were examined in general, the role of natural radioisotope contents of concretes has appeared too. 35 nSv/h dose rate was calculated, attributed to the natural radioisotopes in the original model, which is in the range of the statistical fluctuation of the natural background and 700-times lower than the 25 $\mu\text{Sv/h}$ derived dose constraint for short-term occupational exposure.

To sum up, it can be concluded that dose rates were reasonably low during the maintenance scenario, there is no need for further shielding against decay gamma radiation in the ESS NMX shutter pit.

Related publication

- [1] D. Hajdú, P. Zagyvai, T. Bozsó, J. Somlai: *The role of natural radioisotopes in dose calculations of the NMX shutter pit of the European Spallation Source*, VII. International Conference of Terrestrial Radioisotopes in Environment (2020)

IDENTIFICATION OF WINTERTIME COMBUSTION PROCESS RELATED AEROSOL POLLUTION IN BUDAPEST

*János Osán, Endre Börcsök, Ottó Czömpöly, Árpád Farkas, Péter Fűri, Veronika Groma,
Szabina Török*

Objective

Biomass combustion is one of the major contributors to gaseous and particulate matter pollution especially to carbonaceous aerosol during wintertime. Although European cities have made progress in reducing particulate air pollution in recent decades, due to economic reasons biomass combustion is getting to be popular. Moreover, it is an observable trend that not only firewood but various types of domestic waste are used as fuel for space heating. As fine ($PM_{2.5}$ - where PM_x stands for particulate matter with less than x μm diameter) and ultrafine aerosols ($PM_{0.1}$) are associated with premature mortality and cardiovascular disease, not only the particle number concentration, but also the chemical composition of aerosol particles are of high importance. Whilst the first can be easily investigated by scanning mobility particle sizers (SMPS) with high temporal resolution, the composition and speciation of the different sized particles can be studied by the combination of cascade impactor sampling and total-reflection X-ray fluorescence (TXRF) analysis. To be able to identify the contribution of combustion process related particles, acceptable markers should be defined. Besides levoglucosan, which is unambiguous tracer of biomass burning, the measurement of elemental and organic carbon content is favourable.

Source apportionment techniques, such as positive matrix factorisation (PMF) is an effective tool to define and separate different emission sources and to calculate their contribution. The aim of this study was to identify pollution sources and to quantify their contribution in downtown Budapest based on the results of a 10-day intensive field campaign and PMF modelling. The health effect of ultrafine particles was studied by numerical simulations using a stochastic lung model.

Methods

An intensive wintertime sampling and measurement campaign was carried out in a green belt area of Budapest (Hungary), between 16 and 25 January 2020. High time resolution measurements were performed to monitor the particle number size distribution (10-1000 nm) and black carbon (BC) concentration using an SMPS and an aethalometer, respectively. Size fractionated aerosol samples were collected for 4 hours using a 9-stage May-type cascade impactor four times a day. Sampling was performed onto Si wafers covering the particulate matter size range of 70 nm to 9 μm . For comparison, samples were also collected at Nógrádmegyer (Hungary), a rural village with high utilization of wood and biomass for domestic heating. The size distributions of major (S, Cl, K, Ca, Fe) and trace (Cu, Zn, As, Se, Br, Pb) elemental concentrations were determined by TXRF, which method is capable to reach detection limits down to 0.1 ng/m³ [1].

Source apportionment modelling was performed using the PMF 5.0 software package (US EPA) for the number size distribution data and the size fractionated aerosol samples chemical composition separately. In addition, the Radact version of the stochastic lung model [2] was used to determine the deposition distribution of ultrafine particles in the human respiratory tract.

Results

Stochastic lung model calculations showed that large daily numbers of urban ultrafine particles are deposited in the respiratory tract, which may play a key role in the health effects of particulate matter inhalation [3]. Since the biological effects of the ultrafine and the larger particles differ from each other, it is unavoidable that for a better estimation of the health risks associated with particulate matter inhalation, the number of particles smaller than 100 nm should also be measured in addition to the PM_{10} mass. Emission sources of these particles were identified and their contribution was estimated using the PMF method.

Based on the aethalometer data, the end-of-pipe traffic and biomass burning related BC content could be separated. The contribution of biomass combustion was found to be between 23 and 38% of total BC concentration during the winter campaign. Local biomass combustion source could be identified during an episode with elevated BC concentrations. Besides the characteristic size distribution of potassium, chlorine was also found in the condensation mode similarly to the wood combustion plume sampled at Nógrádmegyer (Figure 1). Trace elements Br, Zn and Pb also followed the size distribution of K [4].

Using the time trends of the measured parameters, the correlation of PMF factors calculated from SMPS data and size fractionated elemental compositions were studied. Number size distribution data was found to be a composition of 6 factors from which three could be identified as combustion process related factor. The 100 nm mode particles could be related to biomass combustion, whilst 16 and 35 nm mode particles are related to fresh traffic emission sources. Using the PMF results of the size fractionated aerosols elemental concentrations these two traffic related sources could be identified and connected to end-of-pipe emission and resuspension, respectively. Also, it was found that the factor related to biomass combustion consists of K, Cl, Zn and Pb in the condensation size range and K, Cu, Zn, Br and Pb in the ultrafine particle range, which suggests that not only firewood but also treated wood as well as other domestic wastes were used for domestic heating. Although the

contribution of black carbon to PM_{2.5} mass was found to be only 6-15% during the campaign, based on the PMF results it can be stated that combustion process related emissions are major anthropogenic sources of ultrafine particles during wintertime.

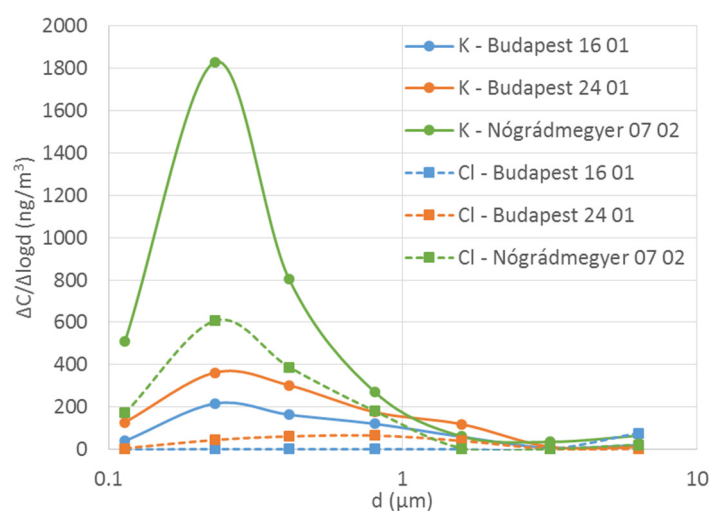


Figure 1: K and Cl size distribution for selected samples collected in Budapest and at Nógrádmegyer. Corresponding BC concentrations: 1.9 $\mu\text{g}/\text{m}^3$, 6.0 $\mu\text{g}/\text{m}^3$ and 6.7 $\mu\text{g}/\text{m}^3$ for the 16 01, 24 01 (Budapest) and the 07 02 (Nógrádmegyer) samples, respectively

Remaining work

Raman microscopy has been successfully used to study carbonaceous particles. In order to study the chemical forms of carbon in aerosol particles, Raman spectroscopy-based analysis of size-fractionated aerosol samples collected on Si wafers is planned.

Related publications

- [1] J. Osán, E. Börcsök, O. Czömpöly, C. Dian, V. Groma, L. Stabile and S. Török: *Experimental evaluation of the in-the-field capabilities of total-reflection X-ray fluorescence analysis to trace fine and ultrafine aerosol particles in populated areas*, *Spectrochimica Acta Part B* **167**, 105852 (2020)
- [2] P. Fűri, Á. Farkas, B.G. Madas, W. Hofmann, R. Winkler-Heil, G. Kudela and I. Balásházy: *The degree of inhomogeneity of the absorbed cell nucleus doses in the bronchial region of the human respiratory tract*, *Radiation and Environmental Biophysics* **59**, 173–183 (2020)
- [3] P. Fűri, V. Groma, S. Török, Á. Farkas and C. Dian: *Deposition distributions of ultrafine urban particles in healthy and diseased lungs*, *Inhalation Toxicology* **32**, 494-502 (2020)
- [4] J. Osán, V. Groma, B. Alföldy, T. Szigeti, O. Czömpöly, E. Börcsök and S. Török: *Identification of fine and ultrafine particles originated from residential wood combustion*, *European Aerosol Conference*, 31 08 – 04 09 2020, Aachen, Germany (virtual), 936 (2020)

STRATEGIC RESEARCH GROUP FOR THE CHALLENGES OF RENEWABLE ENERGY BASED SYSTEMS

Bálint Hartmann, Attila Kazsoki, Bálint Sinkovics, Viktória Sugár

Objective

The primary goal for the third year of the research project was to demonstrate the behaviour of medium voltage networks under varying conditions. Created reference networks were to be integrated to the stochastic simulations.

Methods

In the distribution areas covering more than 50% of the country six reference network models (RNM) were selected, which were topographically verified, too. The clustering methodology was verified with another distribution system operator's medium voltage feeders. The applicability of the synthetic network generation algorithms was described on the presented reference networks, by comparing the node degree and betweenness distributions.

For RNM1 a simulation framework was created to examine the effects of different weather changes with high photovoltaic penetration. The most significant weather event for photovoltaic power generation is the change in cloud coverage, which can be simulated using a cloud shadow model. The typical Hungarian weather conditions were described, with special regard to the typical wind directions and cloud coverage. In the cloud model its diameter, the direction and the speed of the cloud can be altered. The load-flow model uses clear sky irradiation values, dynamic consumer profiles, photovoltaic plant placements (based on the betweenness three scenarios are examined).

Results

As the result of the clustering verification method it was concluded that the Hungarian medium voltage feeders can be described well by the 6 RNM models. By comparing the node degree and betweenness distributions of the RNMs and the synthetic network models, it was found that neither the random graph (Erdős-Rényi), nor the small world graph (Watts-Strogatz) and the scale-free preferential attachment (Barabási-Albert) graph is suitable to approximate the RNMs.

The functionality of the developed simulation framework is proven. Using it, a qualitative estimation can be given of the feasibility of the required increase in photovoltaic penetration. As the results of the simulation in either scenario for RNM1, it can be concluded, that the fast voltage change does not reach the value specified in the standard even in the case of 2030 photovoltaic penetration. In light of the results a comparative analysis of possible smart network development tools was carried out. The key aspects of a new network development best practice were considered, the final methodology is under development.

Remaining work

The research project lasts until the end of 2021 as part of the VEKOP-2.3.2-16-2016-00011 project. The next year's main objective is to finalise documentation and publications.

Related publications

- [1] B. Hartmann: *Comparing efficiency of various solar irradiance categorization methods*, Renewable Energy **154**, 661-671 (2020)
- [2] G. Ódor, B. Hartmann: *Power-Law Distributions of Dynamic Cascade Failures in Power-Grid Models*, Entropy **22**, 666, 1-20 (2020)
- [3] A. Kazsoki, B. Hartmann: *Hierarchical agglomerative clustering of selected Hungarian medium voltage distribution networks*, Acta Polytechnica Hungarica - **17(4)**, 201-219 (2020)
- [4] A. Kazsoki, B. Hartmann: *Methodology for the formulation of medium voltage representative networks in three DSO areas*, Renewable Energy & Power Quality Journal - **18**, 213-218 (2020)
- [5] B. Hartmann, A. Kazsoki, V. Sugár, B. Sinkovics: *Napsugárzás mintázat kategorizálási módszereinek kritikai szemléletű összehasonlítása*, Magyar Energetika - **1**, 18-24 (2020)
- [6] A. Kazsoki, B. Hartmann: *Prosumerek alkotta energiaközösség energiafelhasználásának és napelemes energiatermelés egyidejűség-növelésének lehetőségei*, X. Mechwart András Ifjúsági Találkozó - **1**, 18-24 (2020)
- [7] A. Kazsoki, B. Hartmann: *Középfeszültségű mintahálózatok létrehozása adatbányászati módszerek felhasználásával*, X. Mechwart András Ifjúsági Találkozó - **1**, 78-83 (2020)

STRUCTURE OF OXY-HALIDE COMPOSITIONS FOR USE IN SOLID STATE BATTERIES

Margit Fábrián, István Tolnai

Objective

The novel inorganic and thermally stable oxides are potential substitutes for the toxic and flammable organic liquid electrolytes that are used in Li-ion batteries. The oxy-halide solids are derived from the precursors of crystalline anti-perovskites of metal hydroxides and have the highest reported Li^+ , Na^+ , K^+ conductivity, $\sigma > 10^{-2} \text{ S cm}^{-1}$ at room temperature.

Methods

Li-, Na- and K-ion based oxy-halide materials with nominal compositions: $\text{A}_{3-2x}\text{M}_x\text{O}_{1+y}\text{Cl}_{1-2y}$ ($\text{A}=\text{Li, Na, K}$; $\text{M}=\text{Ca, Ba, Mg}$; $x=0.005$; $y=0$) have been prepared. X-ray diffraction (XRD) measurements were performed using a Bruker AXS D8 Discover diffractometer ($\text{Cu K}\alpha$, $\lambda=1.5406 \text{ \AA}$) radiation. A Renishaw In-Via Reflex μ -Raman spectrometer was used to measure the Raman spectra of the samples using an Ar-ion laser of 488 nm excitation wavelength (50 mW).

Results

Figure 1. shows the XRD intensities of the samples. The formation of anti-perovskite Li_3OCl is verified (Fig 1a), where the peak at $2\Theta=32.7^\circ$ can be indexed as (011) of the cubic Li_3OCl phase with the space group of $\text{Pm}\bar{3}\text{m}$ and a lattice constant of 3.91 \AA . Beside the anti-perovskite phase, the LiCl , Li_2CO_3 , $\text{LiCl}(\text{H}_2\text{O})$, $\text{Li}_4\text{Cl}(\text{OH})_3$ phases were identified. The $\text{LiCl}(\text{H}_2\text{O})$ and $\text{Li}_4\text{Cl}(\text{OH})_3$ phases are due to the absorption of H_2O . In the Na-based samples NaCl can be identified, as well as $\text{NaOH} \cdot \text{H}_2\text{O}$ and $\gamma\text{-Na}_2\text{CO}_3$ phases due to water uptake. In the case of the $\text{Na}_3\text{OCl-Mg}$, no phase(s) could be unambiguously assigned to some of the diffraction peaks based on the present measurements, suggesting that besides the above mentioned compounds we probably have a more complex structure. In the $\text{K}_3\text{OCl-Mg}$ sample KCl , $\text{K}(\text{H}_2\text{O})\text{OH}$ and $\text{K}_2\text{CO}_3 \cdot 1.5\text{H}_2\text{O}$ phases can be identified. Among the three halide chlorides, the KCl exhibited the most intense peaks, besides the minor OH-containing phases.

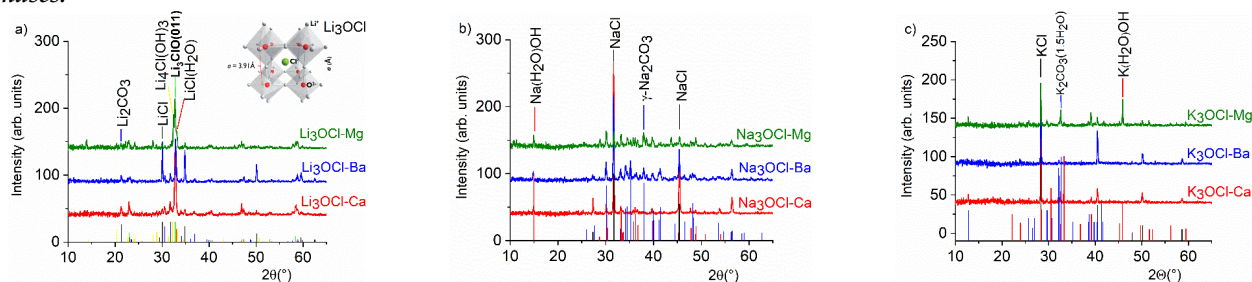


Figure 1: X-ray diffraction patterns of $\text{Li}_3\text{OCl-Ca/Ba/Mg}$ (a), $\text{Na}_3\text{OCl-Ca/Ba/Mg}$ (b) and $\text{K}_3\text{OCl-Ca/Ba/Mg}$ (c) samples.

Figure 2 shows the measured Raman spectra of the three series in the wavenumber range between 3300-3750 cm^{-1} . In case of the $\text{Li}_3\text{OCl-Ca/Ba}$, both samples have a similar spectrum, two well defined bands, one at 3635.3 cm^{-1} which corresponds to OH stretching, and the band at 3609.5 and 3601 cm^{-1} related to the presence of H_2O . The spectrum of $\text{Li}_3\text{OCl-Mg}$ reflects the different local environment, probably corresponding to another incorporation mode of the Mg element. The Raman bands at 3614 and 3619.3 cm^{-1} are assigned to the vibration of the OH⁻ ion. The spectra of the $\text{Na}_3\text{OCl-Ca/Ba/Mg}$ samples all display a band at 3567.5 cm^{-1} connected to H_2O and a multi-band distribution between 3620.7-3648.6 cm^{-1} , due to the vibration of OH. The $\text{K}_3\text{OCl-Ca/Ba/Mg}$ samples all show a sharp band at 3500.2 cm^{-1} , assigned to the H_2O . In case of the $\text{K}_3\text{OCl-Ca}$ sample, an OH stretching band is observed at 3614.9 and 3631 cm^{-1} whereas no stretching peak is observed in the Ba/Mg doped samples.

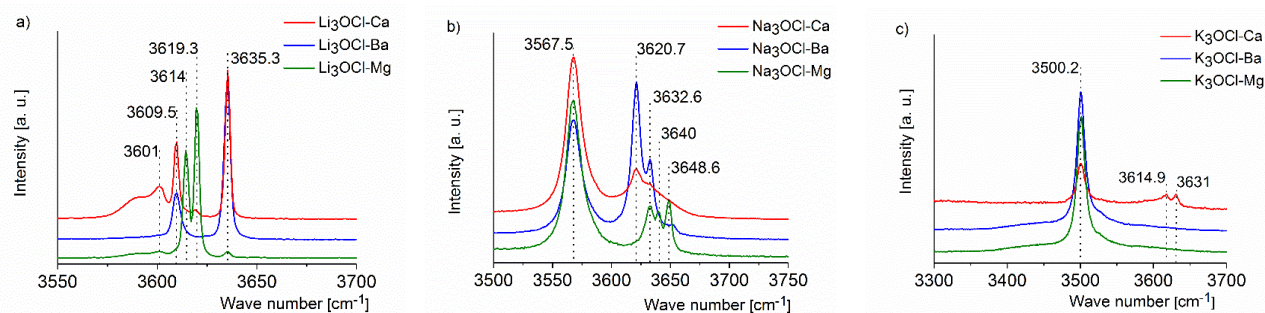


Figure 2: Raman spectra of $\text{Li}_3\text{OCl-Ca/Ba/Mg}$ (a), $\text{Na}_3\text{OCl-Ca/Ba/Mg}$ (b) and $\text{K}_3\text{OCl-Ca/Ba/Mg}$ (c) samples.

During the XRD measurements and Raman spectroscopy investigations, the samples were kept in the air – although not for long period of time - but due to the strong hygroscopic behaviour of the samples, mainly the effect of incorporated water could be detected. Figures 1 and 2 are dominated by the OH- and water-connected phases.

This work was supported by the NKFIH, Nr. 2017-2.3.7-TÉT-IN-2017-00023.

Remaining work

This is the second year of a three-year project. We continue the well-prepared TÉT schedule.

Related publications

- [1] M. Fabian et al: *Structure of oxy-halide compositions for solid state batteries*, 21st ISCMP online conference - invited lecture, 31 Aug-4 Sept 2020, Varna, Bulgaria
- [2] M. Fabian et al: *Structural characterization of oxy-halide materials for solid state batteries*, Phys. Stat. Sol. A **218**, doi.org/10.1002/pssa.202000682 (2021)

X-RAY SPECTROSCOPIC CHARACTERIZATION OF SIZE-FRACTIONATED ATMOSPHERIC AEROSOL PARTICLES

János Osán, Endre Börcsök, Ottó Czömpöly, Veronika Groma, Szabina Török

Objective

Aerosol particles (particulate matter – PM) are among the most harmful pollutants in ambient, indoor and workplace air. The impact of PM pollution in urban areas of many countries exceeds the World Health Organization (WHO) air quality guideline concentrations. Recent epidemiological studies have shown that short term exposure to elevated concentrations of ambient PM might trigger acute effects like heart rate variability, especially the fine (PM_{2.5}) and ultrafine (PM_{0.1}) particles, where PM_x denotes particulate matter with equivalent aerodynamic diameter less than x μm . Submicron particles got special attention recently due to the evidence of their detrimental health effects. The fraction of the inhaled aerosol particles which deposits in the lung strongly increases with decreasing size in the ultrafine region. Emission of submicron particles can be very short-term and can relate to the traffic flow. It is well known that the size distribution of elemental concentrations has a time variation dependent on the sources and meteorological conditions. In order to have a reliable estimation of health effects of the inhaled particles and their source contributions, information on the size-resolved chemical composition of aerosol particles with sufficient time resolution is imperative. Since the toxicity of metals strongly depends on their chemical state, speciation information is necessary to accompany size the distribution of chemical elements in PM samples.

Total-reflection X-ray fluorescence (TXRF) spectrometry is a promising technique for this task. Using TXRF, a suitable aerosol collector (impaction plate) can be directly measured without any sample preparation or handling which would increase the risk of contamination. The present report summarizes the analytical capabilities of the combined methodology of cascade impactor sampling of size-fractionated PM and subsequent TXRF analysis of the deposited particles. Different combinations of cascade impactor and TXRF systems are compared through simultaneously collected samples of the same field campaign. Speciation of carbon and nitrogen was addressed using near-edge X-ray absorption fine structure (NEXAFS) spectrometry in the TXRF geometry.

Methods

Atmospheric PM samples were collected in Budapest, Hungary (suburban background) and at Cassino, Italy (urban location), for 2 to 6 hours. Two types of cascade impactors were used, a 13-stage DLPI (Dekati, Finland) and an in-house made 9-stage May-type impactor. The DLPI works at a 10 l/min flowrate, resulting in aerodynamic cut-off diameters of 10 μm down to 30 nm. The May impactor has, at a 16.7 l/min sampling flowrate, aerodynamic cut off diameters of 18 μm down to 70 nm. Acrylic discs and silicon wafers were used as collecting substrates for the DLPI and May-impactor, respectively. The samples were analysed using a mobile TXRF (S2 Picofox, Bruker, Germany) on-site, and laboratory TXRF (WobiModule, TU Wien, Austria) afterwards. Using laboratory TXRF, detection limits down to 0.1 ng/m³ could be reached [1]. For comparison, inductively coupled plasma mass spectrometry (ICP-MS) was used for elemental analysis of simultaneously collected total PM₁₀ samples collected on filters. Selected samples were also measured at the BESSY II synchrotron radiation facility (Berlin, Germany) using reference-free X-ray spectrometry (XRS) [2].

Results

Since the DLPI has a deposition pattern of several dots in a circular arrangement which are even different for each stage, the mobile TXRF spectrometer used in the field campaign was calibrated against elemental mass depositions at each stage. A nickel test aerosol with a broad size distribution was sampled onto a set of 12 acrylic disc carriers for this task. Mass depositions were determined by a physically traceable, reference-free XRS arrangement, from which stage-dependent correction factors could be revealed [2, 3].

The final result of TXRF elemental analysis of cascade-impactor collected PM samples is the size distribution of elemental concentrations. Fig. 1 shows a comparison between size distributions of major and trace elements obtained by two combinations of sampling and analysis, i.e. DLPI and mobile TXRF, as well as May-impactor and laboratory TXRF. Despite the different size range covered by the two impactors and the different size resolution, a reasonable agreement was found for most of the elements [3]. The size distribution from the DLPI is a little bit more detailed due to the higher size resolution, and higher maxima in the largest size bin were obtained. This most likely occurred because the upper two stages of the May impactor were excluded from the analysis to optimally cover the PM₁₀ size range. In effect, the geometric mean diameter of the largest size bin of the May impactor is only 6.3 μm while for the DLPI it is 8.4 μm . The mismatch of size distributions for Sr, Fe, and Pb, will need further investigations.

After summing the TXRF results obtained for the impactor stages covering the whole PM₁₀ size range, the elemental concentration results could be compared to those of a standard method – e.g. ICP-MS analysis of digested filter samples. The agreement was found to be satisfactory for elements V, Cr, Mn, Fe, Ni, Cu, Zn, As and Pb for several parallel cascade impactor and filter samples of the Cassino field campaign [3].

NEXAFS results indicated the dominance of elemental carbon in the 70-180 nm size range at both the Cassino and Budapest

sites. Absorption peaks related to organic carbon could be identified and are more pronounced in the 180-300 nm fraction. Absorption effects are important for samples, which are highly loaded with soot and organic particles. Nitrogen was found as ammonium and organic-bound in the 70-600 nm size range [4].

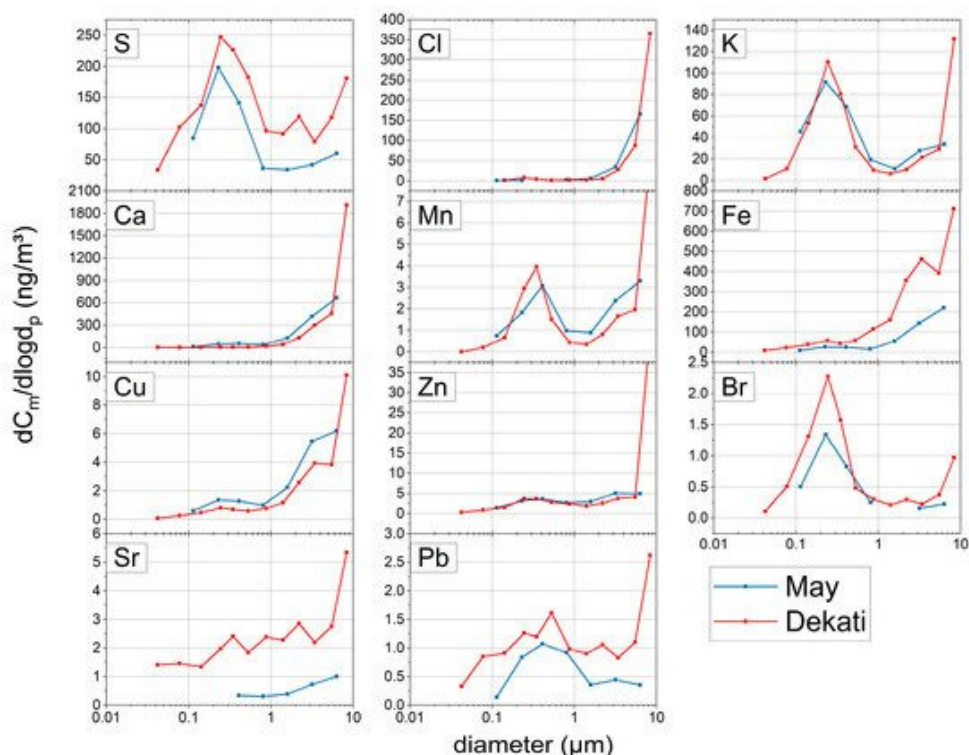


Figure 1: Size distributions of element mass concentrations in PM_{10} from May and DLPI (Dekati) impactors, resulting from a 4-h simultaneously collected set of samples of the Cassino field campaign.

Remaining work

The reliability of TXRF analysis of PM samples collected by cascade impactors will be further addressed through development and characterization of standard sample carriers mimicking the deposition pattern of particles in different cascade impactors.

Related publications

- [1] J. Osán, E. Börcsök, O. Czömpöly, C. Dian, V. Groma, L. Stabile and S. Török: *Experimental evaluation of the in-the-field capabilities of total-reflection X-ray fluorescence analysis to trace fine and ultrafine aerosol particles in populated areas*, *Spectrochimica Acta Part B* **167**, 105852 (2020)
- [2] Y. Kayser, A. Gross, P. Hönicke, J. Osan, B. Pollakowski-Herrmann, S. Seeger and B. Beckhoff: *Reliable chemical analysis of aerosols by reference-free X-ray spectrometry for monitoring airborne particulate matter*, *Spectroscopy* **35**, 42-46 (2020)
- [3] S. Seeger, J. Osán, O. Czömpöly, A. Gross, H. Stosnach, L. Stabile, M. Ochsenkuehn-Petropoulou, L. A. Tsakanika, T. Lympelopoulou, S. Goddard, M. Fiebig, F. Gaie-Levrel, Y. Kayser and B. Beckhoff: *Quantification of element mass concentrations in ambient aerosols by combination of cascade impactor sampling and mobile total reflection X-ray fluorescence spectroscopy*, *Atmosphere* **12**, 309 (2021)
- [4] J. Osán, V. Groma, O. Czömpöly, Y. Kayser, L. Stabile, B. Beckhoff and S. Török: *Chemical state of metals and light elements in size-fractionated aerosol samples*, European Aerosol Conference, 31 08 – 04 09 2020, Aachen, Germany (virtual), 969 (2020)

CHEMICAL EVOLUTION AND RADIONUCLIDE RETENTION STUDIES FOR HIGH-LEVEL RADIOACTIVE WASTE DISPOSAL

Margit Fábíán, István Tolnai, János Osán, Ottó Czömpöly

Objective

The interface between carbon steel and cementitious materials is a key issue in the design of a disposal cell for vitrified high-level radioactive waste (HLW) and intermediate level waste (ILW) in argillaceous and crystalline rock formations for the Hungarian national waste disposal program.

The designs rely upon steel-containers (S235JR) containing the HLW encased in a prefabricated cylindrical concrete/clay buffer material. The concrete is made from CEM II cement and limestone aggregates. The clay is from the Boda Claystone Formation (BCF), the host rock considered for the final disposal program in Hungary. The pH has to be kept at high values during the thermal phase, and for a much longer period after, in order to keep the carbon steel container passivated, to limit corrosion and ultimately to prevent radionuclide release.

The aim of the planned experiments is to gain information on chemical-physical alterations of the steel/concrete and steel/clay interfaces, for different environmental conditions (temperature, groundwater) using different characterization methods. The planned work is an attempt to simulate the conditions which cause the corrosion, whose intensity we plan to measure in laboratory tests. All experimental results will serve as input parameters for modellers. The modelling calculations will be carried out by SCK CEN (Centre d'Étude de l'Énergie Nucléaire) in a later stage of the project.

Quantifying the long-term entrapment of radionuclides (RN) in the solid phases of the host rock around the radioactive waste repository is a crucial step toward understanding diffusion and transport mechanisms. Two distribution areas of the BCF are known, the Gorica Block and the perianticlinal structure of the Boda Block. Albitic claystone is characteristic for the Boda Block, whereas analcime-rich rock types can only be found in the Gorica Block. The main rock-forming minerals of the BCF are: clay minerals (mainly illite and chlorite/smectite), authigenic albite, analcime (Gorica Block only), detrital quartz, carbonate minerals (calcite and dolomite) and hematite. The recent BAF-2 drill core from the Boda Block contains reductive sections with high pyrite. Studies on sorption and diffusion characteristics of RNs in cationic (Ni^{2+}) and anionic form (SeO_3^{2-}) are planned to be studied on clay-rich rock sections of BCF in both crushed and intact forms. Diffusion experiments involving inactive SeO_3^{2-} are especially planned for later microscopic investigations of the diffusion front on both the oxidative (albitic claystone) and on the reductive (pyritic) sections of the BAF-2 core. These studies may deliver information on the possible formation of nanocrystalline precipitates due to redox reactions.

Methods

The Assessment of the Chemical Evolution of ILW and HLW Disposal Cells Work Package is dedicated to identify and model the main reactive processes at the steel/cement and steel/clay interfaces and their consequences in terms of element transfers and microstructures evolutions. All data (from modelling and experiments) have to describe geochemical behaviours as a function of the environmental constraints, representative of conditions expected to be encountered in geological storage facilities.

Two parallel sets of laboratory experiments are in progress in Subtasks 2.2 and 2.3 to gain information on corrosion intensity at the interfaces between carbon steel and a CEM II/B-based concrete and carbon steel and clay. A temperature of 80°C is used for the sake of consistency and comparison with the other experiments performed earlier. Synthetic groundwater of the Boda Claystone is used for hydrating the clay and conditioned cementitious water to set the boundary environmental conditions. The physical and chemical properties of the concrete and the Boda water chemistry have been compiled to further define the initial states of the reactive transport model.

The Fundamental Understanding of Radionuclide Retention Work Package is dedicated to experimental and modelling studies towards a fundamental understanding of radionuclide retention. Our research group focuses on sorption and diffusion experiments on the BCF host rock. Since diffusion and sorption of SeO_3^{2-} on intact BCF rock samples are a major part of the experimental studies, sorption of SeO_3^{2-} is studied on crushed rock samples with a particle diameter less than 63 μm as well. Sorption isotherms (sorbed amount as a function of equilibrium concentration in the liquid phase) are recorded through batch experiments in the 10^{-8} - 10^{-3} M equilibrium concentration regime. Synthetic BCF groundwater, after conditioning, is applied to the crushed rock samples. Diffusion cells prepared from polycarbonate accommodating 4-8 mm thick slices of full diameter (62 mm) core sections are used. The cells contain two compartments of 170 ml volume for the liquid phase. The slices are equilibrated with synthetic groundwater for 1 month. Diffusion experiments involving smaller rock samples are also planned. Proper diffusion cells are under design. To monitor the diffusion in the rock, the changes in concentration of the RN during the experiment lasting several months will be measured. At the end, the rock will be cut and the concentration profile developed inside the rock will be mapped. The measurements of elemental equilibrium concentrations in the liquid phase are and will be carried out using inductively coupled plasma atomic emission spectroscopy (ICP-OES) and total-reflection X-ray fluorescence (TXRF), while on the solid samples microscopic X-ray fluorescence (μXRF), microscopic X-ray diffraction (μXRD) and scanning electron microscopic (SEM) investigations will be performed.

Results

A schematic representation and photograph of the experimental set-up with the cement is given in Figure 1. The reactor cell as well as the materials within it are designed so that the experimental set up represent an axisymmetric geometry. The inner Teflon cylinder contains the carbon steel cylinder embedded in the concrete. There is an external Teflon cylinder filled with conditioned water to keep the degree of water saturation at circa 100%. Holes of 0.7 mm in diameter in the inner Teflon cylinder ensures the connection with the water from the second Teflon cylinder.

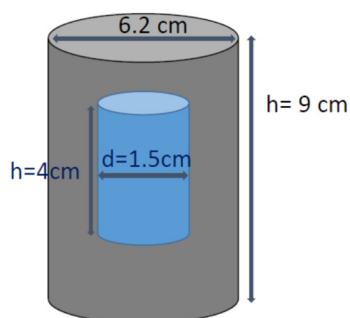


Figure 1. Steel/concrete experiment: dimensions of the concrete cylinder in dark grey and steel cylinder in blue (left), and photograph of the set-up (right).

Three parallel experimental setups were kept at 80°C, for all the steel/cement and for the steel/clay assemblies. The corrosion potential was monitored. After finishing the first cycle (3 months) on 30 September, we took out the first containers, and started to perform different characterizations of the steel/clay and steel/cement interfaces. On the solid samples μ XRF analysis and SEM imaging were performed, and now we are preparing to μ XRD measurements.

Both steel/cement and steel/clay experiments will run until June 2021. The evaluation of the chemical-physical and corrosion properties is in progress for the samples which were taken out after 3 and 7 months.

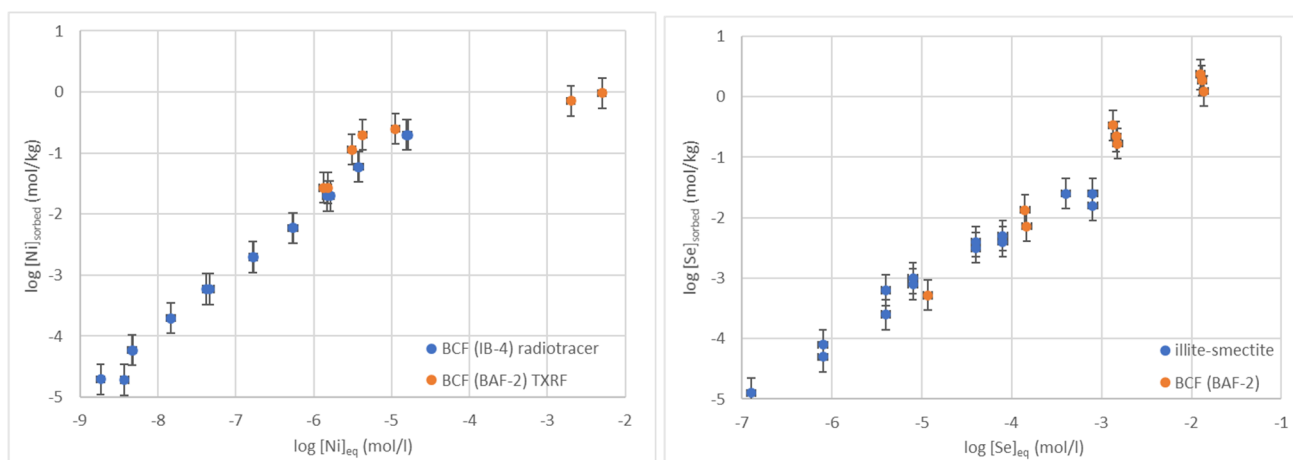


Figure 2. Comparison of sorption isotherms obtained using TXRF and data available in the literature using radiotracer (Ni^{2+} , left panel) and ICP-OES (SeO_3^{2-} , right panel) for quantifying liquid-phase RN concentrations

For the high-concentration regime (10^{-2} - 10^{-5} M equilibrium concentration), batch sorption experiments have been performed using inactive Na_2SeO_3 and NiCl_2 . TXRF was used to determine the elemental concentrations in the liquid phase, showing promising preliminary results compared to the literature (Figure 2). Since sorption isotherms have not yet been recorded for SeO_3^{2-} in BCF, literature data obtained for illite-smectite standard are plotted for comparison. The range of investigation will be extended down to 10^{-8} M liquid phase concentration using ICP-OES. Diffusion cells are equilibrated with synthetic groundwater and the experiments will be initiated in 2021.

This work was supported by the H-2020 European Joint Program on Radioactive Waste Management (EURAD) -847593

Remaining work

This is the first year of a five-year project; we continue the well-prepared schedule.

CONNECTING RUSSIAN AND EUROPEAN MEASURES FOR LARGE-SCALE RESEARCH INFRASTRUCTURES – CREMLIN+

Alex Szakál, Márton Markó, Tamás Veres, Péter Kárpáti, Laura Draskovits, László Rosta

Objectives

The objective of the CREMLIN+ project is to foster the collaboration between European and Russian research infrastructures. The project deals with large-scale infrastructures such as particle accelerators, lasers and research reactors. EK is collaborating with the Forschungszentrum Jülich (FZJ) and the Petersburg Nuclear Physics Institute (PNPI) to develop a cold neutron source and a connected guide system to effectively transport the neutrons to the experimental stations. The planned cold source and guides will be a state-of-the-art system for several reasons: The cold source will be a low-dimensional moderator (LDM) filled with liquid para-hydrogen. The connected neutron guide system will be designed to exploit effectively the higher brilliance of the source.

Methods

Although several Monte-Carlo calculations have been done to calculate the brilliance of a low-dimensional moderator, the concept was not yet proven experimentally. The experimental validation without building the full-scale cold source is challenging because the mock-up has to be put into a neutron environment similar to that provided by the reactor itself. Placing the mock-up into one of the horizontal channels close to the reactor core has several drawbacks e.g. limited access to the moderator cell to experiment with changes in the cell geometry, safety issues, etc. To overcome these drawbacks, we will use one of the horizontal channels of the Budapest Research Reactor (BRR) which provides a significant flux of fast neutrons. A pre-moderator with the mock-up version of the LDM cell on top of it will be placed in the beam. A closed cycle refrigerator system with a cryostat will be used to cool down and produce the liquid para-hydrogen in the LDM cell. The neutron moderation capability of the cell will be measured using a neutron pin-hole camera device developed at the Budapest Neutron Centre (BNC). This technique, combined with time-of-flight analysis, will provide information about the spatial and spectral properties of the moderated neutrons. The measurements will be compared with the results of Monte-Carlo calculations.

The neutron extraction system has to be adapted to the low-dimensional moderator to fully benefit from its potential. The cold source provides a high-intensity cold beam but the thermal spectrum, which could be used in the experiments to extend the neutron momentum range, is also present. The guide system which provides the thermal and cold spectrum is called a bi-spectral extraction system. It is a challenging task to design these systems because the thermal and cold sources are separated spatially, but the two beams should be homogenized in the neutron guide. Simulation of these extraction systems is performed by using analytical calculations and Monte-Carlo (McStas) simulations.

Results

The design of the CMTF (Cold Moderator Test Facility) has begun. The 3 major components of the test station are in the conceptual design phase. 1) The moderator cell: the optimization has shown that a bare-type LDM cell has twice as high a neutron brightness as the volume moderator vessel ($\text{Ø}140 \times 40$ mm) currently in use in BRR. The parameters of the LDM cell will be varied in the following range: radius 10-25 mm, length 90-180 mm. 2) The neutron beam take-off system at the BRR channels number 4 and 5 is being considered and the design of a bunker shielding has started. 3) A camera-obscure principle device was developed and built within the H2020 BrightnESS project for testing the source and beam transport properties of various facilities.

The optimization of the geometry of the moderator cells and the modelling of the expected spectrum from the low dimensional moderators at the PIK reactor is being planned by the project partners and a conceptual design of the PIK cold source is underway. The use of the CMTF at BRR is also meant for the validation of these modellings and it can also be used to compare different solutions for the bi-spectral extraction system.

Remaining work

The CREMLIN+ tasks are part of a larger project, namely the modernization of the BRR cold source, which served 20 years for the cold neutron suite of instruments. In order to replace and improve the capabilities of the moderator and guide assembly the tasks above will contribute to achieve a higher performance for the BRR instrumentation. We are at the beginning of a 4 year project which started in Feb. 2020. Most of the milestones and deliverables listed above are ahead of us and being implemented.

Related publication

- [1] Rosta L, Mezei F: *Liquid-H₂ cold neutron moderator development at the Budapest Neutron Centre*. Workshop of the PIK Reactor Neutron Optics Subcommittee. St.Petersburg, November 16, 2020.

RADONORM: TOWARDS EFFECTIVE RADIATION PROTECTION BASED ON IMPROVED SCIENTIFIC EVIDENCE AND SOCIAL CONSIDERATIONS – FOCUS ON RADON AND NORM

Balázs G. Madas

Objective

The RadoNorm project under EURATOM Horizon 2020 aims at managing risk from radon and NORM exposure situations to assure effective radiation protection based on improved scientific evidence and social considerations. It is designed to initiate and perform research and technical development in support of European Union Member States, Associated Countries and the European Commission in their efforts to implement the European radiation protection Basic Safety Standards. The proposed multidisciplinary and inclusive research project will target all relevant steps of the radiation risk management cycle for radon and NORM exposure situations.

Methods

In order to reduce scientific, technical and societal uncertainties, RadoNorm initiates and performs research and technical developments, integrates education and training in all research and development activities, and disseminates project achievements through targeted actions to the public, stakeholders, and regulators. The activities are structured in eight Work Packages (WPs, Figure 1). EK coordinates the Dosimetry WP (WP3), and contributes to the Effects and Risks (WP4), Education and Training (WP7), and Communication, Dissemination and Exploitation of Results (WP8) work packages. In WP3, EK specifically leads the Tasks entitled Computational microdosimetry supporting the preparation and evaluation of experiments (Task 3.5) and Comparison of the effects of homogeneous and inhomogeneous dose distributions (Task 3.6).

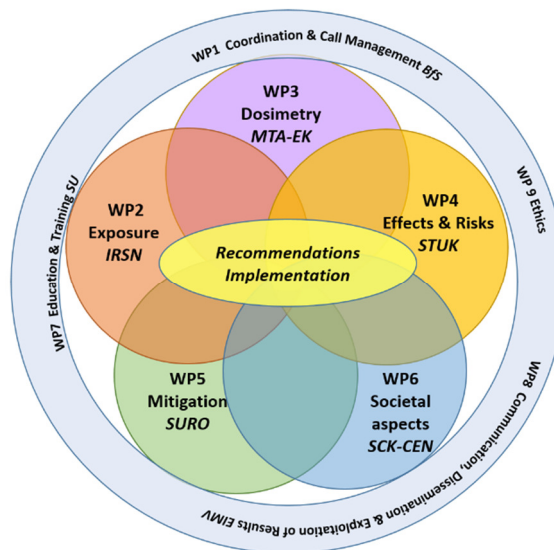


Figure 1: Overall structure of RadoNorm Work Packages.

Results

Besides the overall Kick-Off Meeting and the Kick-Off-Meeting of the Dosimetry Work Package in September, there were various meetings to strengthen the collaboration both within and between work packages. While we faced new challenges due to the COVID-19 pandemic, all activities EK involved in has been launched successfully.

Remaining work

As the project was started in September 2020 and runs until 2025, most of the work remains to be performed. Besides the scientific tasks, EK will also organize the Annual Meeting of RadoNorm in 2021.

PROGRESS ON THE EURAD SCF EUROPEAN JOINT PROGRAMME

Márton Király, Márta Horváth, Richárd Nagy, Nóra Vér, Zoltán Hózer

Objective

The European Joint Programme on Radioactive Waste Management (EURAD) project began in 2019. The Centre for Energy Research Fuel and Reactor Materials Department is involved with the Spent Fuel Characterization (SFC) work package to develop characterisation techniques that will allow us to more fully understand the physiochemical evolution of irradiated spent fuels (pellets and cladding) under normal and credible accident scenarios following reactor discharge, during (wet and dry) interim storage, transport to and emplacement in a geological displacement facility.

Methods

In the five years of the project, two separate experiments are conducted on two zirconium-niobium fuel cladding alloys used in WWER-type NPPs, the E110 and the E110G. The first task is to study the creep of cladding samples near the operating temperature under internal pressure. The samples are either untreated as-received claddings, or heat treated and hydrogenated up to 1000 ppm at 600 °C. The second task is to study the ductility and embrittlement of claddings under various hydrogen treatments using the mandrel method to simulate pellet-cladding mechanical interaction. The upper limit of the hydrogen content of the samples is 3200 ppm.

Results

Only the first creep and mandrel tests have been performed in 2020. Two sets of creep test were completed, in which samples heat treated and hydrogenated at 600°C and were subsequently tested at 400°C in inert atmosphere with 11 MPa inner pressure. The diameter change was registered with laser scanner micrometre at regular intervals. The result confirmed a decrease in creep velocity for the hydrogenated samples compared to the heat treated and as-received samples. This might be caused by the hardening effect of the hydrogen that was first absorbed and then precipitated in the zirconium lattice as zirconium hydrides. The two tested alloys behaved in a similar manner.

The mandrel ductility tests were conducted at room temperature in the apparatus designed in our laboratory. The as-received cladding samples were very ductile, the 8 mm long cladding ring samples reached over 80% increase in inner diameter before failure. As the hydrogen content of the samples increased, so did the maximum measured force, but the diameter increase before failure decreased. The mode of failure changed after 1500 ppm hydrogen, as the ductile necking and large plastic deformation was replaced with ruptures along definite axial cracks. The least ductile samples were those containing around 3000 ppm of hydrogen, as these samples hardly showed plastic deformation and ruptured into several pieces at twice the force as the as-received samples. The gradual decrease in ductility can be seen in Figure 1. The decrease in ductility is almost linear up to 2000 ppm hydrogen, after that a plateau is reached. This is well in line with our ring compression ductility tests where the change in ductile to brittle behaviour was reported at 2000 ppm hydrogen as well.

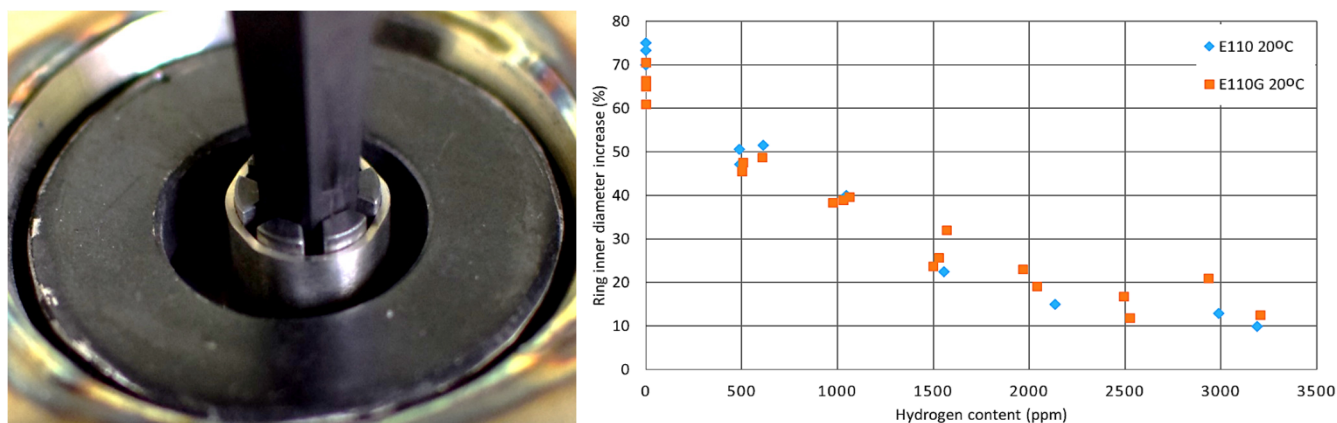


Figure 1: The mandrel test on a zirconium cladding sample (left) and the decrease in ductility (maximum reached inner diameter before failure) with the growing hydrogen content for the two tested cladding types (right).

Remaining work

In the following years additional creep tests will be carried out on different cladding materials, and the mandrel tests will be continued at higher temperatures. The project end with a Deliverable Report towards the European Commission in 2024.

Related publications (If your results were published in any conferences or workshops last year, or will be published this year (abstract accepted for presentation) should also be mentioned here.)

- [1] M. Király, M. Horváth, R. Nagy, N. Vér, Z. Hózer: *Segmented mandrel tests of as-received and hydrogenated WWER fuel cladding tubes*, Nuclear Engineering and Technology, Available online form 26 March 2021

MELODI VIRTUAL WORKSHOP 2020 ON THE EFFECTS OF SPATIAL AND TEMPORAL VARIATION IN DOSE DELIVERY

Balázs G. Madas

Objective

MELODI (Multidisciplinary European Low Dose Initiative) is a European radiation protection research platform with a focus on research on health risks after exposure to low-dose ionizing radiation. EK is one of its members since 2013. A major activity of MELODI is the establishment and updating of a long term (>20 years) Strategic Research Agenda (SRA) for research on low dose risk for radiation protection in Europe.

Methods

In order to support this activity, a series of dedicated Workshops on different topics was launched in 2018. The Workshop in 2020 was focused on the effects of spatial and temporal variation in dose delivery. Originally, it was planned jointly with the International Conference on Individual Monitoring of Ionising Radiation (IM2020) in Budapest between 21st and 23rd April, 2020. Due to the COVID-19 pandemic, however, the IM2020 had to be cancelled, while the MELODI Workshop had to be postponed and made a virtual event on November. There were six sessions in total. One session focused on the effects of dose rate. Three sessions covered the effects of spatial variation in dose delivery, which were organized according to the relevant spatial scales (Figure 1): radiation quality (smallest scale), internal exposures (including the mid-scale), and partial body exposures (largest scale). Besides these, there was an introductory session. The Workshop also included the Ceremony of the MELODI Award given each year to excellent young scientists in low dose research.

Results

Similarly to previous MELODI Workshops, the meeting was highly multidisciplinary with well-known speakers in the fields of radiation epidemiology, radiation biology, dosimetry and modelling. The talks summarized the state of the art in order to set priorities for launching new pertinent research activities related to the effects of dose rate, radiation quality, partial body exposures, and internal exposures. After the sessions, the chairs initiated and lead the discussions, which had to be continued in separate meetings for different topics in 2021. Although, the excitement and liveliness of a face-to-face meeting were missing, the Workshop reached its goal by initiating preparation of manuscripts presenting the state of the art in these fields as well as making suggestions on how to organize future studies.



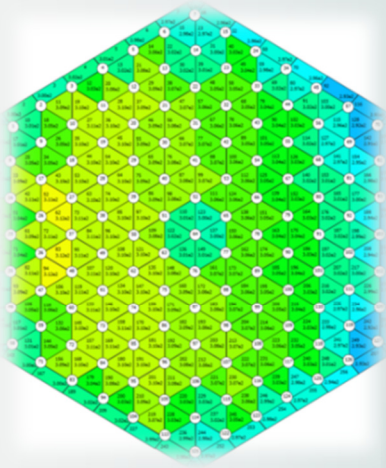
Figure 1: Relevant scales of spatial variation in dose delivery: partial body exposures (upper row), “partial organ exposures” (middle row), and “partial cell exposures”, i.e. radiation quality (bottom row). The first and the last one are considered in radiation protection by tissue weighting factors and radiation weighting factors, respectively.

Remaining work

The manuscripts have to be prepared to be published as a theme issue of Radiation and Environmental Biophysics. EK is responsible for the coordination of the review article on internal emitters, and for the preparation of an introductory piece of editorial of the theme issue.



II. RESEARCH AND DEVELOPMENT RELATED TO NUCLEAR POWER PLANTS



ACTIVITIES OF EK AS MAIN CONSULTANT OF PAKS NPP

Zoltán Hózer, Katalin Kulacsy, Tamás Pázmándi

Objective

EK, together with NUBIKI (Nuclear Safety Research Institute), has been the main consultant of Paks Nuclear Power Plant (NPP) for many years. The main consultant supports the NPP in solving safety-related technical issues and helping with strategic planning. The work is done by the most experienced and highly qualified members of the staff on the basis of yearly work plans. In 2020 EK undertook the following separate tasks, done by different (groups of) experts:

- development of a limitation in the local linear heat rate change that would assure the safety of the fuel rods' cladding by keeping the cladding hoop stress under the design limit;
- re-evaluation of the primary coolant activities used for dose and release calculations considering the new fuel types;
- analysis of the radiation hardness of the SODAR meteorological measurement system;
- review of the changes proposed by the NPP expert for treatment of the iodine spikes following power changes in operational limit document.

Methods

Each task required different method, which can be summarized as follows.

A new methodology was established in which 10 cm-long fictive rodlets, each representing one axial node of a VVER-440 fuel rod, were subjected to a constant-power irradiation followed by a power increase in simulations performed with the steady-state fuel behaviour code FURROM-2.1.1. The linear heat rates during irradiation and after the ramp, the final burn-up, the duration of the ramp and the axial position (through cladding temperature and the ratio of the local burnup to the average) were varied within the possible limits. The linear heat rate changes and burnups were recorded when the hoop stress exceeded the design limit.

A consistent model was introduced for the simulation of defective fuel rods and for the estimation of sources from tramp uranium in primary coolant using isotope inventory data of the new "slim" fuel type. The simulation of water purification system was updated with recently precised filter efficiencies for the minimum and maximum purification flowrates. The water chemistry measurements of the four units of Paks NPP were evaluated for several years.

In the last couple of years, radiological consequence assessments have been conducted for receptor points outside the building of the NPP in case of beyond design basis accidents. Dose consequences were determined also for the location of the SODAR measurement system. Based on the literature and expert judgement, effect of the radiation on the performance of the SODAR system was estimated, feasibility of methods for reduction of the radiation field was investigated.

The iodine spiking data from literature and from NPP measurements were reviewed paying special attention to power change ratios.

Results

The individual results of the tasks were as follows.

A burnup-dependent linear heat rate change limit was established, which ensures that the design hoop stress limit is not violated. This limit is significantly lower than that given by the fuel vendor for the previous types of fuel.

The typical values of activity concentrations for nominal power operation and transients were determined. Beyond the primary water activity concentrations, the coolant activities in the refuelling pool and in the spent fuel storage pool were also estimated.

Based on the assessments conducted in the previous years, about 15.3 Sv external exposure from the radioactive plume and the ground deposition can be estimated for the first week in case of the largest possible release scenario. Based on scientific publications it could be confirmed that damage of electronic devices is not expected below 100...200 Gy. Consequently, it was found that even in case of the largest radioactive release there is not expected any adverse effect on the functioning of the SODAR measurement system. Thus, it is not necessary to introduce protective measures for reduction of radiation field, but recommendations were given for radiation monitoring and the application of temporary shielding to improve the radiation hardness of the system.

It was concluded that the new approach for the treatment of the iodine spikes following power changes will facilitate the decision making on the need of fuel assembly sipping during refuelling periods. The limitation of the evaluations to 20% power change is supported by measured data.

Remaining work

The 2020 tasks have been completed.

Related publications

- [1] K. Kulacsy: *Investigation of the dual PCMI limit*, EK TFO-2020-751-04-01-M1, in Hungarian (2020)
- [2] Z. Hózer, B. Somfai, Zs. Kerner, T. Pázmándi: *Re-evaluation of the activities in the primary circuit used for dose and release calculations*, EK-TFO-2020-751-5-1-M1, in Hungarian (2020)
- [3] T. Pázmándi: *Justification of the radiation hardness of the SODAR meteorological measurement system*, EK-SZV-2020-751-08-01-M0, in Hungarian (2020)
- [4] Z. Hózer: *Treatment of the iodine spikes following power changes*, EK-TFO-2020-751-9-1-M0, in Hungarian (2020)

WALL THICKNESS MEASUREMENT OF E110 SLIM CLADDING TUBE

Richárd Nagy, Hózer Zoltán

Objective

Numerous tests were carried out on E110 and E110G (Zr1%Nb) alloys in the last few years, in order to reveal physical parameters of ballooning and burst. Pure and pre-test-treated samples were applied in these measurements such as "as-received", oxidized and hydrogenated samples. Now, we aimed to measure E110 slim alloy samples by the same methods. One of the most important initial parameters needed is the wall thickness of the „as-received” sample.

Methods

Video measurement was carried out observing the kinetics of the bulge formation prior to the crack opening. Crack opening and propagation was recorded by 100.000 frames/s optical fast camera. Ballooning and burst tests of E110 and E110G tubes presented a hot spot appearance at the position where crack opening would be occurred. This hot spot appearance was proofed and the magnitude of temperature-rise was determined by infrared camera and an article was published [1] this year.

Continuation of the ballooning and burst measurement series, "as-received" E110 slim tubes were prepared for next ballooning and burst tests on 700, 800 and 950 °C. Our purpose was to determine the wall thickness of all tubes prior to the tests.

A mechanical micrometre (M105) was used in this measurement. 85 mm long samples were cut by lathe. 11 individual data were measured 5 mm deep in the tube. The average of these data has provided wall thickness in perpendicular directions. Micrometre was calibrated by Mitutoyo laser profilometer. Calibration polynomic was determined for our mechanical micrometre.

Calibration

The mechanical micrometre (0-25 mm/0,01 mm) was calibrated by Mitutoyo LSM-503S laser micrometre. This instrument has two standard Mitutoyo Dimensions of Gauge (30.0050 mm and 0.9980 mm). The diameters of two random copper electric wires (1.595167 mm and 2.983511 mm) were determined by laser micrometre using the average of 200 measurements (STDERR 0,257%) and by mechanical micrometre too. The experienced calibration polynomic was measured as $X = 1.000288 x + 0.001240$, where X is the calibrated value, x is the measured diameter.

Results

1. table: Specifications of the fuel cladding tubes from the manufacturers.

Alloy	Wall thickness	Outer diameter	References
E110	0.685 mm ^{+0.1 mm} _{-0.05 mm}	9.1 mm ^{+0.1 mm} _{-0.05 mm}	[2]
E110 slim	0.571 mm ^{+0.003 mm} _{-0.0003 mm}	8.90 mm ^{+0.045 mm} _{-0.045 mm}	[3]

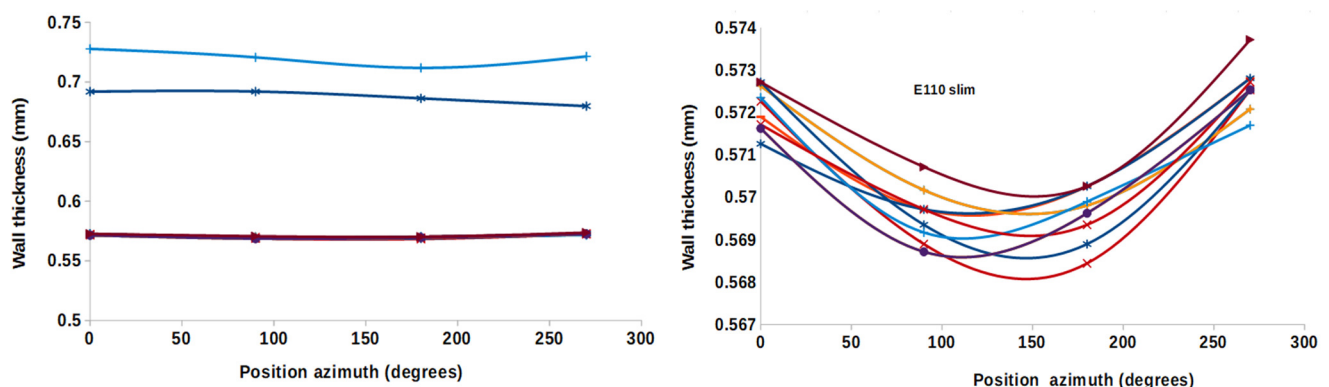


Figure 1: Left figure: the wall thickness of Zr-4 (top), E110 (middle) and E110 slim (bottom) samples.

Right figure: the ovality of E110 slim cladding tube.

In Figure 1 the wall thickness of Zr-4, E110 and E110 slim, and also the ovality of the E110 slim are shown with respect to position along the circumference. The top curve represents the wall thickness of E110, at the bottom wall thickness of E110 slim is shown. According to the factory specification, the wall thickness of the E110 slim must be between 0.568-0.574 mm. In our measurement the average wall thickness of this tube is 0.5714 mm \pm 0.0004 mm [4]. As it is seen in Figure 1 left side, Zr-4

and E110 samples have a little asymmetry in their wall thickness. Similarly, a little ovality has been revealed in the wall thickness of E110 slim within our accuracy. This uncertainty is much less than the ovality of Zr-4 or E110 samples.

Remaining work

In the next year, several pre-test-treated E110 slim (oxidized, hydrogen filled) samples are planned to test in the ballooning and burst facility.

Related publications

- [1] R. Nagy, M. Király, P. Petrik, Z. Hózer: *Infrared observation of ballooning and burst of nuclear fuel cladding tubes*, NED, **371**, January 2021, 110942 (2020)
- [2] E. Perez-Feró, Cs. Győri, L. Matus, L. Vasáros, Z. Hózer, P. Windberg, L. Maróti, M. Horváth, I. Nagy, A. Pintér-Csordás, T. Novotny: *Experimental Database of E110 Claddings Under Accident Conditions*, AEKI-FRL-2007-123-01/01, Report, Budapest, November, 2007
- [3] Э110о.ч. *Quality Certificate*, TVEL, №317-19, (2020)
- [4] R. Nagy, *Wall thickness measurements of E110 and E110 slim fuel cladding tube*, EK-FRL-2020-130-1-1-M0, in Hungarian (2020)

EXPERIMENTS FOR FUEL ROD BEHAVIOUR MODELLING

Eszter Barsy, Zoltán Hózer

Objective

This PhD research is aimed to model the azimuthal distribution of oxidation of the Zr-1%Nb cladding. It is done by a standalone code (numerical model) which simulates the oxidation of a ruptured cladding in steam [1]. This kind of modelling is crucial for supporting the planned redefinition of acceptance criteria.

In this phase of the project, the objective was to assist the calculations with experimental results. The experimental design matrix (Table 1.) was designed in a way that the changes in the oxygen concentration of the cladding over time on high temperatures can be observed.

Methods

Seven 8 mm ring samples were chosen for the experiments. One was an E110 and the others were E110G from the 2015 batch. The setup consisted of a steam generator, an electric resistance furnace and a quench bowl. The temperature was set to 1000 °C and the steam flow was 2-4 mg/cm²/s (with 12 v/v % Ar). The samples were inserted one-by-one into the furnace in a quartz sample holder for a specific oxidation length of time. After the high-temperature steam oxidation the samples were either slowly cooled in room temperature or were dropped into a dish of cold water (quenching). The mass of the samples was measured before and after the oxidation. These oxidised samples will be used in heat treatment experiments (in vacuum) to examine the changes in oxygen distribution due to high temperatures.

Results

The experimental results on oxidation (Figure 1.) are consistent with previous results [2], the extent of cladding oxidation in the case of E110G is smaller as shown by the ECR% (equivalent cladding reacted). These samples are redundant because they will differ only by the length of time of the heat treatment (Table 1. Column 8-9).

Sample	Material	Initial mass (g) $\pm 10^{-5}$ g	Ox. mass (g) $\pm 10^{-5}$ g	Mass gain (g) $\pm 10^{-5}$ g	ECR%	Cooling	Heat treatment T (°C)	Heat treatment t (s)
ESZT-00	E110	0.94263	0.99272	0.05009	15.15	normal	1000	3600
ESZT-01	E110G	0.92428	0.94730	0.02302	7.10	normal	1000	3600
ESZT-02	E110G	0.93489	0.95869	0.02380	7.26	quench	1000	3600
ESZT-03	E110G	0.92852	0.95209	0.02357	7.24	quench	-	0
ESZT-04	E110G	0.93365	0.95712	0.02347	7.17	normal	-	0
ESZT-05	E110G	0.93260	0.95628	0.02368	7.24	normal	1000	1800
ESZT-06	E110G	0.92399	0.94763	0.02364	7.29	normal	1000	10800

Table 1: Experimental design matrix

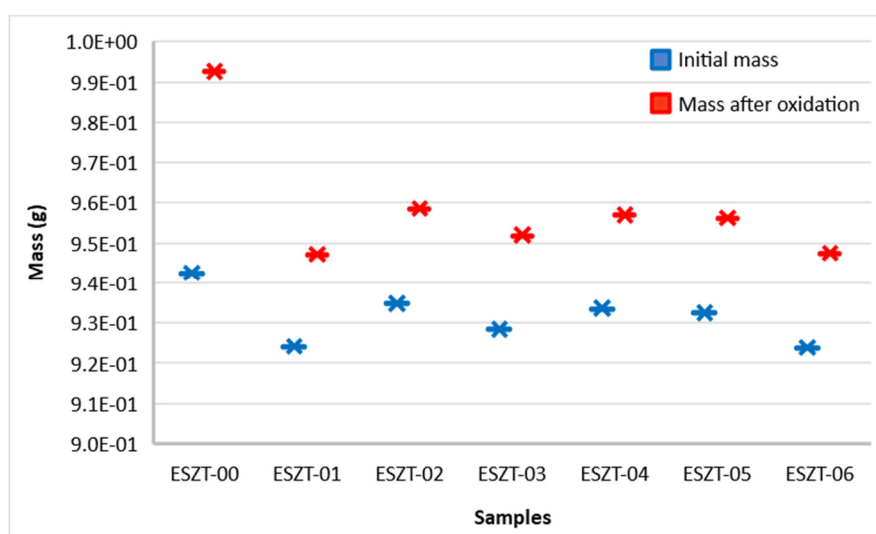


Figure 1: Mass gain of samples

Remaining work

The project will be continued in 2021. The aforementioned heat treatment experiments will be conducted in 2021. The experimental results will be used for the development of the numerical model. The model will be extended axially too, so it will be able to give results on full length rods.

References

- [1] E. Barsy, P. Szabó, K. Kulacsy, Z. Hózer: *The non-uniform high-temperature oxidation of Zr-1%Nb cladding - A numerical model*, Progress in Nuclear Energy, **133**, 103613 (2021) ISSN 0149-1970
- [2] E. Kozsda-Barsy, K. Kulacsy, Z. Hózer, M. Horváth, Z. Kis, B. Maróti, I. Nagy, R. Nagy, T. Novotny, E. Perez-Feró, A. Pintér-Csordás, L. Szentmiklósi: *Post-test examinations on Zr-1%Nb claddings after ballooning and burst, high-temperature oxidation and secondary hydriding*, Journal of Nuclear Materials **508**, 423-433 (2018)

IDENTIFICATION AND HANDLING OF DEFECTIVE FUEL RODS

Zoltán Hózer, Imre Szalóki*, Péter Szabó, Gábor Radócz*, Anita Gerényi*

*BME NTI

Objective

It was requested by the Paks NPP that the experience of identification and handling of defective fuel rods was summarised in a handbook type report, including basic theoretical considerations and typical operational data on the related phenomena.

Methods

The experts of EK and BME NTI were involved in the analyses of defective fuel rods behaviour for the Paks NPP. Large number of technical reports and publications were produced during the last decades and those documents served as the basis for the comprehensive report.

Results

Three chapters of the handbook were produced in 2020 with the following main content:

1. Radioactive isotopes in the coolant of primary circuit
 - 1.1. Formation of fission product
 - 1.2. Formation of transuranic elements
 - 1.3. Activation and corrosion products
 - 1.4. Decay of radioactive nuclides
2. Fission product release from defective fuel rods
 - 2.1. Mechanism of activity release
 - 2.2. Main characteristics of fuel rods
 - 2.3. Activity release during steady state conditions
 - 2.4. Activity release during transients
3. Monitoring fuel rod integrity
 - 3.1. Coolant activity concentration measurements in the primary circuit
 - 3.2. Activity concentration measurements during transients

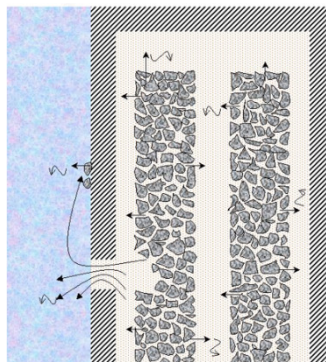


Figure 1: General scheme of activity release from defective fuel rod

Remaining work

Two chapters of the handbook will be produced in 2021:

4. Estimation of the number of leaking fuel rods and other characteristics of leakers
5. Selection of fuel assemblies with leaking fuel rods using sipping tools

Related publication

- [1] Z. Hózer, I. Szalóki, P. Szabó, G. Radócz, A. Gerényi: *Review of Experience on Identification and Handling of Defective Fuel Rods*, EK-FRL-2020-701-1-1-M0, in Hungarian (2020)

DEVELOPMENT OF RECONSTITUTION TECHNOLOGY OF IRRADIATED SPECIMENS

*Ildikó Szenthe, Ferenc Gillemot, Márta Horváth,
Dávid Cinger*

Objective

Development of laser welding reconstitution technology for irradiated specimens and process validation has been carried out for irradiated Charpy inserts with 5x10 mm cross section. Validation of the technology had two main objectives: to prove that the welds do not suffer plastic deformation or failure during the standard testing of the reconstituted specimens, and the heat affected zone of the welding is narrow enough to remain at least 10 mm wide unaffected middle zone for testing in accordance with the requirement of the ASTM-E1253 standard.

Methods

Remote controlled laser welding technology has been developed for reconstitution of half thickness Charpy size fracture toughness specimens from 18 mm length irradiated austenitic steel inserts. The welds are only 2 mm wide with a very narrow heat affected zone. The new technology required verification tests, proving that the reconstituted specimens fully replace the standard ones. The following tests have been used: hardness testing, slow bending test on tensile machine, tensile tests, fracture toughness test, and temperature measurement near the welds (2 and 3 mm away from the welding).

Results

Hardness tests performed before and after welding proved that the hardness of the weld and the heat affected zone only slightly differ from the unirradiated base material. Bending tests of the reconstituted specimens verified that the strength of the welds is satisfying the standard requirements, even more since the specimens were loaded without notch in the middle section (see Figure 1. left side). Standard reconstituted fracture toughness specimens have also been tested to prove that the welds and the heat affected zone don't absorb deformation energy during the test. Thermocouple measurement 2 and 3 mm away from the laser welding ensured that the middle zone of the specimens wasn't overheated during welding.



Figure 1: Results of the bending and fracture toughness tests

Remaining work

Development of laser welding reconstitution technology for irradiated specimens, process validation for irradiated Charpy inserts with other dimensions.

GAMMA-RAY MEASUREMENT AND ANALYSIS OF SPENT FUEL ASSEMBLIES OF PAKS NPP (2020)

Péter Kirchknopf, István Almási, Péter Völgyesi

Objective

For safety reasons, the fuel manufacturer has to set a maximum burnup limit for its assemblies. To guarantee operational safety, the NPP staff decreases this limit by a so-called 'engineering factor'. This factor accounts for the uncertainty of the NPP's reactor physics calculations. The long-term goal of this project is to prove that the uncertainty of the burnup calculated by the NPP is well within the scope of the currently used engineering factor. This would allow the staff to increase the burnup limit, thus achieving better fuel utilization while maintaining safety.

Methods

This year we performed in-situ high-resolution gamma-ray spectrometry (HRGS) measurements on nine selected spent fuel assemblies, which included assemblies with 4.7% initial enrichment. All assemblies were measured from three sides that were rotated by +/-120° relative to each other. The spectra were collected with an Ortec GEM10P4-70 coaxial type high-purity germanium (HPGe) detector. We measured the $^{134}\text{Cs}/^{137}\text{Cs}$ and $^{154}\text{Eu}/^{137}\text{Cs}$ fission product activity ratios, which correlate with the burnup value. After calculating the net peak areas with the Ortec GammaVision software, we used the intrinsic efficiency calibration method to obtain the mentioned activity ratios. We calculated the values for the end-of-operation dates using the known cooling times of the assemblies.

Results

The results (Table 1) were sent to the NPP, so that the reactor physicists can compare them with their own calculations. Axial scanning results (Fig. 1) show the similarity of $^{134}\text{Cs}/^{137}\text{Cs}$ and $^{154}\text{Eu}/^{137}\text{Cs}$ profiles along the height of an assembly. With the analysis done, we have completed our objectives. The results will be presented at a conference later this year [1].

Table 1: Measured activity ratios calculated for the end-of-operation dates. Each measurement lasted for 10,000 s live time. The 2σ relative uncertainties for $^{134}\text{Cs}/^{137}\text{Cs}$ and $^{154}\text{Eu}/^{137}\text{Cs}$ are 0.7% and 2.0%, respectively.

Assembly ID	Initial Enrichment [%]	Declared Burnup [GWd/MTU]	$^{134}\text{Cs}/^{137}\text{Cs}$ activity ratio			$^{154}\text{Eu}/^{137}\text{Cs}$ activity ratio		
			0°side	-120°side	+120°side	0°side	-120°side	+120°side
470_1	4.7	48.59	2.008	2.025	1.986	0.0723	0.0733	0.0712
470_2	4.7	48.59	1.992	1.982	1.992	0.0713	0.0713	0.0715
470_3	4.7	48.59	2.001	2.011	2.001	0.0690	0.0727	0.0750
420_1	4.2	50.14	2.044	2.045	2.072	0.0718	0.0725	0.0742
420_2	4.2	50.14	2.034	2.070	2.065	0.0727	0.0728	0.0744
420_3	4.2	50.14	2.040	2.068	2.055	0.0710	0.0743	0.0721
382_1	3.82	47.76	2.010	2.025	2.039	0.0707	0.0716	0.0709
382_2	3.82	47.76	2.017	2.020	2.034	0.0703	0.0708	0.0730
382_3	3.82	47.76	2.017	2.034	2.032	0.0698	0.0709	0.0710

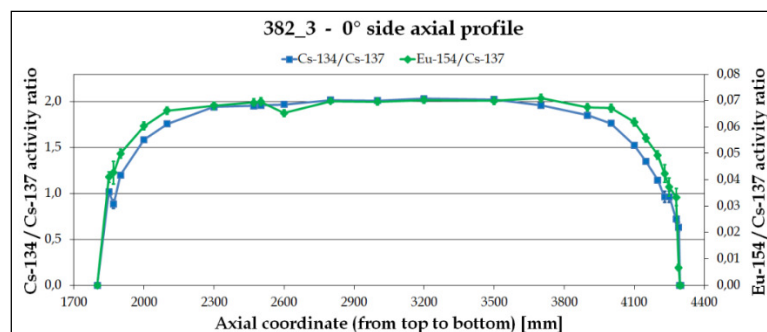


Figure 1: Axial profile measurement results for assembly 382_3 from the 0° side. Each measurement lasted for about 600 s live time.

Remaining work

The work for the year 2020 has been completed. As of 22/06/2021, a new contract for this project for 2021 is in preparation.

Related publication

- [1] P. Kirchknopf, I. Almási, G. Radócz, I. Nemes, I. Szalóki, P. Völgyesi: *Safeguards investigations based on gamma spectrometry to determine the activity ratio of fission products in spent fuel assemblies of VVER-440 Nuclear Reactor*, ANIMMA 7th International Conference (2021), accepted abstract

ANALYSIS OF DISSOLVED AND PARTICULATE CORROSION PRODUCTS FOUND IN THE PRIMARY COOLANT CIRCUIT OF THE PAKS NPP

Zsolt Kerner, Éva Kovács-Széles

Objective

Between 2016 and 2020, corrosion particles and dissolved corrosion products found in the primary cooling systems of the reactors in the Paks Nuclear Power Plant (NPP) were analysed during two shut down periods in every year to detect the origin or source of corrosion, to describe the transfer process of corrosion products and to detect the changes.

Methods

25-40 water samples were taken in each period. All were filtered on a 0.4 µm pore size membrane. Particles were characterized by scanning electron microscopy (SEM). The concentrations of corrosion products (Fe, Co, Ni, Cr, Zr, Ag) in the dissolved and in the particulate fraction were measured by inductively coupled plasma mass spectrometry (ICP-MS). Silver was measured separately after chemical enrichment using ion-exchange chromatography in the first three years. The activity of most of the corrosion products was determined by gamma-spectrometry, but the ⁶³Ni and ⁵⁵Fe contents were done by the liquid scintillation technique after radiochemical separation using dimethylglyoxime and methyl isobutyl ketone. The specific activity and the residence time of the particles in the reactor zone was calculated.

Results

In normal operation, there is hardly any corrosion product in the primary cooling water. During shutdown and start-up periods, the main components of steel (Fe, Ni, Cr, and Ti) appear, accompanied by oxygen. Zirconium can also be observed periodically. Most characterized particles can be classified into one of the following types:

- iron rich particles: These often contain Cr and Ni, and sometimes Zr, Mo and Ag, and the typical size is a few micrometres.
- chromium and iron rich particles: Typical size is 10-120 µm.
- zirconium rich particles, mostly as ZrO₂: Typical size is 1-10 µm.
- aluminosilicate and magnesium silicate particles: Typical size is <10-100 µm, rounded in shape
- mineral particles containing Ca, Na, Cl, S
- mixed particles: These are rich in several elements at once, for example zirconium and iron or iron and chromium are common.

During the shutdown periods usually the ⁵⁹Fe, ⁵¹Cr, ⁵⁵Fe and ⁹⁵Zr have the highest activity in the particle fraction, and ⁵⁴Mn, ⁵⁸Co and ⁶⁰Co in the dissolved fraction. Concentrations in the particulate fraction decrease in the Fe > Cr, Ni > Mn > Co, Ag order, and in Ni > Mn, Fe > Cr > Ag, Co order in the dissolved fraction. Fe became the main dissolved corrosion product during the start-up period only. ⁶³Ni is mainly dissolved during the shutdown, but it is equally present in dissolved and particle forms during the start-up. The total activity of the dissolved fraction is higher during the shutdown and lower during the start-up compared with the particulate fraction. Co and Ag can be found in both fractions. The dissolved ^{110m}Ag activity is usually high while the primary circuit is open.

All corrosion products show concentration and activity peaks during the shutdown and restart periods, but the time and the extent is different. Collecting this data can be useful for understanding the chemical changes and transfer properties of corrosion products during transient states.

^{110m}Ag/Ag and ⁶⁰Co/Co have the highest specific activity (10⁵-10⁶ Bq/µg) followed by ⁵⁴Mn/Fe, ⁵¹Cr/Cr and ⁵⁸Co/Ni and finally ⁵⁹Fe/Fe (10-100 Bq/µg).

The effective residence time of the corrosion products in the reactor zone can be calculated from the specific activity. The residence time determined from the specific activity of short-lived isotopes follows the order of the half-lives. Residence times of long-lived isotopes can be longer than a reactor campaign e.g. the long-lived ⁶³Ni isotope (half-life: 100 years). The calculated values of residence time in case of ⁶³Ni isotope is 3-4 years for the block No. 1 and usually around 1 year for the block No. 2 and 3 and <100 days for No. 4. Block No. 4 is the youngest one and it has the best corrosion condition. Its steam generators have not undergone the chemical decontamination of 20 years ago, unlike the others. The difference between the blocks occurs in all investigated isotope cases. There has been no systematic change in the last 5 years.

Remaining work

This activity determination project has been extended for the next five years.

Related publication

- [1] É. Kovács-Széles, Zs. Kerner and N. Vajda: *Analysis of corrosion particles originated from primary circuit of block No. 1-4 of NPP*, Final research report for MVM PAKS NPP, EK-SBL-2020-766-02-M0, in Hungarian (2020)

RENEWING THE REFUELLING NEUTRON MONITORING AND REACTIVITY MEASUREMENT SYSTEMS AT PAKS NPP

*G. Házi, S. Kiss, S. Lipcsei, J. Páles, Z. Dezsó, Cs. Horváth, G. Makai,
T. Parkó, I. Pócs, Z. Kálya*

Objective

The Refuelling Neutron Monitoring System and the Reactivity Measurement System for start-up measurements at Paks NPP were both aged, the development of a new combined system fulfilling both functionalities had therefore been started in 2014. The most important requirements of the new system were:

- Measurements during both refuelling and start-up,
- Redundant configuration,
- Handles the whole neutron flux range in the reactor core,
- Based on fixed detectors,
- Based on the already installed cabling,
- Adds new functionalities,
- Based on 6 detectors instead of the original 9 detectors of the old systems without impairing the original functionalities.

Methods

ANEREM (Hungarian acronym) is the name of the newly developed combined system carrying out both refuelling neutron monitoring and start-up measurements. Since the operating periods of the refuelling and the start-up measurements do not overlap, the combination of the two systems does not deteriorate the nuclear and operational safety. In order to increase its reliability, the new system contains six autonomous measurement chains of the following main properties:

- Operates continuously during the fuel cycles including refuelling,
- Handles the full neutron flux range from 1 cps to 10^{10} cps,
- Provides simpler operation and lower probability of failures by fixed detector setting,
- Covers the remaining lifetime (over 20 years) of the reactors by using CFUL08 fission chamber,
- Utilizes extant cabling. Connections between the devices placed near the reactor tank and near the Main Control Room (MCR) are established via extant cabling,
- Implements digital communication. The large distance is handled according to the industrial RS-422A standard,
- Accomplishes autonomous measurement. The chains measure the detector signal autonomously without any external control,
- Each measurement chain provides two isolated outputs, in order to serve two redundant subsystems.

ANEREM is built of two redundant signal processing subsystems achieving two main functionalities:

Refuelling Neutron Monitoring operation mode

Based on the monitored neutron flux the system continuously checks for limit violations and automatically generates alarms and status information, i.e.

- system active,
- warning level,
- alarm level,
- alarm,
- out of service

to the operators of the MCR, the Emergency Control Room and the Refuelling Machine.

Reactivity Measurement operation mode

The system supports the reactor physics analysis of the core by determining reactor physics parameters during the start-up of the reactor. It helps to carry out

- reaching the first criticality,
- control rod functionality test,
- Moderator Temperature Coefficient (MTC) measurement,
- control rod drop test,
- reaching criticality with control rods,
- control rod differential/integral reactivity worth measurement.

Results

The first installation of the new system was achieved in two phases in order to guarantee the highest safety and availability: only one of the two redundant subsystems was installed replacing one redundant half of the old refuelling system and this

configuration worked for a whole fuel cycle. Factory acceptance tests (FAT) of ANEREM (see Fig. 1 and 2) for Paks NPP were successfully accomplished at Unit 3 in April 2018. The first installation was postponed to Unit 4 due to organizational reasons, therefore the FAT were repeated in October with Unit 4 configuration. The first system was installed at Unit 4 in February 2019 and the last was installed at Unit 2 in August 2020. The project finished with the installation of the full configuration at Unit 4 in September 2020.

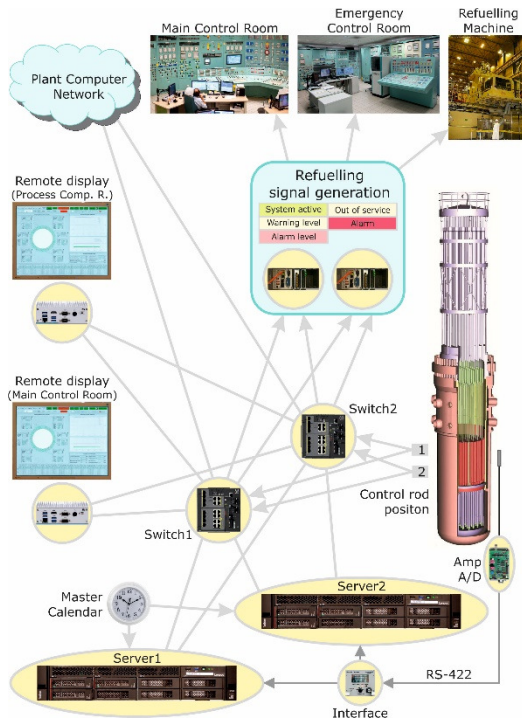


Figure 1: Architecture of the ANEREM system



Figure 2: Cabinet of ANEREM components near to the MCR

Related publications

- [1] S. Kiss, S. Lipcsei, G. Házi, Z. Dezső, T. Parkó, I. Pósz, M. Ignits, L. Hományi: *Renewing the refuelling neutron monitoring and reactivity measurement systems at Paks NPP*, *Kerntechnik* **83:4**, 354-364 (2018)
- [2] S. Kiss, S. Lipcsei, G. Házi, Z. Dezső, T. Parkó, I. Pósz, M. Ignits, L. Hományi: *Developing a New Neutron and Reactivity Monitoring System for Paks NPP*, 25th International Conference Energy for New Europe, 5-8 September 2016, Portorož, Slovenia, Nuclear Society of Slovenia, pp. 402.1-402.10 (2016)

STUDSVIK CLADDING INTEGRITY PROJECT

Barbara Somfai, Zoltán Hózer

Objective

The Studsvik Cladding Integrity Project (SCIP) is an OECD/NEA supported international program operated by Studsvik, launched in 2004 and – with the 4th stage – prolonged to 2024. SCIP has focused on studies of the behaviour of nuclear cladding materials. The Centre for Energy Research joined the project in 2014 with the financial support of Paks Nuclear Power Plant. As we gained a lot of useful knowledge by participating in the SCIP III we joined the SCIP IV project which will last from 2019 to 2024.

Methods and the scope of the experimental work

The main areas of SCIP IV are treated in four tasks. Task 1 is focused on fuel at back-end conditions. Creep and hydride reorientation under dry storage conditions, fuel in transport or handling accidents and treatment of failed fuel are investigated. The possible effects due to fuel-cladding bonding in high burnup fuel rods are examined. The conditions and mechanism for hydride reorientation in irradiated cladding material will be determined, in order to predict both the hydride reorientation and ductile-to-brittle transition behaviour of the material, based on the understanding of these parameters. The strength of weak or slightly damaged fuel rods under transportation and handling operations will be investigated. The aims are

- to verify that weak or slightly damaged rods will not degrade or jeopardise cask safety functions during transportation and storage,
- to generate valuable experimental data on the mechanical response of irradiated fuel rods under transport accident conditions,
- to characterise the particulates which might be released from high burnup fuel rods due to impact events,
- to generate experimental data to support safe encapsulation and dry storage of failed fuel rods.

Various characterisation methods will be applied to assess the form and extent of residual water before and after typical vacuum drying procedure.

In Task 2, LOCA issues, in particular fuel fragmentation, relocation and release are studied, with special focus on non-standard fuel, pressure and pre-transient microstructure. The main tasks are

- to investigate how sub-grain structure impacts fragmentation behaviour,
- to carry out microscopy examinations on fuels with high burnup that fragment to a large extent in LOCA like conditions,
- to study high burnup fuel that appears resistant to fine fragmentation,
- to determine fine fragmentation burnup threshold for large grain, doped and additive fuel, for MOX fuel and for gadolinia fuel and compare them to the performance of standard fuel,
- to investigate relations between burnup and temperature dependence of fragmentation and pretest fuel microstructure,
- to confirm the influence of cladding strain on fuel fragmentation, relocation and dispersal for nonstandard fuel types,
- to study the degree of fragmentation that might depend on the rod pressure and the rate of depressurisation, causing a fragmentation shockwave that attenuates in the fuel column away from the burst opening in a LOCA transient,
- to evaluate transient fission gas release and axial gas communication inside the fuel rods as function of burnup and as function of temperature.

LOCA transients in spent fuel pool are investigated as well in order to improve knowledge on cladding corrosion and fuel rod performance during and after transients in air-steam mixtures.

In task 3, the microstructure and microchemistry influencing pellet cladding interaction crack propagation is studied by means of advanced microscopy.

In task 4, modelling support to the experiment planning and to the data analysis is given by the participants and will stimulate understanding of the mechanisms important for transient fuel performance.

There will be progress reports issued for tasks 1-3 once a year.

Results

The project is still at early stage where we are discussing and planning the experiments. We do participate in the LOCA working group where we investigate the possible tests and suggest the test conditions and parameters for the program group.

Remaining work

The project will end in 2024, much of the work is still ahead of us.

Related publication

- [1] B. Somfai: *Summary report on the results of the SCIP IV project in 2020*, EK-FRL-2020-962-1-1-M0, in Hungarian (2020)

REVIEW OF SGTR AND LOCA AVAILABLE EXPERIMENTAL DATA FOR THE R2CA PROJECT

Zoltán Hózer, Péter Szabó

Objective

The review of experimental data on reactor incidents and accidents were needed to provide the basis for code validation and development activities in the framework of the EU Reduction of Radiological Consequences of design basis and extension Accidents (R2CA) project and to serve as background of current knowledge on related phenomena.

Methods

The available experimental databases were reviewed focusing on

- fuel failure,
- fission products release from the fuel rods and
- activity transport up to the environment during Loss of Coolant Accident (LOCA) and Steam Generator Tube Rupture (SGTR) events.

This review also covered available information obtained from the monitoring of normal operation and transients in NPPs and from some accidental situations.

The report included the description of each test series in individual chapters. Short summaries were produced to identify the test objectives, introduce the tested materials, test facility, measured parameters and Post Irradiation Examination (PIE) data, and present the general conclusions drawn after the completion of the tests. The main characteristics of test series were summarized in form of matrices.

The task carrying out this international review was coordinated by EK experts.

Results

The present review of experimental databases covered a 43 test series, which characterize the phenomena taking place during LOCA and SGTR events in PWRs and VVERs. The project partners indicated that at least 18 test series were already used earlier for code validation purposes and there are intentions to use at least 21 tests series for further validation activities within the R2CA project. The experimental data can be used for the support R2CA tasks in several areas including model development and validation activities:

- burst tests data can be used for the improvement and validation of transient fuel behaviour codes,
- integral LOCA tests allow us to carry out further validation of fuel behaviour codes,
- fission product test data are crucial for the testing of severe accident codes,
- fission product transport experiments provide unique possibilities for severe accident code validation,
- iodine spiking data can be used to develop and improve activity release models which can be applied in SGTR analyses,
- hydrogen uptake data are useful for the simulation of secondary degradation in defective fuel rods,
- learnings from thermal hydraulic experiments can support the optimization of accident management strategies.

The experimental data from 12 test series were included into the database. Data for other 24 test series are accessible for some of the project partners, but cannot be shared within the project with all partners for different reasons. Some of the experimental data are stored in international databases (e.g. International Fuel Performance Experiments (IFPE) of OECD NEA, OECD projects, IAEA FUEL Modelling at EXTENDED burnup (FUMEX)), while some others are stored by the owners of data in private databases. The data of some old test series or experiments carried out outside of western and central Europe (Russia, USA) are not accessible for the project, but are listed in the database as significant contributions to our knowledge on the SGTR and LOCA related phenomena.

The users of the database can find more information on the given test series in the references, which are grouped into special directories. In some cases, the data available for the test series inside of R2CA project are also given in these directories. The data files are available in their original format as provided by the data owner. It was intended to include all available information on the related experiments and NPP measurements, even if the data are not available for the project.

Remaining work

The planned work was completed.

Related publication

- [1] Z. Hózer (EK), A. Kecek (NRI Rez), K. Dieschbourg (IRSN), T. Taurines (IRSN), M. Adorni (Bel V), N. Müllner (BOKU), M. Massone (ENEA), M. Jobst (HZDR), A. Arkoma (VTT), P. Szabó (EK), R. Lishchuk (ARB), S. Sholomitsky (ARB), M. Schöppner (BOKU), C. Leclere (IRSN), L. E. Herranz (CIEMAT), R. Iglesias (CIEMAT), V. Busser (IRSN): *Report on SGTR and LOCA available experimental data*, D2.1.3m EU R2CA Project (2020)

DEVELOPMENT OF ACCIDENT TOLERANT NUCLEAR FUEL CONCEPTS

Emese Slonszki, Eszter Barsy

Objective

Following the severe reactor accident at the Fukushima Daiichi Nuclear Power Plant in 2011, interest in development of accident tolerant fuel has grown on international level. Several accident tolerant fuel (ATF) programs started at this time. These research programs aimed at developing a new generation of safer fuel systems which will maximize safety and provide economic benefits to utilities. In this work we provide an overview of the current state of development of main ATF concepts. We present which materials have already been irradiated of these materials in a commercial nuclear power plant or research reactor, and how the nuclear authorities handle the licensing of accident-tolerant fuels.

Methods

There are several near-term and longer-term ATF concepts. The improvements cover both enhanced fuels and cladding. Currently, these developments are in the most advanced status in the United States, China, Russia, Korea, and Japan.

In the near-term, nuclear fuel should be one that can be used in a commercial reactor in a short period of time to improve safety and fuel cycle economy. These enhanced ATF concepts include pellet with additives, coated and FeCrAl claddings.

The longer-term solution aimed to offer drastic improvements during beyond design basis accidents. These are the silicide fuels and SiC cladding.

Results

In early 2019, the full-length lead fuel rods with chromium-enhanced fuel pellets and chromium-coated cladding of Framatome were the first complete ATF concepts used in a commercial reactor anywhere in the world. By the end of 2019, both Global Nuclear Fuel and Westinghouse had a short-term ATF concept, those fuel types can be loaded into a commercial reactor. China and Russia are already testing their own short-term ATF concepts in a research reactor.

Insert of short-term Lead Test Assembly into a commercial light water reactor is expected in the coming years, and based on the current results, the long-term concepts can be realized within 10 years.

The licensing of ATF concepts is the result of a complex process of collaboration between authorities and nuclear experts. Extensive in- and out-reactor testing of candidates are necessary.

Remaining work

Centre of Energy Research is also involved in ATF development experiments in the framework of International Atomic Energy Agency projects. Next year, we would like to perform Cr-coated Zr burst tests.

Related publications

- [1] E. Slonszki, E. Barsy: *Development of accident tolerant nuclear fuel concepts*, research report, EK-FRL-2020-253-1-1-M0, OAH-ABA-06/20-M, in Hungarian (2020)

OPTICAL CHARACTERIZATION OF STAINLESS STEEL SURFACES FOR STEAM GENERATOR CORROSION STUDIES

P. Petrik, Z. Kerner, Z. Zolnai, B. Kalas, A. Romanenko, I. Harsányi

Objective

The aim of the project was to develop and apply a high-sensitivity optical surface measurement method for the in-situ characterization of metal surfaces that serve as model materials for the corrosion studies of steam generators. The plans included different extensions of research comprising the development of hardware accessories, evaluation and preparation methods.

Methods

Test samples were temper annealed descaled AISI 321 type stainless steel (Fe/Cr18/Ni9/Ti0.7) sheets purchased from Advent Research Materials, polished using a 0.05- μm colloid silica gel for 30 min. One group of samples were oxidized in an autoclave at 300 °C in ultrapure deoxygenated water for 1 week. The second group of the samples was annealed in a heat cell developed and optimized in the frame of the current project. The sample is heated by a ceramic plate located in the middle of a quartz tube (Fig. 1a) that can be isolated and controlled both in terms of temperature and ambience. The current investigations didn't utilize the latter, only the temperature was controlled measuring in air atmosphere. The tube is UV-grade, therefore the whole wavelength range of the ellipsometer can be utilized. The tube also supports measurements at multiple angles of incidence covering the entire range of angles from 45° to 90°. The plate can be heated up to 600 °C. The temperature was controlled at an accuracy of 0.1 °C. 700 spectral points can be measured in each second that include both amplitude and phase information enabling complex optical modeling of the measured structure.

Results

The refractive index and extinction coefficients were determined for steel samples using the multi-sample approach that increases the accuracy and reliability of the evaluation (Fig. 1b). Proper reference optical data are crucial for the in-situ determination of the sample properties. Fig. 1c shows the thicknesses of the surface overlayer that includes the oxide and the nanoscale roughness before and after the annealing process. The dispersion of the optical functions of the steel substrate and the oxide were parameterized using Lorentz oscillators and the Tauc-Lorentz approach, respectively. During the annealing only the thickness and the optical density of the oxide were fitted. The results showed that a sub-nanometer sensitivity can be achieved even at sample rates down to several seconds and the temperature can be stabilized to 0.1 °C in the range up to 600 °C. A detailed comparison of the sample parameters depending on the different processing methods will be included in a following publication.

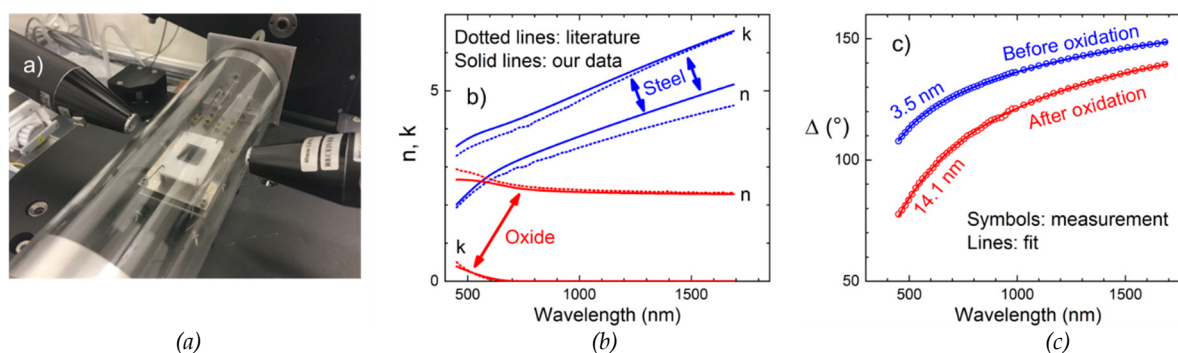


Figure 1: (a) Heat cell developed for in-situ ellipsometry measurements during annealing at temperatures of up to 600 °C in a controlled ambience. (b) Refractive indices (n) and extinction coefficients (k) determined using the multi-sample method from the in-situ measurements during annealing. (c) Measured and fitted ellipsometric angles of the phase shift parameter Δ before and after the heat treatment of a steel plate at 400 °C for two hours. The numbers on the curves show the thicknesses of the surface oxide.

Remaining work

In spite of the pandemic, most of the planned tasks have been performed. However, based on the results, many new ideas emerged that will trigger further collaboration for the development of materials and metrologies. Most of the results will be published beyond the time frame of the project, however, a book chapter summarizing the opportunities for the optical measurement of oxides has already been published in 2020 [1].

Related publication

- [1] P. Petrik: "Optical Characterization of Oxide-Based Materials Using Ellipsometry: Chapter 2", In: Savkina, Rada; Khomenkova, Larysa (eds.) Oxide-Based Materials and Structures, Boca Raton (FL), USA: CRC Press, (2020) pp. 5-29.

UTILIZATION OF LOW-TEMPERATURE HEAT-SOURCES FOR ENERGY PRODUCTION

Attila R. Imre, Bence Bíró, Zalán Csekei

Objective

Low-temperature heat sources can only be used with limited success to produce electricity. One of the potential methods to utilize them is the Organic Rankine Cycle (ORC); similar to the steam Rankine cycle used in normal power plants, applying organic fluids instead of water. The proper choice of the fluid influences the efficiency of the energy production, therefore we are trying to build a theoretically well-supported selection method. Additionally, two special heat sources were investigated to determine the energy-production potential; first the liquid methane of LNG terminals as a source for the so-called cold energy and second, the tertiary cooling water of the research reactor of our campus.

Methods

Analytical method, special computer codes and some commercial codes and databases were used for the calculations.

Results

Concerning the working fluid selection, a group of model-fluids (van der Waals fluids) were investigated. Traditional wet-dry-isentropic classifications of working fluids are insufficient; several materials remain unclassified or misclassified, while materials listed in the same class might show crucial differences. Therefore a novel classification, based on the characteristic points of the T - s diagrams was introduced recently, listing eight different classes. In this study, a map of these classes (using van der Waals equation of states) was presented in reduced temperature vs reduced molecular degree of freedom space; the latter quantity is related to the molar isochoric specific heat. Although van der Waals fluid cannot be used to predict material properties quantitatively, the model gives a very good and proper qualitative description. Using this map, some peculiarities related to T - s diagrams of working fluids can be understood [1].

The final stage of the expansion process has a crucial effect on the ORC design. If it ends in the dry vapour region, it requires extra isobar cooling leading to smaller efficiency, higher investment and operating costs due to the extra recuperative heat exchanger. If, however, the expansion terminates in the two-phase, wet region, the droplets may cause erosion problems, and they may decrease the net efficiency. Hence it is essential to design an expansion, where the process's initial and final states are both saturated ones while all intermediate states are in the dry or slightly wet region. Some preliminary results were shown, how to determine the optimal working fluid for a real expander (characterized by isentropic efficiency) for a given heat source and heat sink with the simplest ORC layout [2].

"Cold energy" refers to a potential to generate power by utilizing cryogenic systems, like Liquefied Natural Gas (LNG). In this case, the cryogenic systems would be used as the cold side of a thermodynamic cycle, while the hot side can be on the ambient temperature. Our study focused on the applicability of some natural working fluids and analyzed their performance upon cold energy utilization in the LNG regasification system. An alternative method, the cryogenic Trilateral Flash Cycle (TFC), was also presented here. Concerning 26 novel LNG terminals, a net power output around 320 MW could be recovered from the cold energy by installing a simple cycle. For the Krk-terminal – which is especially important for Hungary – approx. 6.5 MW could be recovered [3].

With regard to the research reactor at Csillebérc, 10 MW of heat is released into the environment, which we do not utilize in any way and with which we could also do work, thus extracting electricity from this heat. The 45 °C water leaving the research reactor is treated as a heat source (waste heat), and a low heat average temperature circuit is designed to reduce the temperature of the water that we release to the environment and can also be used to generate small amounts of electricity, even for local use. In the course of the related study, a preliminary ORC design was given for the research reactor at Csillebérc that can increase the rate of heat removal and can also generate electricity. The system might be useful to perform similar tasks at the Paks Nuclear Power Plant with minor modifications [4].

Remaining work

We would like to continue the research and in a few years to reach results applicable to design prototypes.

Related publications

- [1] A. R. Imre, R. Kustán and A. Groniewsky: *Mapping of the Temperature–Entropy Diagrams of van der Waals Fluids*, *Energies* **13**, 1519 (2020)
- [2] R. Kustán, A. R. Imre, A. Groniewsky: *The effect of internal efficiency of expander on the working fluid selection*, IIR Rankine 2020 Conference - Advances in Cooling, Heating and Power Generation (2020) PAPER ID: 1170
- [3] S. Daniarta, A. R. Imre: *Cold Energy Utilization in LNG Regasification System Using Organic Rankine Cycle and Trilateral Flash Cycle*, *Periodica Polytechnica Mechanical Engineering*, **64**, 342 (2020)
- [4] B. Bíró, Z. Csekei: *Utilization of the waste heat of Csillebérc research reactor – preliminary study for the waste-heat utilization of the Paks NPP* (in Hungarian: *Csillebérci kutatóreaktor hulladékhőjének hasznosítása - előtanulmány a paksi atomerőművi hulladékhő-hasznosításhoz*), BME GPK TDK Conference (2020)

SIMULATION OF AN UNPROTECTED TRANSIENT OF ALLEGRO USING THE COUPLED KIKO3DMG/ATHLET3.0 CODE

Bálint Batki, István Pataki, András Keresztúri, István Panka

Objective

The main aim of this study was to demonstrate the capabilities of the coupled neutronics/thermal-hydraulics system code KIKO3DMG/ATHLET3.0 for the analyses of reactivity transients in fast spectrum reactors. We focused on a hypothetical transient without SCRAM (ATWS) of the ALLEGRO reactor, during which three-dimensional neutronics modelling is essential. Although ATWS scenarios are highly unlikely events, they are usually parts of the safety analyses required by authorities for nuclear reactors. Furthermore, we validated the KIKO3DMG code and the group constant generation methodology on the temperature reactivity coefficient measurement of the China Experimental Fast Reactor (CEFR).

Methods

The core of the helium-cooled ALLEGRO was modelled using the ATHLET3.0 thermal-hydraulics computer code. The model contains only the active region of the core with fixed inlet mass flow and temperature of the coolant. A gagging scheme was used to flatten the outlet coolant temperature distribution. The nuclear heat generation was simulated by using a neutron point kinetics model and by coupling the KIKO3DMG to the ATHLET3.0 code. For the KIKO3DMG, group constants were calculated in 24-, 12-, 6-, 4- and 3-groups by using the Serpent code and were parameterized as a function of fuel and cladding temperatures and coolant density. We selected an unprotected transient over-power simulating an unintentional control rod withdrawal in the ALLEGRO reactor, leading to a 400 pcm reactivity insertion.

In the case of CEFR, 6-group constants were generated in Serpent and a full-core model was developed in the KIKO3DMG. The temperature coefficient of reactivity measurement of the CEFR was analysed by performing KIKO3DMG simulations.

Results

We found that by using cross-sections in 6 energy groups, the result of the transient hardly differs from the 24-group case, while the calculation time of the transient is reduced by 95%. In general, the differences between the point-kinetics with special assumptions and the coupled calculations are small. Nearby the withdrawn control assembly, the assembly-wise peak temperatures are slightly underestimated compared to the coupled KIKO3DMG/ATHLET3.0 results due to the fixed power distribution and the lack of spatial reactivity effects in the point-kinetics case. An example is shown for the peak fuel temperature in Figure 1. The results confirm that the KIKO3DMG/ATHLET3.0 coupled system code can simulate an unprotected reactivity transient [1].

The calculated value of the temperature reactivity coefficient of CEFR by the KIKO3DMG is between the two measured values as shown in Figure 2. This result validates the group constant generation methodology and the KIKO3DMG code for the investigated quantity.

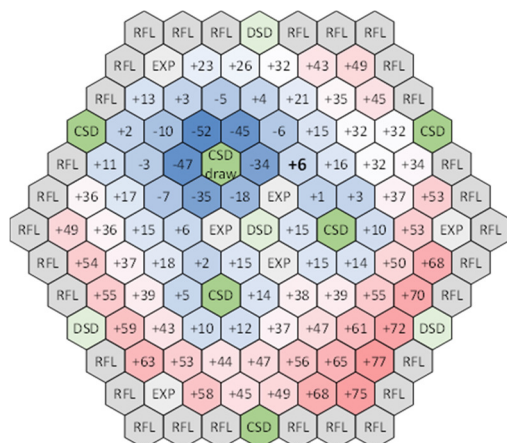


Figure 1: Peak fuel temperature ($^{\circ}\text{C}$) differences between the point-kinetics and KIKO3DMG/ATHLET3.0 results at the end of the transient.

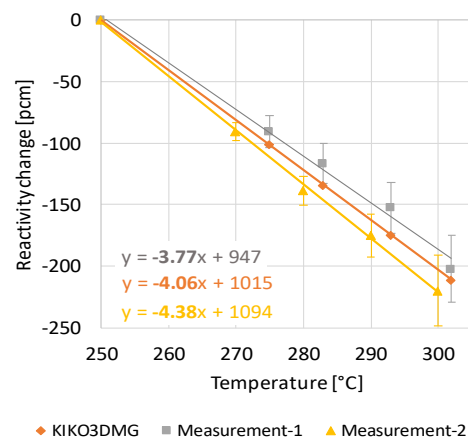


Figure 2: Calculated ($-4.06 \text{ pcm}/^{\circ}\text{C}$) and measured (-3.77 and $-4.38 \text{ pcm}/^{\circ}\text{C}$) values of the temperature reactivity coefficient of CEFR.

Remaining work

There is no remaining work.

Related publication

- [1] B. Batki, I. Pataki, A. Keresztúri, I. Panka: Simulation of an unprotected transient of the ALLEGRO reactor using the coupled neutronics/thermal-hydraulics system code KIKO3DMG/ATHLET3.0, under review at Annals of Nucl. Eng.

HOT DUCT BREAK TRANSIENT WITH TWO- AND THREE-LOOP ALLEGRO MODELS

Gusztáv Mayer

Objective

ALLEGRO is a helium-cooled fast reactor, which is being developed by European research institutes and universities. Its two primary aims are to prove the planned technology for the GEN IV GFR2400 reactor and to test its new ceramic fuel and cladding. The current ALLEGRO design has two primary cooling loops. Since the hot duct of ALLEGRO is led inside the cold duct there is no depressurization of the primary system in case of hot duct break scenario, but there is a huge core bypass. If the hot duct break is aggravated by the failure of the blower in the intact loop, then solely the blower in the broken loop is supposed to ensure the core cooling. In order to mitigate the consequences of this scenario and to increase the cooling capability of the ALLEGRO design a new three-loop ALLEGRO model is proposed.

Methods

The French CATHARE thermal hydraulics code was selected for the calculations, which is developed by CEA, EDF, FRAMATOME and IRSN. In this work the two-loop ALLEGRO input deck of the earlier EU VINCO project was selected as a starting point, which was extended by third primary, secondary and tertiary loops. The advantage of the three-loop model compared to the two-loop model in case of hot duct break is that the third loop remains intact during the transient and in this way it ensures better core cooling. In the two-loop model the primary blower inertias were set to 10 kg*m*m each, while in the new three-loop model they were varied from 6.7 to 20 kg*m*m.

Results

According to Figure 1 the blower inertia plays a major role in the maximum cladding temperature values. It can be seen that in case of the three-loop model the peak cladding temperature can be decreased by more than 120 °C if the inertia of each blower is increased from 6.667 to 20 kg*m*m. The results showed (Figure 1.) that the peak cladding temperature is lower by 31 °C in case of the three-loop model than that in the two loop model, even if the total blower inertias of the two designs were kept at the same value (in the case when the two-loop model has a total blower inertia of 2*10=20 kg*m*m and the three-loop model has 3*6.667=20 kg*m*m). Further calculations pointed out that the break size has a significant effect on the PCT values.

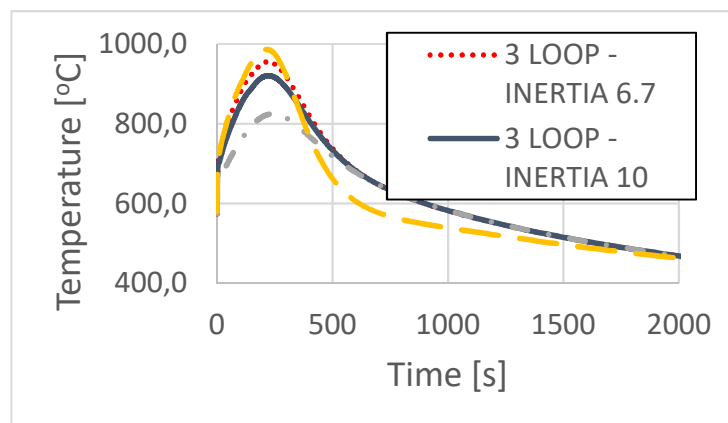


Figure 1: Maximum cladding temperature values of the two- and three-loop models using different primary blower inertias. The total blower inertia is the sum of total inertia of all blowers in the primary system.

Related publication

- [1] G. Mayer: Hot duct break transient with two- and three-loop ALLEGRO model, Nuclear Engineering and Design, **370**, 110911 (2020)



III. NUCLEAR SECURITY, DOSIMETRY AND SPACE RESEARCH



LOGIC OPTIMIZATION FOR THE RM-RADTEL RADIATION TELESCOPE

Boglárka Erdős, Attila Hirn

Objective

This document reports on the work of Boglárka Erdős' PhD studies, which is focused on selectivity of silicon charged particle detectors for space weather and space dosimetry measurements and contamination of the measured energy bins. During the reporting period, the work was mainly focused on calculating the possible detector responses and optimizing the initial logic for the binning of the D3S-RADTEL charged particle telescope for space weather measurements.

Methods

The D3S-RADMAG radiation monitor and space weather instrument concept is being developed to provide a marketable product combining the radiation and magnetic field measurement capabilities into one payload to be directly usable within the D3S hosted payload concept of the European Space Agency (ESA). The Radiation Monitor Unit (RM-RAD) of the instrument includes a sophisticated, complex silicon detector based telescope, called RADTEL. It is a single axis charged particle telescope with six independent silicon sensitive volumes for measuring the fluxes and energies of protons, electrons, and heavy ions. The ranges of interest in terms of energy are 3 MeV–500 MeV for protons, 30 keV–8 MeV for electrons, and approximately 1 MeV/n–500 MeV/n for heavier ions which needs to be specified later in the study. The detectors are connected in coincidence or anticoincidence with a complex logic system to determine the type of particle and its energy and to restrict the field of view. The telescope responses were modelled with a Monte Carlo tool called GRAS (Geant4 Radiation Analysis for Space) that was developed by the ESA and based on the Geant4 toolkit. The geometries that were required for the simulations were defined in Geometry Description Markup Language (GDML), which were based on Standard Tessellation Language (STL) (file format commonly used by 3D printers) files created with a Computer-Aided Design (CAD) program. For the simulation, a simple spectrum, the descending branch of the function $1/E$, was used for both protons and electrons in the corresponding energy range of interest. For the first iteration of the logic, only a beam of particles was used, but for the second iteration a full isotropic spectrum with the whole simplified geometry was modelled. For the optimization, two following method was used. First the energy deposition in the detectors were examined and then the response functions were calculated and looked at. Based on these, the logic with the most optimal energy selection was chosen. In most cases the optimization cannot be done on each energy bin individually since there is a tradeoff between channels. Energies deposited in detectors are so close to each other and even overlapping, that perfect energy selection is impossible to be done, so a sufficiently appropriate option should be chosen. After deciding on a logic, the first used simple spectrum can be rescaled to several characteristic realistic spectra to calculate the relative accuracies and contaminations and possible corrections to these. Based on these percentages, a few changes in the logic may be justified for better results.

Results

The response functions for a possible option for the proton logic is presented in Fig. 1. Energy selection is good in the channels, but a high energy contamination can be seen on all channels, due to the overlapping of deposited energies which cannot be fully cut off by the logic. Also, "double bumps" are present in some of the response functions, because one energy bin can correspond to two or three coincidence possibilities which cannot be always seamlessly separated. Fig. 2 shows the response functions for the possible electron logics. For electrons, the energy bins are not completely separated, making interpretation more difficult, but with post-processing corrections, it can still be used to get information about the electron spectra. In the future, these logics need to be finalized and post processing corrections need to be calculated as well, but the analysis confirmed that the detector design can be used to provide the requested data [1].

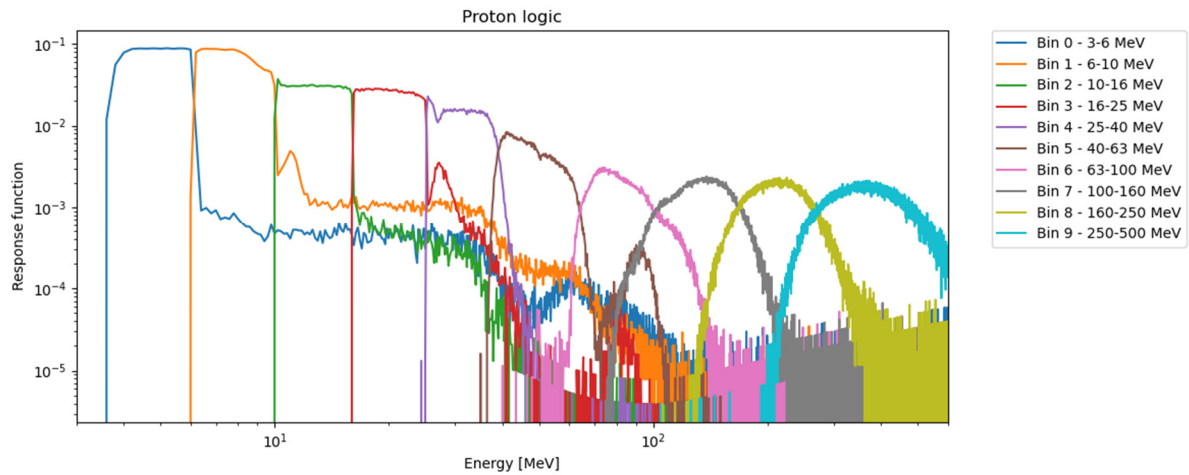


Figure 1: Detector response functions for the most recent version of the proton logic with the isotropic $1/E$ spectrum

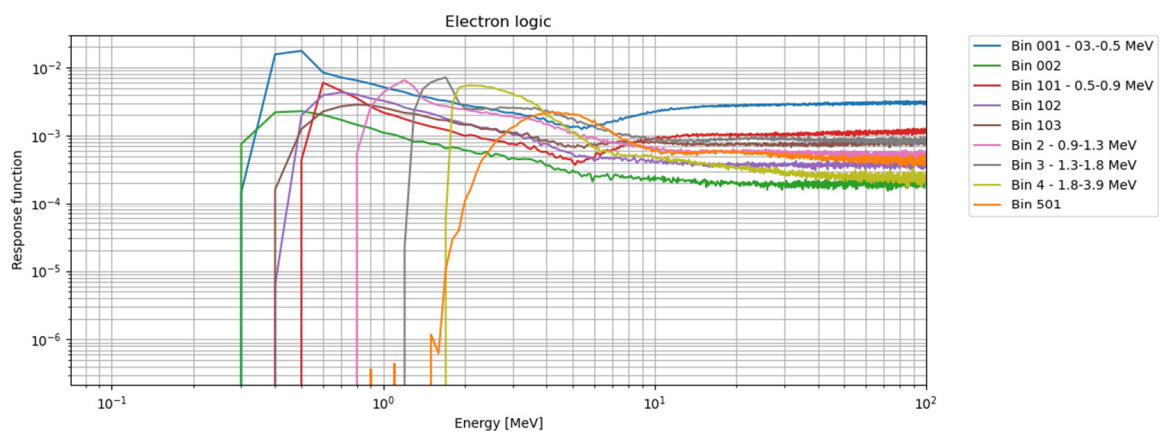


Figure 2: Detector response functions for the most recent version of the electron logic with the isotropic $1/x$ spectrum. Bins 002, 102, 103, and 501 are bins that will be used for corrections and post processing on ground

Remaining work

The logic for both protons and electrons will be finalized in early 2021. An algorithm for post-processing of the electron spectra will be defined. The logic for heavy ions will be determined in 2021.

Related publication

- [1] B. Erdős, A. Hirn and B. Zábóri: *D3S-RADMAG Radiation Performance Analysis Report*, D3S-EK-PL-AN-001_02_01 (2020)

DEVELOPMENT OF METHODS TO IMPROVE PRECISION OF ENVIRONMENTAL RADIATION MEASUREMENTS

Tamás Pázmándi, Dorottya Jakab, Péter Zagyvai

Objectives

Accurate and detailed evaluation of uncertainties and characteristic limits of environmental measurements as well as the adequate statistical analysis of the resulting data sets is required to support basic environmental monitoring objectives (e.g. providing information to support decision making). For their effective implementation, there is a need for methods that are easy-to-use in practice, hence such easily applicable evaluation procedures have been developed. In order to ensure reliable and representative monitoring of environmental radioactivity levels, increasing the accuracy, the precision and the detection capabilities of radioactivity measurements is also necessary, therefore we established proposals for such developments.

Methods

In line with the enhancement of local and national systems, the applicability of proposals for evaluation procedures and improvements that can be used both in routine and occasional environmental monitoring had to be examined. A nationwide survey has been carried out, then evaluated to assess the current environmental control practices, and several methods have been tested in practice through the on-site environmental monitoring system at KFKI Campus. These improvements were based on the use of the existing system's elements and were achievable by modifying the sampling and measurement procedures and the evaluation methods. To support their effective use, easily applicable evaluation procedures were developed that are compatible with standard spreadsheet software. With the goal of improving the general accuracy of the prevalent measurement uncertainty and characteristic limit evaluation procedures, such as the analytical (propagation of uncertainty) and stochastic (Monte Carlo simulation-based) methods, conditions affecting their reliability were examined. We have reviewed the available statistical methods and evaluated their applicability, with consideration of the specificities characterizing environmental data sets (spatially and temporally correlated values, non-normally distributed samples, presence of outliers and inclusion of data below the detection limit).

Results

The general accuracy of central finite-difference approximation as an alternative approach to analytical uncertainty propagation was verified. We showed that in addition to the presence of non-Gaussian input quantities or those that are non-linearly related to the measurand, their contribution to the overall uncertainty also affects significantly the resulting probability density function (PDF) and numerical results (estimation of measurand and its associated standard uncertainty, coverage interval's endpoints), hence also affecting the conformity of uncertainty propagation-based methods (either analytical or numerical differentiation-based) with the stochastic evaluation. Uncertainty evaluation procedures were complemented by including quantification of uncertainty component contributions, for which various methods have been described whose applicability has been investigated. Beyond the obvious gain of identifying key sources of measurement uncertainty to be reduced to increase overall precision, another practical relevance is the indication of non-compliance with conditions for uncertainty propagation and the need for an alternative evaluation procedure (i.e. stochastic method) to provide valid uncertainty statement. We illustrated that the stochastic method is more general since it is not limited by such restraining conditions as the uncertainty propagation. We showed the theoretical differences between analytical and stochastic methods for characteristic limit calculations and developed an easy-to-use scheme for stochastic calculation.

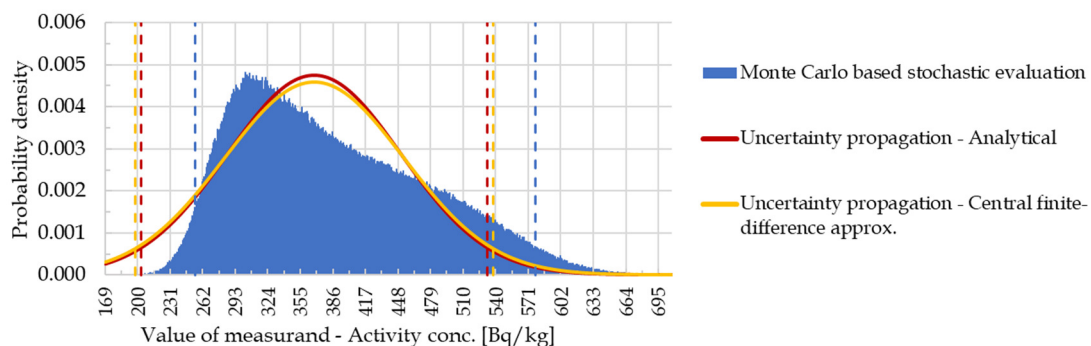


Figure 3: Illustration of differences between PDFs and coverage intervals obtained by stochastic and analytical uncertainty evaluation methods on a gamma spectrometric measurement example, with presence of a non-Gaussian type input quantity (efficiency correction factor) that is inversely proportional to the measurand and has dominant uncertainty contribution

Related publications

- [1] D. Jakab, T. Pázmándi, P. Zagyvai: Development of methods to improve precision of the measurement results of environmental radiation monitoring systems - Part 2: Methods for reduction of measurement uncertainties and

characteristic limits of environmental radiation measurements, Research report, EK-SVL-2019-270-02-01-01, In Hungarian (2020)

- [2] D. Jakab, T. Pázmándi, P. Zagyvai: Development of methods to improve precision of the measurement results of environmental radiation monitoring systems - Part 3: Integrated statistical analysis of environmental radiation measurements, Research report, EK-SVL-2020-270-01-01-01, In Hungarian (2020)

DEVELOPMENT OF GUIDELINES FOR DETERMINING THE INTERNAL EXPOSURE OF WORKERS

Annamária Pántya, Tamás Pázmándi, Péter Zagyvai

Objective

The aim of the work is to develop official guidelines for determining the internal exposure of workers for occupational intakes of radionuclides. In recent years, a number of international recommendations have been issued regarding internal dosimetry. In Hungary their application can be recommended in the determination of occupational radiation exposure for promoting the harmonization of such services. The guidelines present the principles of individual monitoring and internal dosimetry and offer guidance and recommendations for the practice. An adequate level of control of internal radiation exposure takes place in several steps, which requires the joint work of several participants. It is essential to establish adequate occupational radiation protection and a related routine monitoring program to perform sampling and measurements appropriately, to record measurement data properly, and to accurately determine the dose based on the available data. As a consequence, assessment of internal doses is subject to uncertainty relating to activity measurements, to biokinetic and dosimetric models and to the exposure scenario. In order to demonstrate these uncertainties and differences of results of diverse methods, the practice was investigated and an example was presented.

Methods

During an incident ^{14}C -labelled compound entered a person's body. To determine the effective dose of the worker, we made several estimates using the appropriate recommendations and recent published scientific papers, taking into account the available measurement data and the circumstances of the case.

^{14}C is a soft beta emitter, so the amount of intake can only be measured through an excretion sample. Liquid scintillation (LSC) measurement techniques were used to examine urine samples. The worker performing ordinary work was routinely monitored by the employer for internal exposure with spot urine samples. However, a more accurate determination of internal radiation exposure requires urine sample collected over 24 hours. The uncertainties of the measurement data to be used for dose estimation were chosen as recommended by international guidelines for in vitro measurement data, scattering factor (SF) of 1.1 was applied for complete 24-hour collection of samples; 1.6 was used in case of deduced (e.g. by volume normalization) 24-hour urine samples; and 2 for spot samples. The ^{14}C content of the urine samples was well measurable in the examined period, the activity could be determined from the given samples with low measurement uncertainty. The fluctuation of the initial measurements and the large standard deviation of the results can be explained by the uncertainty from the spot sampling. Range of the measurement results of the 24-hour urine samples was limited. The calculation methods used in the dose estimates can be divided into two major groups. In conventional calculations, the administered activity is determined from the measurements and the intake is multiplied by the dose conversion factor for the isotope to obtain the committed effective dose. In the other type of the calculations, we deduce the extent of radiation exposure from the estimated number of decays in the body.

Results

Different calculation methods were used for the evaluation of the committed effective dose. (1) According to the ICRP recommendation commonly used for routine dose calculations, 99% of the incorporated nuclide has a short biological half-life and only 1% is excreted with an assumed biological half-life of 40 days. Since in this specific case we received measurement results from only 3 days after intake, the determination of the intake moment was extremely uncertain. Estimated effective dose derived in this way was quite high (1320 mSv), however deviations of several orders of magnitude are possible using the dose conversion factors given in the recommendation. This overestimation is also highlighted in the ICRP recommendation, especially in cases where carbon compounds other than carbon dioxide entered the body. (2) For the calculations performed with the IMBA software developed according to the ICRP recommendations, we selected the parameters best suited for the case, according to which organic-bond ^{14}C isotope was inhaled in vapour format. The software calculates the possible intake by fitting of the measurement data and based on this we got 562 mSv for the effective dose, less than half of that with the ICRP method. (3) According to ISO 27048, the measurement data and the daily excretion rate of the ^{14}C isotope were taken into consideration, intake was calculated and then the committed effective dose (222 mSv) was determined. (4) The value of the effective dose is significantly influenced by the course of the clearance curve. Since the short-term components were not known in this case, but a sufficiently long set of measurement data was available, a direct method taking into account the course of the excretion curve was elaborated and used to determine the effective dose (23 mSv). In this case, the contribution of the components with a short biological half-life cannot be determined precisely, but it has been demonstrated by calculations that these components contribute only up to 10% to the effective dose. Assessments confirm the important role of routine monitoring in the detection of possible incorporation, however, it has been shown that dose estimation by general recommendations and parameters does not give accurate results in cases where the incorporated radioisotope is a compound for which an exact biokinetic and dosimetric model does not exist.

Related publications

- [1] A. Pántya, T. Pázmándi, P. Zagyvai: *Development of guide for monitoring internal exposure: Part 2*, Research report, EK-SVL-2019-263-03-01-01, in Hungarian (2019)
- [2] A. Pántya, T. Pázmándi, P. Zagyvai: *Development of guide for monitoring internal exposure: Part 3*, Research report, EK-SVL-2020-263-01-01-01, in Hungarian (2020)
- [3] A. Pántya, T. Pázmándi, P. Zagyvai: *Determination of the effective dose of ^{14}C incorporation*, Internal report, EK-SVL-2020-xxx-01-01-01, in Hungarian (2020)

INVERSE EXPOSURE RATE EFFECT, ITS POTENTIAL EXPLANATIONS, AND THEIR IMPLICATIONS ON THE RISK OF LOW DOSES

Emese Drozsdik, Balázs Madas

Objective

One of the assumptions of the present system of radiation protection is that the harmful health effects of ionizing radiation is lower at a given cumulative dose if the dose rate is smaller. Several epidemiological studies of lung cancer among uranium miners, however, have shown evidence for the opposite, i.e. the risk of lung cancer is lower at a given cumulative exposure if the exposure rate is higher. This phenomenon is called the inverse exposure rate effect. It is an important question whether this phenomenon is specific to radon exposure or also applies to other chronic radiation exposures. The aim of the present study was to prepare to review and compare the proposed explanations of inverse exposure rate effect, and discuss their implications regarding the risk of and protection against low doses.

Methods

For this purpose, it is necessary to examine which processes can lead to inverse exposure rate effect and whether they are specific to radon. A potential explanation for inverse exposure rate effect is related to bystander responses. Another explanation for inverse exposure rate effect may be the induction of hyperplasia in the deposition hot spots.

Results

Inverse exposure rate effect decreases as the exposure rate decreases, and essentially disappears at average fluences of around one alpha-particle per target cell nucleus. This fact is compatible with the observation that bystander effects dominate the direct effects at low dose rates, but saturate if all cells are hit by an alpha-particle. However, this explanation does not take into account the heterogeneous dose distribution within the bronchial airways.

On the other hand, there is experimental and histological evidence that chronic irritation and cell death may result in hyperplasia in the exposed tissue. As the heterogeneous deposition of inhaled radon progeny results in high local doses at the peak of the bronchial bifurcations, local hyperplasia may occur in these deposition hot spots upon chronic radon exposure. It has also been shown that the average tissue dose, and the average hit number and dose of target cells decrease by the increase of the measure of hyperplasia potentially leading to inverse exposure rate effect.

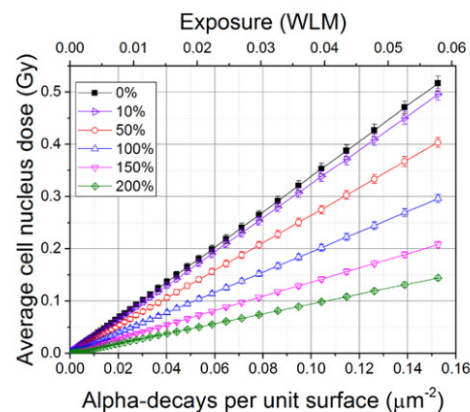


Figure 1: Average cell nucleus dose for basal cells as the function of alpha-decays per unit surface. The different curves refer to different numbers of basal cells relative to their normal number. In case of exposure in working level month (WLM), deposition hot spots are considered, and mucociliary clearance is neglected.

An important difference between the explanations proposed that while bystander effects are expected to occur in any kind of radiation exposure, the induction of hyperplasia requires locally high doses specific to radon exposure. In this way, the bystander explanation implies that low dose rates result in higher risk in general, while the hyperplasia explanation suggests that inverse exposure rate effect is specific to radon progeny and some other internal alpha-emitters.

Related publication

- [1] E. J. Drozsdik, and B. G. Madas: *Inverse exposure rate effect, its potential explanations, and their implications on the risk of low doses* (In prep.)

ENVIRONMENTAL RADIATION MONITORING WITH DETECTORS IN A NEW GENERATION SCALABLE NETWORK – DOZINET 2.0

Attila Hirn, János Volk, István Apáthy, Sándor Deme, Gáborné Endrődi, András Gerecs, Ákos Horváth, Miklós Szappanos, László Tósaki, Erika Tunyogi

Objectives

In the frame of the DoziNet project, initiated in 2019, it was demonstrated that the radiation detector system developed by the Space Research Laboratory for sounding rocket experiments could be combined with the communication units and protocol developed and used by the Nanosensors Department for self-organizing scalable networks and that the combined system could be integrated into the network of Geiger–Müller (GM) probes installed and operated by the Environmental Protection Service at the KFKI Campus. The primary objectives of the 2nd phase of the project (DoziNet 2.0) in 2020 were to make the DoziNet unit more compact, to extend the network of GM probes with 5 relocatable DoziNet units and to optimize the system for use on radiation protection vehicle (DoziMobile).

Methods

The concept behind the development was to provide uniform mechanical design for different applications, uniform electronic design with optional modules to be implemented when required and software specific for the given application. Requirements were to be compatible with

- passive/active GPS antenna,
- communication through USB (laptop connected directly to the unit), GSM or LoRaWAN,
- power supply from batteries, optionally solar cells or mains electric power,
- integral data storage with subsequent data download and visualization and real-time data editing.

Results

The prototype of the DoziNet/DoziMobile instrument was manufactured. Operation of the DoziMobile was demonstrated in an environmental dose rate measurement at the KFKI Campus (Fig. 1 and Fig. 2). The results of the car-borne survey were in good agreement with former measurements carried out by manual measurements on site. Sampling rate, data collection frequency and alarm levels could be set by the user. Preset colour coding and autoscaling are both implemented in the visualization module of the software. Results of the study on the use of DoziMobile in Nuclear Accident Prevention and Protection are documented in [1].

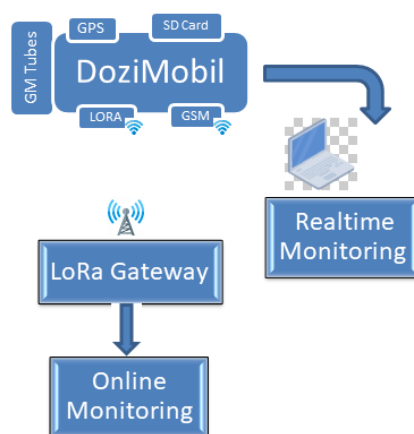


Figure 1: DoziMobile unit attached to a dedicated console on the right-side A-pillar of the radiation protection vehicle. The processing laptop is on the dashboard of the vehicle

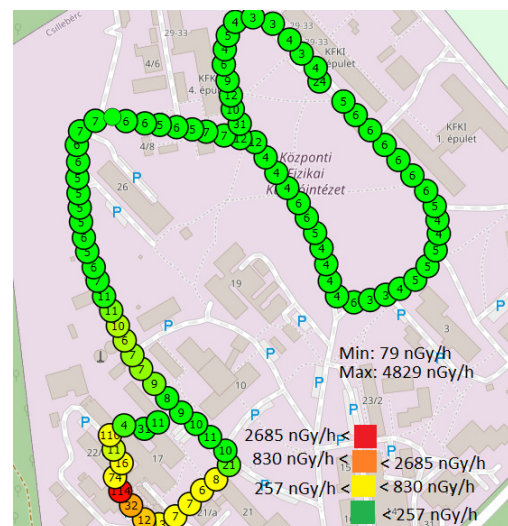


Figure 2: Dose rate mapping measurements at the KFKI Campus using the DoziMobile unit – autoscaling visualization mode

Remaining work

Due to the worldwide pandemic in 2020, the manufacturing and integration of the relocatable DoziNet units will be finished in the first quarter of 2021.

Related publication

- [1] S. Deme, I. Apáthy, Zs. Csalótzky, A. Hirn, M. Szappanos, E. Tunyogi, J. Volk: A Dozimobil sugárázsmérő gépkocsi alkalmazása nukleárisbaleset-elhárításnál, DOZINET-EK-MAN-AN-001_01_00, in Hungarian (2020)

METASTATIC POTENTIAL OF HELA-CELLS DOES NOT INCREASE DIRECTLY AFTER RADIATION EXPOSURE

Balázs Madas, Kinga Kovács, Andrea Strádi, Szabolcs Polgár, Boglárka Erdős, Inna Székács, Emese Drozsdik, Attila Hirn, Róbert Horváth

Objective

Ionizing radiation is frequently applied in cancer therapy. New treatment modalities include targeted radionuclide therapy either alone [1] or in combination with chemotherapy [2]. While radiation therapy increases local tumour control, it remains controversial whether ionizing radiation increases the metastatic potential of cancer cells. One of the potential mechanisms of radiation-induced metastasis is the direct release of tumour cells into the circulation requiring the detachment of the cells. The objective of the present study was to measure how ionizing radiation affects cellular adhesion, especially its initial stage after cell attachment on a biomimetic surface.

Methods

For this purpose, an automatic irradiation facility (Cs-137) has been developed providing parallel irradiation opportunity for 96 wells of a biosensor microplate with different doses. The employed optical biosensor records the wavelength shift from a nanostructured waveguide, being proportional to the cell adhesion strength (contact area and protein density within the contact zone). Absorbed doses were measured by thermoluminescent dosimeters (TLDs) in each well. Monte Carlo simulations were performed to describe the radiation field within the irradiation facility. As a model system a cervical cancer cell line (HeLa) was studied.

Three different experimental setups have been used distinguished by the sequence of irradiation and cellular attachment to the surface. In the first setup, cells were first attached to the surface of the biosensor, and then irradiated. In the second setup, cells were irradiated in suspension, and then the attachment process was monitored. In the final setup, cells were irradiated during the adhesion process, after direct attachment. The wavelength shift as the function of time was measured for different absorbed doses. The maximum wavelength shift as a function of dose was also analysed.

Results

Figure 1. shows that adhesion of HeLa cells is not affected by ionizing radiation, independently whether cells are attached, in suspension, or during the adhesion process were irradiated. This suggests that radiation therapy does not increase the metastatic potential of cancer cells directly by decreasing their adhesion. However, this study does not exclude the other three potential mechanisms of radiation induced metastasis.

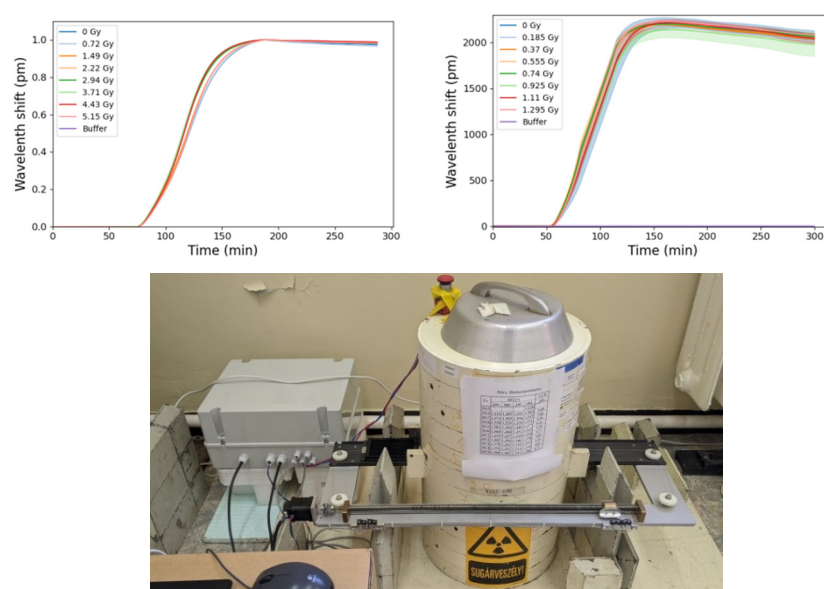


Figure 1: Wavelength shift as a function of time if cells attached are irradiated (upper left panel), or they are irradiated during the adhesion process (upper right panel). The bottom panel shows the irradiation facility.

Remaining work

Experiments with longer follow-up after irradiation are required to quantify the effects of radiation on cell survival.

SIMULATION OF INDIVIDUAL RADIOSENSITIVITY

Árpád Farkas, Péter Fűri

Objective

Subjects with different age or gender, or patients with lung diseases have different lung geometry and breathing pattern. This has a strong effect on the deposited number of the inhaled radon progenies and their spatial distribution within the respiratory tract. This implies that the dose and dose distribution due to the inhaled radon decay products will also be influenced by the above characteristics of healthy and diseased subjects. Due to the possible different health outcomes, age, gender and health status and the associated inherent anatomical and physiological characteristics can be considered as indicators of individual radio-sensitivity.

The main objective of this work was to investigate the effect of age, gender and airway disease on the deposition distribution of the inhaled radon progenies in the human respiratory tract, and to calculate the absorbed doses in the nuclei of the basal and secretory cells of subjects from different age, gender and health-status groups.

Methods

The standard Stochastic Lung Model (SLM) has been extended to realistically simulate the deposition distribution of the inhaled radon progenies in subjects belonging to specific population groups. The new version of the SLM is able to scale down and up the dimensions of the airways according to the height of the subject. The modified model is also able to simulate the presence of lung diseases (asthma, emphysema, chronic obstructive pulmonary disease COPD) by assuming modified airway architecture and dimensions (e.g. bronchial diameters and lengths, alveolar volumes). As the next step, we determined the radiation burden of the radiation sensitive cells by simulating the tracks of the alpha particles emitted by the deposited short-lived radon progenies.

Results

Our computer simulations demonstrated that the absorbed doses in the nuclei of the radio-sensitive basal and secretory cells are strongly influenced by the age of the subject. Assuming the same radon progeny activity concentration, much more energy is absorbed in the bronchial cell nuclei of a 5-year-old child than in an adult's basal or secretory cell nuclei (Figure 1). Our simulations revealed that health status is also influencing the radiation burden of the airways, severe COPD patients receiving about twice higher cellular doses than their healthy counterparts.

Our results demonstrate that for an adequately personalized radon-dosimetry, the individual anatomical and physiological or pathological particularities have to be taken into account.

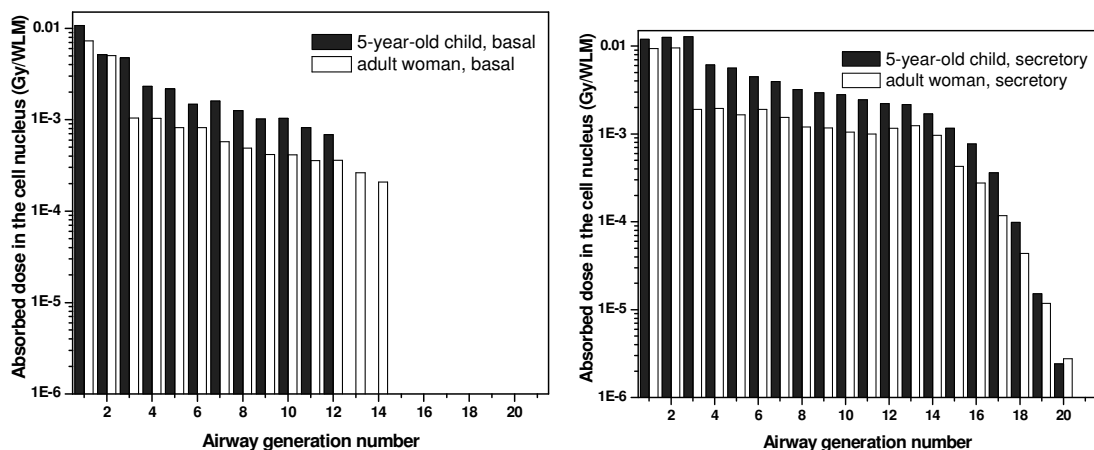


Figure 1: Absorbed doses in the nuclei of the basal and secretory cells of a 5-years-old child and an adult woman for one Working Level Month radiation exposure

Related publications

- [1] P. Fűri, Á. Farkas, B. G. Madas, W. Hofmann, R. Winkler-Heil, G. Kudela, I. Balásházy: *The degree of inhomogeneity of the absorbed cell nucleus doses in the bronchial region of the human respiratory tract*. Radiation and Environmental Biophysics, **59**, 173-183 (2020)
- [2] Á. Farkas: *Simulation of the effect of mucociliary clearance on the bronchial distribution of inhaled radon progenies and related cellular damage using a new deposition and clearance model for the lung*. Radiation and Environmental Biophysics, **59**, 651-661 (2020)
- [3] P. Fűri, I. Balásházy, W. Hofmann, R. Winkler Heil, G. Kudela, Á. Farkas, B. G. Madas: *Effect of mucociliary clearance on radiation burden from inhaled radon progenies in a healthy woman's lung*. Submitted to Radiation Protection Dosimetry.

NEW 3D SPECTRAL DATA DISPLAY SOLUTION FOR THE WHOLE BODY COUNTER

Attila Gábor Nagy, Gáborné Endrődi

Objective

The whole body measurement methods use the sum of the counts of all the gamma spectrometry channels. The detector measures approximately the entire body of the subject and provides one data for each channel. This means that if somebody is being measured, we can get data about her or his body radioactivity, but cannot tell anything about where the source of this activity can be found in the body. If we have this extra information, it could be very useful in human measurements, because if there is contamination in the body, with this new method we can tell where the source of the activation is.

Methods

For achieving our goal, we had to find a way to extract the spectral data from the detector, as many times as we want, not just at the end of the measurement. To realize this, we used a Canberra software, which can be scripted in REXX programming language. During the measurement this utility can extract all the channels/data (4096 in this case), the real-time and almost every data about the detector and actual measurement. This tool is very useful but only gives data in files or screen and has to be started by the user. To overcome this problem, we made a graphic GUI (Graphic User Interface), which records the spectral data to files, and from the file extracts the spectral data creates a 3D OpenGL powered graph. This graph is online so it shows the results as the measurement develops. There are 10 gamma spectrums in 3D form, which you can zoom and scroll.

Results

To test the new method, we chose to measure point sources because it is the simplest geometry setup. We have made several tests with Caesium Europium Cobalt sources. A test placing a Cs137 source in the middle of moving length of the detector can be seen in Figure 1. The Caesium peak is around the 1432th channel in this case (4096 channel setup), we can see in the figure that as the detector moves towards the source, the peak height is increasing, it reaches the highest point at the 6th spectrum, then the detector starts to move away from the height of the peak is decreasing.

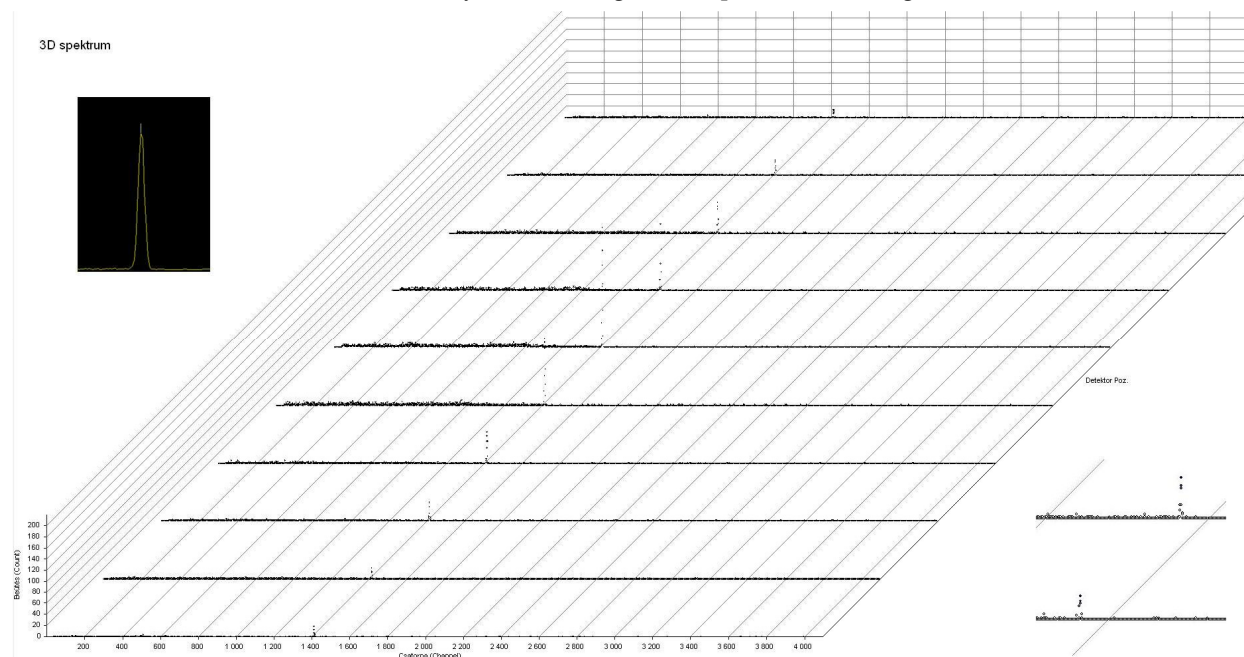


Figure 4: Cs¹³⁷ point source measurement, in the little black picture we can see the information we have got from the usual method, on the right bottom two Cs peaks are zoomed (the graph is a screen shot of the program)

We had similar results from different sources. Using multiply sources for this task is not too easy because the sources have quite different activities, for example the Europium source has a few thousand counts on every peak, but Caesium has at most few hundreds, so it is not easy to display them together.

Remaining work

1. Find different graphic methods to display better the result, make the output Gnu-plot program compatible
2. Colouring the peaks, possibility of logarithm axes
3. Show lengthwise spectral data.

CHARACTERIZATION OF RADIATION EXPOSURE AND ITS BIOLOGICAL EFFECTS AT DIFFERENT SPATIAL SCALES

Tariq Hailat, Emese Drozsdik, Balázs Madas

Objective

Most experiments in radiation biology are performed to estimate the relationship between biological effects and radiation dose. While the difficulties of measuring the biological effects are well-recognized, less attention is paid to the problems of quantifying radiation dose. It is particularly difficult in case of incorporated alpha-emitting radioisotopes. The objectives of this research were i) to develop a Monte-Carlo code in order to estimate and compare the radiation doses absorbed by the salivary gland upon administration of different alpha-emitting radiopharmaceuticals, and ii) to describe the dosimetric properties of sulfosalicylic acid-ferrous-polyvinyl alcohol-glutaraldehyde hydrogel (SSA-Ferrous-PVA-GTA) dosimeters.

Methods

For these purposes, i) a computational model was developed to quantify dose rate (as the function of time), total dose, and total hit numbers of the salivary gland cell nuclei and to estimate their surviving fractions [1], ii) nuclear magnetic resonance relaxometry (NMR) and ultraviolet-visible (UV-Vis) spectrophotometry techniques were applied to characterize the dose-response function of the dosimeter from 0 Gy to 40 Gy using a linear accelerator with different beam energies and dose rates [2].

Results

Considering the effectiveness of alpha-particles in cell killing, the hit number calculations explain why salivary gland is destructed upon administration of 10 MBq Ac-225 in secular equilibrium with its progeny as it is observed clinically. 3 MBq of another alpha-emitting radionuclide in transient equilibrium with its progeny results in similar doses and similar hit numbers. Therefore, it is expected to be similarly toxic to the salivary gland as 10 MBq Ac-225. The results clearly show that biokinetics of the progenies, and in particular their washing out probabilities are major determinants of salivary gland toxicity.

Linear dose-response relationships were observed in the range of 0-40 Gy for all recipes applied, and the highest dose-response was obtained at 40 mM SSA and 4 mM Fe²⁺ concentration for both measurement techniques. A small increase in absorbance and relaxation rate (R_2) values was observed up to 8 hours after irradiation. After 8 hours of irradiation, it was almost stable up to 60 hours. The hydrogel dosimeter performance was found to be independent of dose rate and radiation beam energy. The result of absorbance measurement was almost constant with different scanning temperatures.

Remaining work

The next question is whether SSA-Ferrous-PVA-GTA dosimeters can be applied for alpha-particle dosimetry as potential indicators of spatial inhomogeneities in dose distributions.

Related publications

- [1] B. G. Madas, E.J. Drozsdik, and T. F. Hailat: *Report KFL-2019-319-01-01-D* (2020)
- [2] K.A. Rabaeh, T. F. Hailat, M. M. Eyadeh, M. Z. Al-Shorman., S. M. Alheet, B. G. Madas, and S. I. Awad: *Dosimetric properties of sulfosalicylic acid-ferrous-polyvinyl alcohol-glutaraldehyde hydrogel dosimeters using magnetic and optical techniques*, *Radiation Physics and Chemistry* **177**, 109106 (2020)

DOSIMETRY MEASUREMENTS IN PULSED IONIZING RADIATION FIELDS CREATED BY GAMMA-CHOPPER

Attila Gulyás, Károly Bodor, János Pető, Gergely Dósa, Péter Völgyesi

Objective

A test campaign has been carried out by the Detector Testing Laboratory of the Centre for Energy Research in the frame of a research contract supported by the Hungarian Atomic Energy Authority (OAH). The aim of this project is to create test procedures for pulsed ionising radiation fields, for measuring instruments and for a Gamma-chopper machine. Measurements and analysis in/of pulsed fields were our main focus, but with the additional aim to investigate the possibility of dosimetry calibration without X-ray source and to develop that possibility with methods and specifications. There are no standards in this area and thus no adequacy with them; therefore test measurements should be quite useful and required.

Methods

The research project includes a number of activities related to radiation protection needs in the calibration of measuring instruments. We have developed an experimental machine with a rotary disc, which chops the stationary (continuous) field. Laboratory test measurements with the combination of radiation source, chopper, detector and analysis of the time characteristic of dose-rate were carried out using self-developed procedures to create pulsed fields, which conforms to ISO/TS 18090 Radiological protection – characteristics of reference pulsed radiation technical specification.

Results

Based on the experiences of the test campaign, the chopping method has good capabilities to create reference repeated pulsed fields. The main consideration in the design and creation was adjustability on the widest possible scale in all aspects (e.g. pulse width and frequency). However, unmet needs (e.g. single pulse) envisage further expansion of the machine's capabilities. As a final result, test procedures (e.g. vibration and visible light/shadow diagnostic) have been established and carried out. For calibration, the basic procedure is easy and similar to stationary field setup except for the placement of the chopping disc in the path of the radiation field. In this process, more sizing procedures (e.g. in the rotary collimator geometry) and quasi-static experiments had to be made to increase accuracy, precision and compliance, and decrease uncertainties. There are two ways to do the instrument calibration: making the function of the pulsation time characteristic and/or the size of dose-rate jump in the pulse. The measurement data of the ThermoFisher Scientific Mk2+ electronic personal dosimeter (EPD) were compared directly to the reference ionization chamber data (STEP OD-02) as well as to themselves as a function of the change in the time characteristics of the pulsed field (Figure 1), generated by chopping a ^{137}Cs radiation field. As can be seen, the results are quite consistent. At given disc, the measuring points are defined by the set speed of the rotary disc; the pulse frequency and the widths are calculated from it. The resulting examined pulse time range covers four orders of magnitude. In these cases the dose-rate jump from the background (base line) is more than three orders of magnitude during the pulse. The slope of the line fitted to the dose-time data gives the perceived average dose-rate. This average dose-rate is normalized to the result of the longest pulse time, which is the most similar to continuous irradiation conditions. Further test results prove that the counting-type EPD Mk2+ dosimeter shows no deficiency compared to the reference detector in the way of the size (maximum three orders of magnitude) of dose-rate jump calibration. The reference detector was a ThermoFisher Scientific TruDose EPD which was developed for pulsed fields. The pulsed field formed by the Gamma-chopper is suitable for modelling and examining the scattered field of a direct beam of a pulsed irradiating X-ray machine. Our results can be used to support the measurement technology and thus the radiation protection of equipment producing pulsed radiation fields, which are also useful for the OAH, as well as licensing and inspection activities.

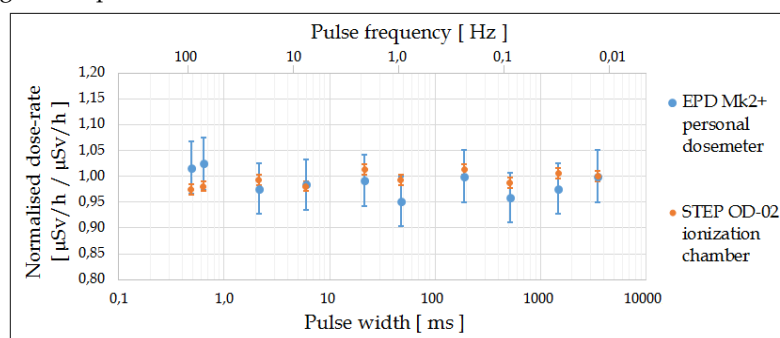


Figure 1: EPD Mk2+ and STEP OD-02 dose-rate comparison as a function of the pulsation time characteristic of the ionizing radiation field created by Gamma-chopper and the line fitting uncertainty is marked ($k=2$)

Remaining work

The project is being continued because we intend to achieve the single pulse capability with a self-developed machine (fantasy name: Gamma-guillotine) to be able to measure the dead time of the detectors, in accordance with IEC/TS 62743.

EFFECTIVE USE OF DOSE PROJECTION TOOLS IN THE PREPAREDNESS AND RESPONSE TO NUCLEAR AND RADIOLOGICAL EMERGENCIES: PART 1

Tamás Pázmándi, Csilla Rudas

Objective

The research in this 3-years long project is focused on the assessment and application of dose projection software, and the main objective is the evaluation of uncertainties in atmospheric dispersion modelling and dose estimation in case of accidental radiological releases. In the first phase of the research, the dose projection capabilities of the involved software were reviewed and compared, and limitations were identified. Selection of the initial and boundary conditions of the benchmark analysis was established and the output quantities and format were decided.

Methods

A benchmark analysis will be carried out with two different dose projection tools to better understand the uncertainties of the dose projection conducted for a radiological release. The assessment performed through a benchmark study will use the SINAC decision support system developed in the Centre for Energy Research and the MACCS engineering-level computer code developed at Sandia National Laboratories. The work was carried out with the participation of the Nuclear Safety Research Institute (NUBIKI).

Results

The two codes use similar basic physical principles: the SINAC uses Gaussian puff dispersion model, while the MACCS code uses Gaussian plume model for atmospheric dispersion calculation. Consequently, with proper selection of input data, no significant differences in the model performance are expected. A principal difference between the two codes is the used coordinate system: MACCS uses a polar, while SINAC uses a Cartesian coordinate system (and geographic coordinate system for handling the meteorological input data from numerical weather prediction models). However, this difference is not a limiting factor if the are to be compared.

The source term and the meteorological input data used by the two codes are in principal the same. The number of nuclides calculated by MACCS is larger, but a consistent set of nuclides can be identified. Both codes are capable of using fixed/constant or time dependent meteorological data sets. SINAC uses a larger set of precipitation types, but a consistent set of precipitation type can be identified.

The comparison of the dose modules of SINAC and MACCS showed that in both codes the dose equation for an early exposure pathway in each spatial element is computed based on the product of the following quantities: radionuclide concentration, usage factor, duration of exposure, dose conversion factor and shielding or protection factor. The quantities used in the dose equations depend on the exposure pathway. The followings are common exposure pathways in codes for different organs: cloudshine, groundshine, skin beta dose, acute (short-term) dose equivalent from direct inhalation of the cloud, lifetime (long-term) dose commitment from direct inhalation of the cloud, total acute (total short-term dose) dose equivalent from all pathways, total committed dose for lifetime (total long-term dose) from all pathways.

In the benchmark study, a simple release scenario was defined. The simulation of the radioactive dispersion will be carried out with a Gaussian puff model in SINAC and with a Gaussian plume segment model in MACCS, for which the common release characteristics were defined. The meteorological conditions for the simulation were selected to be spatially and temporally fixed. Due to the difference in the calculation grid of SINAC and MACCS, the receptor points were defined along a straight line in the wind direction and in the plume centreline at the following distances from the release point: 5.0 km, 7.5 km, 10.0 km, 12.5 km and 15.0 km. The output quantities of the benchmark assessments were selected. The results of the atmospheric dispersion and ground deposition will be the air concentration [Bq s/m³] at effective release height and at 1 m height, and the ground activity [Bq/m²]. Gamma dose rate [Sv/h] will be determined for cloudshine and groundshine. Furthermore, the following dose values will also be compared: effective cloudshine and groundshine dose [Sv], the effective committed inhalation dose [Sv], the equivalent inhalation thyroid dose for adults and the total effective dose [Sv].

Remaining work

In the next phase, the development of the involved software will be carried out to meet the requirements of the case study. Dose assessment calculation will be performed for the selected case, with deterministic input parameters. The uncertainty bands of the input parameters will be chosen. In the final phase of the work, the estimation of uncertainties will be carried out with perturbing the input parameters according to their previously decided uncertainty intervals. The final results of the research will be the assessment and visualization of output uncertainties of the dose projection with a comparison of the performance and effectiveness of the software packages.

Related publication

- [1] T. Pázmándi, Cs. Rudas, A. L. Győri, G. L. Horváth, G. Lajtha: *First Phase: Comparison of SINAC and MACCS software, definition of benchmark scenario*, EK-SVL-2020-345-01-01-00 (2020)

NEUTRON IRRADIATIONS FOR RADIATION-HARDNESS TESTING OF ELECTRONIC SEALING SYSTEMS

Dorottya Jakab, József Pálfalvi, Tamás Pázmándi

Objective

The objective of the work is the neutron radiation-hardness testing of electronic sealing systems developed by the International Atomic Energy Agency (IAEA), which is a necessary step in preparing newly developed safeguards equipment for authorization. The electronic seals are built from commercial-off-the-self electronic components of which radiation-hardness must be tested to indicate any necessary changes to achieve the required radiation tolerance. The Centre for Energy Research (EK) is involved in this project in the neutron irradiations of the equipment units.

Methods

The neutron irradiations have been performed at the Biological Irradiation Facility (BIO), which is the 5th horizontal channel of the Budapest Research Reactor (BRR). The main features of the BIO are the remote-controlled internal filters, the outer collimator with manually operated and changeable filters and absorbers (see in Fig. 1), and the computerized control dosimetry system, suitable for real time monitoring. These functions enable to form a large variety of neutron spectra, thereby providing a versatile platform for neutron irradiations.

In order to determine the ideal filter/absorber arrangements to assure the conformity of the thermal and fast neutron fluences to the pre-defined radiation levels required for IAEA safeguards equipment, and also to simulate the neutron energy spectra corresponding to the filter arrangements, a series of Monte Carlo calculations have been performed. For the experimental determination of the actual neutron fluxes passive activation detectors were used: for the thermal neutron flux measurements detectors consisting of two thick gold ($^{197}\text{Au}(n,\gamma)^{198}\text{Au}$) foils sandwiching a cadmium foil were used, whereas for the fast neutron flux testing sulfur ($^{32}\text{S}(n,p)^{32}\text{P}$) fast neutron threshold activation dosimeters were applied. These simulation- and measurement-based evaluations were also used if the adjustment of the neutron beam parameters were required based on the feedbacks received by the developer of the electronic seals.

The electronic devices placed at the end of the outer collimator were simultaneously irradiated with thermal (<0.5 eV) and fast neutrons (100 keV...10 MeV). The exposure times were determined in accordance with the achievement of the required fluences. The functionality of the different types of electronic devices was continuously monitored during the irradiations using computer programs that track device failures. Several irradiations were also performed using variant filter arrangements (e.g. with different thickness of internal Bi filter, or with inserting outer absorbers and filters of PMMA, Cd, B_4C) to establish reliable correspondences between the fluxes and the detected error rates. Post-irradiation functionality tests and activation measurements of the exposed units were also performed.

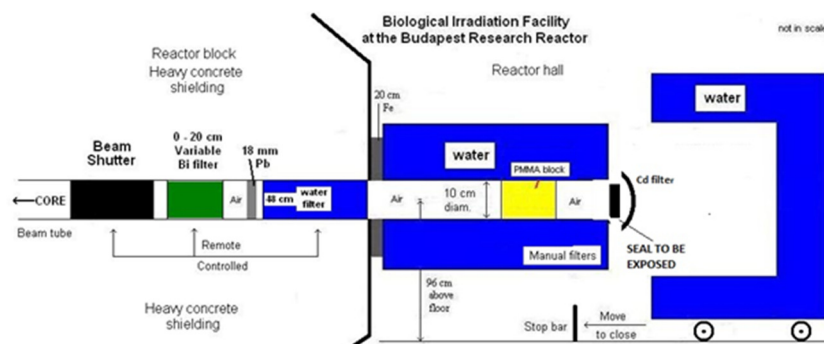


Figure 1: Schematic view of the neutron irradiation test arrangement in the Biological Irradiation Facility [1]

Results

The thermal and fast neutron irradiations allowed the neutron radiation-hardness testing of the IAEA electronic sealing systems to implement the necessary changes in the hardware and firmware to achieve the required level of radiation tolerance.

Remaining work

Since the work is performed in several campaigns within the framework of long-term agreement between the IAEA and the EK, the project continues.

Related publications

- [1] J. Pálfalvi, D. Jakab: *Neutron radiation-hardness testing of electronic seals*, EK-SVL-2020-348-01-01-00, in Hungarian (2020)
- [2] D. Jakab, J. Pálfalvi: *Neutron radiation-hardness testing of electronic seals*, SVL-56/2020, in Hungarian (2020)
- [3] D. Jakab, J. Pálfalvi: *Neutron radiation-hardness testing of electronic seals*, EK-SVL-2020-348-02-01-00, (in Hungarian (2021)

BUDAPEST NEUTRON MONITOR STATION

Attila Hirn, István Apáthy, Antal Csőke, Sándor Deme, Andrea Strádi, Balázs Zábóri

Objective

The intensity of cosmic rays entering Earth's atmosphere is determined by, and is therefore an indicator of the level of solar activity. As solar activity approaches a maximum, the importance of monitoring cosmic rays and understanding their effects and the corresponding dose levels increases. When a transient solar event, such as a solar storm occurs and if it is strong enough, solar cosmic rays can affect electronics and even humans at ground level; this phenomenon is called "Ground Level Enhancement (GLE)". Data from the neutron monitors can be utilized for research on geomagnetic storms, dose effectiveness of cosmic rays and the GLE warning system, predicting changes in cosmic ray intensity and the environmental impact of cosmic rays. Neutron monitor stations are generally used worldwide as a basic space weather research and data service system to monitor the real-time status of the space weather environment of our planet and to provide input data set(s) for operational space weather prediction systems, like in the frame of the Space Safety programme of the European Space Agency (ESA). The main objective of establishing a neutron monitor station in Budapest, Hungary is to complement the international network of neutron monitor stations with a station at mid magnetic latitude at about 450 m above sea level.

Methods

A de facto standard NM-64 type neutron monitor station will be established at the KFKI campus, in the Buda Hills, Hungary. The neutron monitor will include BF₃-filled proportional counters enclosed by polyethylene tubes (neutron moderator) surrounded by lead rings, producing low-energy neutrons from the nucleon component of the incident secondary cosmic rays. In year 2020, a trade-off analysis was performed on the expected costs, the environment (e.g. distance from the Budapest Research Reactor, shielding by neighbouring buildings), and the local infrastructure to select the exact location of the neutron monitor. Literature survey was conducted on the design of and the practices used at other neutron monitor stations in Europe in order to finalize the conceptual design.

Results

Room 303 in the ground floor building 25/3, with a flat roof, located in the Northern part of the KFKI campus was selected for the location of the neutron monitor station. Instead of removing snow from the roof, the system will include a snow depth sensor and correction for the snow effect caused by accumulation of snow on top of the roof will be performed. For comparability of measurement data, the 2061 type Cylindrical BF₃ Neutron Detector, from LND Inc., with effective length of 1956 mm and effective diameter of 149 mm will be used, which is commonly used in the European neutron monitor network. Each neutron counter will have its own front end electronics and counter unit. Data from the counters, the Global Positioning System (GPS) receiver providing the real-time clock, the barometer and the snow depth sensor will be collected with a common system controller and power supply unit. Data packages will be forwarded from the controller unit to a PC, which also serves as interface to the servers forwarding data to the neutron monitor network and to the public.

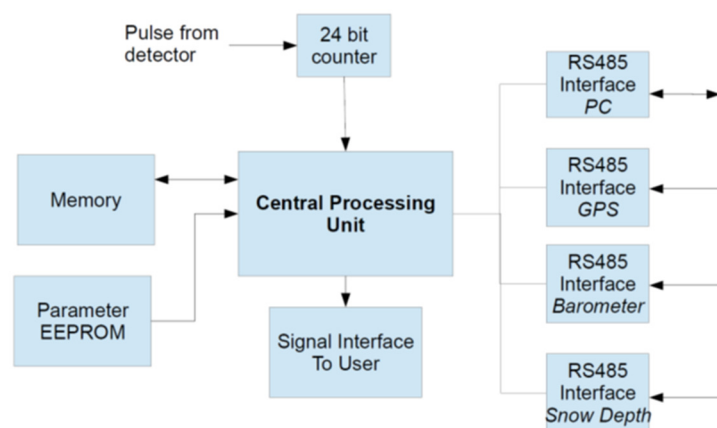
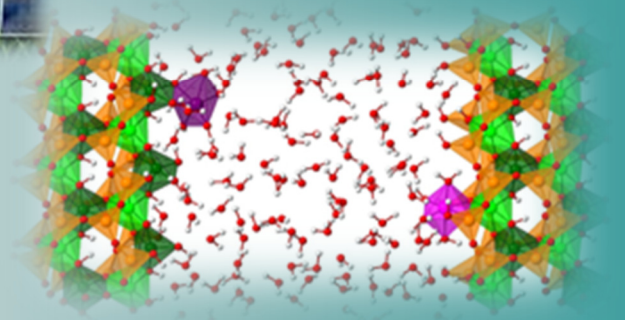


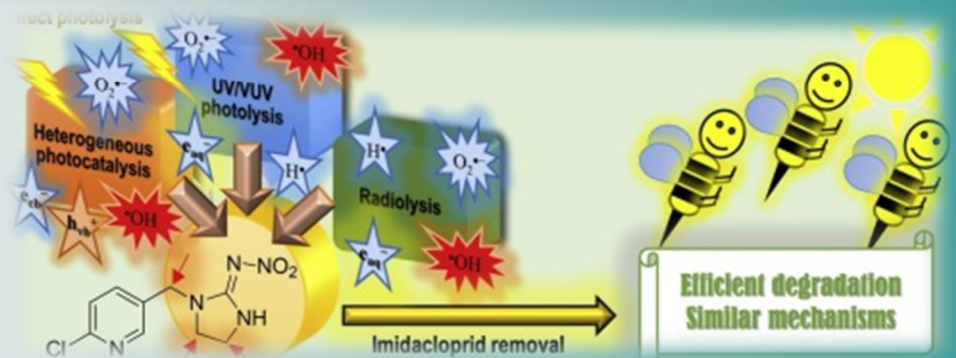
Figure 1: Electrical block diagram of the neutron monitor system
EEPROM (Electrically Erasable Programmable Read-Only Memory)

Remaining work

In year 2021, the architectural and mechanical plans will be finalized, the room for the neutron monitor station will be prepared, the detectors and the associated mechanical and electronic units will be procured and developed, and the neutron monitor will be assembled. Commissioning of the neutron monitor station is due in the first half of 2022, after which the nominal operation can be started.



IV. ENERGY AND ENVIRONMENTAL STUDIES



CATALYTIC SYSTEMS FOR EFFICIENT WATER ELECTROLYSIS

Tímea Benkó, Krisztina Frey, Sahir M. Al-Zuraiji, Zsolt Kerner, Dávid Lukács, Tamás Ollár, Antal Koós, Levente Tapasztó, József S. Pap

Objective

Detailed investigations were carried out on surface-modified working electrodes in order to enhance their efficiency in water electrolysis. We investigated water-insoluble Cu and Fe complexes as modifiers with a catalytic effect in the oxygen evolving reaction (OER), and layered these molecular units onto semiconducting oxides by exploiting hydrophobic interactions. Thin layers of molybdenum sulfide were prepared as electro-active carriers and modified by a rationally designed deposition method for Pt-nanoparticles to achieve as high as possible performance in the hydrogen evolving reaction (HER). The work was supported by the VEKOP 2.3.2-16-2016-00011, the NKFIH 132869/2019 and the NKFIH 128841/2018 grants.

Methods

The ligands, complexes (OER) and the MoS_{2-x}O_x 2D-layers (HER) were synthesized by known methods. Electrochemical experiments were conducted on a Bio-Logic SP-150 or a GAMRY Reference 3000 potentiostat. The working electrodes for the OER included boron doped diamond (BDD), indium tin oxide (ITO), fluorine-doped tin oxide (FTO), and the nanostructured semiconductor α -Fe₂O₃/Ti (provided by a collaborator). For the HER, the 2D-layers of MoS_{2-x}O_x were prepared on a graphite (HOPG) support by the CVD method. MoS₂ were decorated with platinum by electrochemical deposition. The size and the shape of the Pt nanoparticles were determined using scanning electron microscopy (SEM), and scanning tunnelling microscopy (STM). The electrochemical methods used included linear sweep (LSV), cyclic (CV) and square wave voltammetry (SWV), and controlled potential electrolysis (CPE). The produced O₂ or H₂ was quantified by a Shimadzu Tracera 2010 gas chromatograph equipped with a BID detector and a sampling loop. The surfaces of the as-prepared/used electrodes were investigated by X-ray photoelectron spectroscopy (XPS), SEM with energy dispersive X-ray (EDX), Raman and infrared (IR) spectroscopy. Spectro-electrochemistry was carried out by a Cary 60 UV-visible spectrophotometer and a 3-electrode cell.

Results

Encouraged by the successful utilization of a water-insoluble Fe^{II} complex made with the 2-(2'-pyridyl)benzimidazole (PBI) ligand as an additive-free catalyst ad-layer on an ITO electrode [1], we pursued other Fe compounds. The five-coordinate [Fe^{III}Cl₂(tia-BAI)] complex (tia-BAI⁻ = 1,3-bis(2'-thiazolylimino)isoindolate(-)) was found to be a suitable pre-catalyst for the OER providing the active form *via* the exchange of chloride ligands to water molecules [2]. The tia-BAI⁻ pincer ligand confers water-insolubility on the Fe-(tia-BAI) assembly, but it tolerates the presence of water in acetone and produces an electrocatalytic current associated with molecular OER catalysis. Upon addition of water to [Fe^{III}Cl₂(tia-BAI)] in acetone, the changes in the Fe^{3+/2+} redox transition and the UV-visible spectra could be associated with solvent-dependent equilibria between the aqua and chloride complex forms. Immobilization of the complex on the ITO substrate by means of drop-casting resulted in OER in a borate buffer. The detected O₂ at pH 8.3 indicates >80% Faraday efficiency by a TON>193. Analysis of the elemental composition of the complex/ITO assembly by SEM-EDX and XPS before and after CPE, and re-dissolution tests suggest that an immobilized molecular catalyst is responsible for the OER and its de-activation occurs by depletion of the metal. According to initial LSV experiments under visible light irradiation, some of these Fe-ligand units are suitable surface catalysts in photo-electrocatalytic OER, when combined with the photo-reactive carrier α -Fe₂O₃/Ti. The Fe-ligand/ α -Fe₂O₃/Ti hybrid system exceeded the photocurrent of α -Fe₂O₃/Ti by 1.5-2-times, which points to the next steps in the investigation.

The OER by a Cu(II) complex, [Cu^{II}(py-BAIH)(ClO₄)(NCCH₃)](ClO₄), with a similar pincer ligand, py-BAIH = 1,3-bis(2'-pyridyl)iminoisoindoline, took a surprising mechanistic pathway described below. Under homogeneous conditions in an acetonitrile-water mixture, electrochemical and spectroscopic investigations, supported by DFT calculations, suggest that the reaction starts with the oxidation of the ligand while detection of a Cu³⁺ species was not possible, making its role in OER catalysis unrealistic. Utilization of the immobilized complex/ITO in CPE led to OER with a 69% Faradaic efficiency. During 20 h of electrolysis the complex dissolved to the aqueous phase and worked as a stable homogeneous catalyst without CuO_x/Cu(OH)₂ formation on the ITO. UV-vis and IR spectroscopy indicated the presence of [Cu^{II}(ind)(OH)] in the buffer. SEM-EDX and XPS showed the almost complete dissolution of the complex from the ITO (or FTO) surface. Hardly any Cu species persisted on it. This is consistent with the results on the homogeneous system and DFT calculations. In conclusion, the ligand-centred redox activity may be the key to a stable homogeneous system, saving the catalyst from oxidative degradation [3].

For the HER catalysts, the size of the Pt-nanoparticles on the 2D MoS_{2-x}O_x surface was controlled by electrochemical deposition parameters. This method can be used to determine the relationship between Pt particle size and H₂ production efficiency and allows for the determination of the optimal size of nanoparticles for the HER. These modified chalcogenide surfaces are highly durable in electrocatalytic HER, some of which are close in performance to the industrial Pt/C.

Related publications

- [1] S. M. Al-Zuraiji, T. Benkó, L. Illés, M. Németh, K. Frey, J. S. Pap: *Utilization of Hydrophobic Ligands for Water-Insoluble Fe(II) Water Oxidation Catalysts - Immobilization and Characterization*, J. Catal. **381**, 615 (2020)
- [2] S. M. Al-Zuraiji, D. Lukács, M. Németh, K. Frey, T. Benkó, L. Illés, J. S. Pap: *An Iron(III) Complex with Pincer Ligand – Catalytic Water Oxidation through Controllable Ligand Exchange*, Reactions **1**, 16 (2020)
- [3] T. Benkó, D. Lukács, K. Frey, M. Németh, M. Móricz, D. Liu, L. Vayssieres, É. Kováts, N. May, M. Li, J. S. Pap: *Redox-Inactive Copper in a Molecular Water Oxidation Electrocatalyst*, JACS Au, submitted.

METHANE DRY REFORMING ON IN AND CeO₂ PROMOTED Ni/Al₂O₃ CATALYSTS

Miklós Németh, Andrea Beck, Gergely Nagy, Anita Horváth

Objective

The development of viable and economical, non-coking and highly active catalysts for synthesis gas production by CO₂ (dry) reforming of methane (DRM: CH₄+CO₂⇌2CO+2H₂) was the aim of this work. Lately, the value of the addition of an indium modifier to inhibit coking on silica-supported nickel has been discovered in our laboratory. This research was extended to explore the potential of the In promotion, studying its effect on the Ni/Al₂O₃ catalyst and to compare it with the often applied ceria promotion. Moreover, the simultaneous effect of ceria and In additives was also investigated.

Methods

For catalyst synthesis, Al₂O₃ and 8 wt% CeO₂/Al₂O₃ supports (prepared by wet impregnation of alumina with Ce-nitrate) were used. Ni or Ni and In together were introduced by the deposition precipitation (DP) method, providing 3wt%Ni and 0.3wt% In loading. Catalyst characterizations by Temperature Programmed Reduction (TPR), X-ray diffraction (XRD), Transmission Electron Microscopy (TEM) with elemental mapping, X-ray Photoelectron Spectroscopy (XPS) and Diffuse Reflectance Infrared Fourier Transform Spectroscopy (DRIFTS) to measure the adsorbed CO were performed. The catalytic properties were investigated under temperature ramped CH₄-decomposition experiments and during a 6-hour DRM reaction at 650 °C in plug flow reactors. Coke formation in both cases were analysed by Thermogravimetric Analysis (TGA) and Temperature Programmed Oxidation (TPO), respectively.

Results

The presence of the indium promoter increased the Ni size on both the Al₂O₃ and the CeO₂-Al₂O₃ supports and widened the size distribution, but the average particle sizes ranged only between 4.5-5.7 nm. Elemental mapping revealed the presence of In in NiIn bimetallic particles and also on the oxide support. TPR and XPS suggested that indium promoted the reduction of nickel-oxide but some of the Ni²⁺ still remained in the surface Ni-aluminate after reduction in all the samples. Regarding the CeO₂ distribution, ceria rich territories were not necessarily overlapped with areas where Ni(In) particles were numerous. CO chemisorption followed by DRIFTS measurements on the In-promoted samples showed an enhanced ratio of linear/bridged CO species and a strong red shift for all carbonyl bands compared to the corresponding reference Ni samples, which can occur only if Ni is alloyed with indium, inducing geometric and electronic effects. XPS proved that ceria had a higher surface concentration with a higher ratio of Ce³⁺ centres after reduction due to indium promotion.

Temperature ramped CH₄ decomposition followed by TGA pointed out firstly that the NiIn/CeO₂-Al₂O₃ sample is the least active in CH₄ decomposition and produces only an easily oxidizable, probably amorphous surface carbon, and secondly that indium alone (without ceria) has an effect on the morphology and/or the oxidation kinetics of graphitic coke deposited from methane.

In the DRM test reaction at 650 °C, the highly active Ni/Al₂O₃ and Ni/CeO₂-Al₂O₃ samples coked heavily and the reactors were blocked by carbon. The co-presence of ceria and indium additives resulted in the least coking but also the least activity. This shows that there is a sensitive compromise between activity and coking tendency. In this sense indium promotion seems to be more efficient than ceria, because it still causes a low coking at a higher activity.

The similarity of average Ni particle size among the catalysts highlighted that the particle size itself is not the main governing parameter for the different catalytic properties during the reaction, but it is rather the Ni-promoter interaction. In the reduced state of the catalyst, indium is alloyed with nickel, while a small amount is mixed with CeO₂ and alumina. In³⁺ incorporated in the ceria lattice results in more Ce³⁺ with higher stability at the interface of Ni and ceria-indium-oxide providing an additional new platform for CO₂ activation. The extra CO₂ transformation resulting in more reactive oxygen or H₂O (via reverse water gas shift reaction) fosters the gasification of surface carbon. On the other hand indium alloyed with nickel lowers the CH₄ dissociation activity via electronically perturbing the surface nickel sites, and due probably to the retarded carbide formation, slows down the transformation of reactive surface carbon into inactive coke. Based on all the results, it is found that in the 3%Ni0.3%In/CeO₂-Al₂O₃ catalyst indium plays a double role as a reducible oxide-modifier, and also as a metal modifier and it decreases coking to a very low 1.3 wt% carbon content during a 6-hour reaction via a fine interplay between the In/InO_x over/around the nickel particles interacting with the CeO_x-Al₂O₃ matrix.

Remaining work

A detailed DRIFTS investigation on the same samples will be summarized very soon in the form of our next submission.

Related publication

- [1] A. Horváth, M. Németh, A. Beck, B. Maróti, G. Sáfrán, G. Pantaleo, L. Liotta, A. M. Venezia and V. La Parola: *Strong impact of indium promoter on Ni/Al₂O₃ and Ni/CeO₂-Al₂O₃ catalysts used in dry reforming of methane*, to be submitted.

PREVENTING THE DEVELOPMENT OF ANTIBIOTIC RESISTANCE IN WASTEWATER MATRICES BY HIGH ENERGY IRRADIATION

Renáta Homlok, Krisztina Kovács, Tünde Tóth, Erzsébet Takács, László Wojnárovits, László Szabó

Objective

The objective was to establish the conditions for the high-energy-radiation-induced destruction of antibiotics by following the change in both biodegradability and antimicrobial activity in a synthetic effluent wastewater matrix.

Methods

Electron beam (EB) treatment was performed using a vertically mounted Tesla Linac LPR-4 type linear electron accelerator. In order to assess the applicability of this technique for eliminating the sub inhibitory effects of antibiotics on the selection of resistant bacteria, a microbiological assay was introduced. The test is based on the dynamics of a mixed (sensitive/resistant) bacterial population in response to the presence of antibiotics in a concentration range well below the minimum inhibitory concentration (MIC) in a synthetic wastewater matrix. Sensitive and resistant subtypes of *Staphylococcus aureus* in a 1:1 ratio are added to the test medium, after an appropriate incubation period. The number of resistant cells on the antibiotic-containing plate and the total number of cells on the control plate without antibiotic were counted. Then the fraction of resistant strains compared to all the colonies (sensitive and resistant) were determined.

Results

Using advanced oxidation treatment, the selective pressure on the bacterial population favouring the predominance of resistant mutants can be eliminated. This is achieved when the fraction of resistant bacteria, within a statistically insignificant deviation, is the same as in the control sample. In other words, the difference between the control sample and the sample containing the antibiotic (piperacillin) is no longer significant in terms of the ratio of resistant and susceptible bacteria population. A synthetic effluent wastewater was designed to be a kinetically appropriate reflection of a real sample while containing the antibiotics at sufficiently high concentration for microbiological assay. We were looking for the absorbed dose that could eliminate the effect of antibiotics on microorganisms in a modelled wastewater, so that we could reduce the resistance to the given antibiotic in the given matrix.

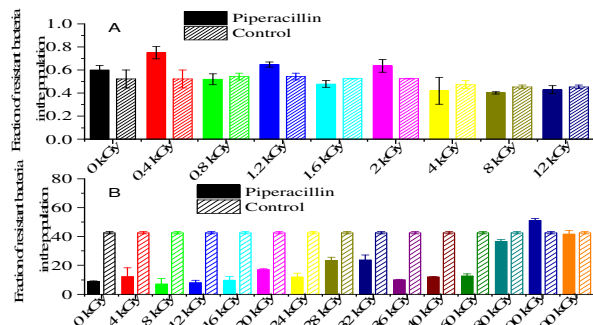


Figure 1: (A) Fraction of resistant bacteria in a population that was spiked with piperacillin sample irradiated in pure aqueous solution. (B) Fraction of resistant bacteria in a population that was spiked with piperacillin sample irradiated in model wastewater solution. The control did not contain antibiotics in either case.

In piperacillin aqueous solutions at 4 kGy as a starting point, there is no significant change from the control sample, and it can be stated that the selective pressure has eventually been eliminated (Fig. 1A). It was shown in our previous studies that in case of penicillin derivatives several products form that can retain the biological activity of the original molecule. When irradiation is done in a complex wastewater matrix, markedly different system is generated, which can eventually give rise to considerably different outcomes. In case of piperacillin we can see that the population is dominated by the sensitive strain until 60 kGy, this phenomenon might be explained in terms of substantial fitness costs of being resistant.

At higher doses we assume that probably products from humid acid exhibits some effect on the population, as we can see in the case of piperacillin (Figure 1B), the population becomes dominated by the resistant mutant.

It should be mentioned that although at first sight it appears to be delighting that the amount of resistant subtypes is suppressed, it must be recognized that they are under continuous effect of the antibiotic and this circumstance might lead to slow but further mutation event.

Remaining work

Using this method, we plan two series of experiments in the next year, in one of them wastewater matrix with antibiotic and bacteria, in the other one wastewater matrix with only bacteria will be used. During these experiments, we will add bacteria to the samples prior to irradiation. The results of these two experiment series will be compared.

BIOGENIC CARBON CONTENT DETERMINATION OF CATALYTICALLY CONVERTED BIOMASS

Tamás Korányi

Objective

The optimization of measuring conditions for direct liquid scintillation counting (LSC) of biomass originated samples for the determination of the biogenic carbon content of catalytically converted biomass.

Methods

The determination of the biomass content of biocarbon/fossil carbon mixtures (cellulose, lignocellulose and lignin derivatives) by radiocarbon (^{14}C) liquid scintillation counting (LSC) and by accelerator mass spectrometry (AMS). This determination depends on the fact that there is no ^{14}C in the fossil-carbon.

- Direct LSC: The product mixture was dissolved directly in the scintillation cocktail and its biogenic carbon content was measured in LSC equipment. This method is only applicable using colourless or slightly coloured samples.
- AMS-graphite method: Samples were burned and the carbon dioxide thus produced was graphitized in sealed reaction tubes. AMS measurements of the graphitized samples were performed in Debrecen at ATOMKI (Mihály Molnár).

Results

The cooperation with our Dutch partners, who moved in the meantime to Austria, (Prof. Katalin Barta and Bálint Fridrich, University of Graz) has been continued. We published a review paper (see below) and analysed a sixth sample series by ^{14}C LSC using direct counting. Despite their increased biogenic carbon contents, only the cellulose originated samples gave measurable signals. Therefore we decided to continue these measurements by the AMS-graphite method in Debrecen.

Our new Swedish partner (Prof. Christian Hulteberg, Lund University) sent us catalytically converted lignin - vacuum gas oil (VGO) samples where lignin is the starting biomass material. Due to their dark brown colour we were not able to measure their ^{14}C content by our direct LSC method, and therefore they were analysed by AMS in Debrecen. The original VGO did not contain any biocarbon, but all catalytically treated VGO reference samples contained a definite 4 - 8 % modern carbon. The biocarbon content of lignin originated samples is 2-3 times larger than in their counterparts containing only VGO. The detailed results are not shown because they were not published yet.

Remaining work

We plan to enhance the precision of ^{14}C detection from biomass samples by LSC. We assume that colour and free radicals in the sample mixture causes chemiluminescence and these effects can be eliminated by treating the solutions by novel proper chemicals.

Related publication

- [1] T.I. Korányi, B. Fridrich, A. Pineda, K. Barta: *Development of 'Lignin-First' Approaches for the Valorization of Lignocellulosic Biomass*, *Molecules* **25**, 2815 (2020). DOI: 10.3390/molecules25122815.

DEGRADATION OF PROPRANOLOL IN DILUTE AQUEOUS SOLUTION BY HIGH ENERGY IONIZING RADIATION

Krisztina Kovács, Tünde Tóth, László Wojnárovits

Objective

The aim of this present study was to demonstrate that the beta-blocker, propranolol (PRO) can be efficiently degraded in one-electron oxidation and reduction reactions.

Methods

The samples in the end-product experiments were irradiated in a panoramic type ^{60}Co - γ irradiation chamber (dose rate = 10 kGy h⁻¹) with doses 0, 0.2, 0.4, 0.6, 0.8, 1, 2.5, 5, 7.5 and 10 kGy under different conditions. The initial PRO concentration was 0.1 mmol dm⁻³. The samples before and after irradiation were characterized using a JASCO 550 UV-Vis spectrophotometer with a 1 cm optical length cell and applying appropriate dilutions before taking the spectra. The transient intermediates of degradation reactions were investigated by the pulse radiolysis technique using 4 MeV accelerated electrons with an electron pulse length of 800 ns and utilizing kinetic spectrophotometric detection with a 1 cm path length cell. In order to identify and quantify the participating free radicals with different reduction potentials, redox titration measurements were conducted. The time (dose) dependence of degradation was characterized by chemical oxygen demand (COD) and total organic carbon (TOC) content measurements.

Results

In water radiolysis, hydroxyl radicals and hydrated electrons are responsible for the degradation reactions in dilute aqueous solutions of different solutes. The transient intermediates formed in PRO solutions showed absorption maxima at 325 and 380 nm. These intermediates were identified as hydroxyl cyclohexadienyl type radicals (OH adducts). The presence of OH adducts was proven by a redox titration experiment with $\text{K}_3[\text{Fe}(\text{CN})_6]$. In the hydroxyl radical + PRO reaction, aminium type radicals may also form. The rate constant measured for the PRO + hydroxyl radical reaction was $7.6 \times 10^9 \text{ mol}^{-1} \text{ dm}^3 \text{ s}^{-1}$. Hydroxyl radicals showed higher reactivity towards PRO, which has a naphthalene component than towards other beta-blockers possessing a benzene ring. The hydrated electrons ($k = 8.5 \times 10^9 \text{ mol}^{-1} \text{ dm}^3 \text{ s}^{-1}$) can also effectively contribute to PRO degradation. Based on pulse radiolysis and UV-Vis measurements, the contribution of hydroxyl radicals and hydrated electrons to the degradation was shown to be similar. At higher doses (1-10 kGy) light scattering was observed in the samples when hydroxyl radicals reacted with PRO, indicating the formation of scarcely soluble products in water. In an N_2 saturated solution containing *tert*-butanol, this phenomenon was not observed (hydrated electron reaction). The efficiency of the decomposition was measured based on the decreases of the chemical oxygen demand and total organic carbon content values.

Remaining work

The separation and identification of degradation products is an important task for the understanding of the degradation mechanism of PRO. In order to get a comprehensive picture about the degradation processes, we intend to perform mass spectrometric measurements in the future.

BIMETALLIC GOLD CATALYSTS IN AEROBIC SELECTIVE OXIDATION OF ALCOHOLS

Gergely Nagy, Andrea Beck

Objective

The PhD work of Gergely Nagy aimed at obtaining a better understanding of the selective alcohol oxidation on gold-based catalysts by searching for correlations between the catalyst structure and the catalytic properties in order to support the development of improved catalysts. Special attention was paid to the effects of a second metal (Ag, Ru, Ir) and of the support material (SiO₂, Al₂O₃, MgO, MgAl₂O₃ and hydroxyapatite (HAP)) as well as to other influencing factors which can modify these effects in the reaction.

For 2020 the following tasks were planned: (i) completion of the publication process of the paper on the alumina supported AuRu and AuIr catalysts, (ii) finalising the thesis for the pre-defence, (iii) pre-defence, (iv) submission of the thesis after final corrections.

Methods

For structural characterisation of the supported bi- and monometallic catalysts synthesized typically by sol adsorption, and in some cases also by solvated metal atom deposition methods, the following techniques were used: prompt- γ -activation analysis, transmission electron microscopy, UV-vis spectroscopy, X-ray diffraction, X-ray photoelectron spectroscopy, temperature programmed oxidation, reduction, CO₂ and NH₃ desorption, CO adsorption measurements followed by diffuse reflectance Fourier-transform infrared (DRIFT) spectroscopy. The catalysts were studied in selective liquid phase oxidation of benzyl alcohol and glycerol (the latter in a bilateral co-operation) with oxygen, and several catalysts also in CO oxidation.

Results

1. On Au-Ag/SiO₂ catalysts, CO oxidation occurs via at least two different mechanisms which have different active temperature ranges. The reaction mechanism changes with increasing temperature. The two mechanisms have different active centres. Hydrogen reduction favours the formation of the active centres of the high temperature mechanism. Furthermore, the centres of the low temperature activity must contain gold atoms.
2. The presence of nanoscale gold particles alone is not a sufficient condition for the benzyl alcohol oxidation in an organic solvent. The presence of a proper promoter is also needed (e.g. basic surface sites or added base, water, a second metal) for the catalysis. Promoters can assist in the deprotonation of benzyl alcohol (basic centres, water), modify the charge state of Au centres (second metal, acid-basic properties of support) thus helping the adsorption of the substrate and the β -hydride elimination, or contribute oxygen activation (second metal), which favours the regeneration of the Au centres. The quality of the OH groups affects the selectivity.
3. There is a strong synergetic effect between gold and silver on a SiO₂ support in base-free benzyl alcohol oxidation if on the surface of bimetallic particles the concentration of gold atoms is larger. It implies that the adsorption of the substrate requires a minimum contiguous gold surface. The trend of Au:Ag atomic-ratio-dependent change in catalytic activity is similar to that previously published for glucose oxidation, which indicates the similarity of the active centres in the two reactions.
4. Adding silver to gold (Au:Ag = 4:1 atomic ratio) results in improved activity of the AuAg/Al₂O₃ catalysts made by both sol adsorption and solvated metal atom deposition methods in the selective oxidation of glycerol. For the sol derived catalyst it was demonstrated for the first time that silver promotes the further oxidation of glyceric acid to tartronic acid.
5. Au-Ru and Au-Ir bimetallic nanoparticles were made in aqueous media in a way which have not been used before; Au and Ru, or Au and Ir precursor ions were co-reduced by NaBH₄ in the presence of polyvinyl alcohol (PVA) stabilizer. According to the STEM-EDS examinations, the modifier metal (Ru, Ir) is enriched on the surface of the bimetallic particles. This structure remains on the aluminium-oxide support after calcination and following reduction at 400 °C.
6. Based on the activity per unit of the total molar amount of the metals, the Au-Ru/Al₂O₃ and the reduced Au-Ir/Al₂O₃ were somewhat less active than the Au/Al₂O₃ for benzyl alcohol oxidation in the presence of a base (K₂CO₃), while the Ru/Al₂O₃ and the Ir/Al₂O₃ had a negligible activity. However, based on the comparison of the estimated activity per unit of the surface Au atoms, a synergetic effect between Au and Ru, and in reduced state between Au and Ir is suggested.

Remaining work

Completion of the doctoral procedure (defence).

Related publications

- [1] G. Nagy, T. Gál, D. F. Srankó, G. Sáfrán, B. Maróti, I. E. Sajó, F.-P. Schmidt, A. Beck: *Selective aerobic oxidation of benzyl alcohol on alumina supported Au-Ru and Au-Ir catalysts*, *Molecular Catalysis* **492**, 110917 (2020)
- [2] G. Nagy: *Study of Gold Containing Bimetallic Catalysts in Selective Aerobe Oxidation of Alcohols*, PhD thesis, submitted in 2020

EVOLUTION MODELS OF THE POWER GRID BASED ON THE RATE OF SYSTEM DEVELOPMENT AND SETTLEMENT STRUCTURES

Bálint Hartmann, Viktória Sugár, Kazsoki Attila

Objective

Since the introduction of small-world and scale-free properties, there is an ongoing discussion on how certain real-world networks fit into these network science categories. While the electrical power grid was among the most discussed examples of these real-world networks, published results are controversial, and studies usually fail to take the aspects of network evolution into consideration. Consequently, there is a broad agreement that power grids are small-world networks and might show scale-free behaviour; although very few attempts have been made to find how these characteristics of the network are related to grid infrastructure development or other underlying phenomena. In this work the authors used the 70-year-long historical dataset (1949–2019) of the Hungarian power grid to perform network analysis, which is the first attempt to evaluate small-world and scale-free properties on long-term real-world data.

Methods

The authors have assembled the network data using various sources, including hand-written notes, anniversary books, statistical publications, maps and personal consultations. Since none of the sources were consistent, certain pre-processing and standardisation had to be made. In the database, a new node was created when a substation was first constructed, regardless of the installed switchgear and the type of the busbar. A new edge was created when a power line was put into operation. Double lines are handled as single connections. Infrastructural elements were removed from the database in the year of decommissioning. The final database spans over 70 years and includes 400 nodes and 774 edges.

Results

It was observed that most network properties stabilized at practically constant values after the initial phase of grid evolution. This phase took approximately 20 years and was closed by the introduction and deployment of the 220 kV voltage level, which has connected distant nodes of the network, and formed a meshed topology. Four periods of grid development were identified, during which the clustering coefficient (and thus the small-world coefficient) of the network has significantly increased (Fig. 1). All of these periods were related to the introduction of new voltage levels and the creation of meshed/looped topological formations, which is atypical in single voltage level subnetworks of the power grid. The authors have concluded that power grids show small-world behaviour only if they consist of multiple voltage levels. Power-law and exponential fits to cumulative node degree distributions have shown that power-law fits perform poorly for nodes with high connectivity, thus the use of exponential fits should be preferred.

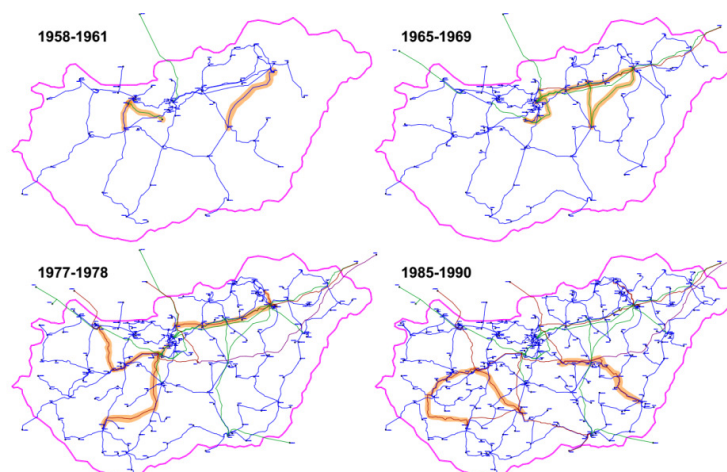


Figure 1: Four periods of network development activities, which have significantly increased the clustering coefficient of the network.

Remaining work

The remaining work consists of the survey of the development of grid systems at settlement scale. For this step, case study settlements were chosen which represent main Hungarian urban fabric types.

Related publications

- [1] B. Hartmann, V. Sugár: *Searching for small-world and scale-free behaviour in long-term historical data of a real-world power grid*, Scientific Reports (under review, pre-print available: <https://arxiv.org/abs/2010.09315>)

BIVALENT RADIONUCLIDE ADSORPTION ON CLAY MINERALS

Annamária Kéri, Ottó Czömpöly, János Osán

Objective

The investigations of the high-level waste (HLW) repository have so far demonstrated the achievability of long-term safety. The evolution of the geochemical environment in the nearfield of the HLW site however requires further studies to reduce the uncertainties and to optimize the repository design. The unaltered bentonite backfill, which consists of predominantly clay minerals, plays a particularly important role in the near field to ensure a stable and suitable chemical environment. Argillaceous formations are considered as host rocks in several European countries, and also in Hungary the Boda Claystone Formation (BCF) is being studied. The sorption behaviour of radiocontaminants (e.g. UO_2^{2+} , Ni^{2+}) is mostly determined by their interaction with clay mineral-water interfaces. However, the stability of the uranium retention mechanism and the exact nature of the sorption complexes have remained unclear.

Methods

A combination of *ab initio* simulations and X-ray absorption spectroscopy (XAS) calculations [1] was used for the study of uranyl adsorption. The structure relaxations and the molecular dynamics simulations were performed based on the density functional theory (DFT) using the Gaussian plane wave method as it is implemented in the QUICKSTEP module of the CP2K code. The theoretical XAS spectra were calculated based on molecular configurations derived from *ab initio* structure optimizations. Real space multiple scattering theory was used for extended X-ray absorption fine structure (EXAFS) as it is implemented in the FEFF 8.40 software.

Concentration dependence of the partition coefficient (R_d) of Ni^{2+} between the solid and liquid phases – sorption isotherm – was recorded on crushed BCF core samples and petrographic thin sections in the high concentration region (10^{-3} – 10^{-5} M) of the liquid phase. Total reflection x-ray fluorescence (TXRF) and microscopic X-ray fluorescence (μ -XRF) measurements were used for elemental analysis of the liquid and solid phases, respectively.

Results

The relaxed structures of the different bidentate uranyl adsorption models at the two most relevant montmorillonite edge surfaces were determined (Figure 1) and their relative energies were calculated to determine the most stable adsorption complexes [2]. The results show that uranyl prefers to bind to the octahedral sheet through two so-called bridging oxygen atoms (Figure 1a,b) or it sits into the defect of the *cis*-like site binding to the (110) montmorillonite edge surface through one octahedral and one tetrahedral bridging oxygen (Figure 1c). The structural parameters (interatomic distances and coordination number) of uranium- (bridging, axial and water) oxygen agreed well for the most stable models with two octahedral bridging oxygens [2].

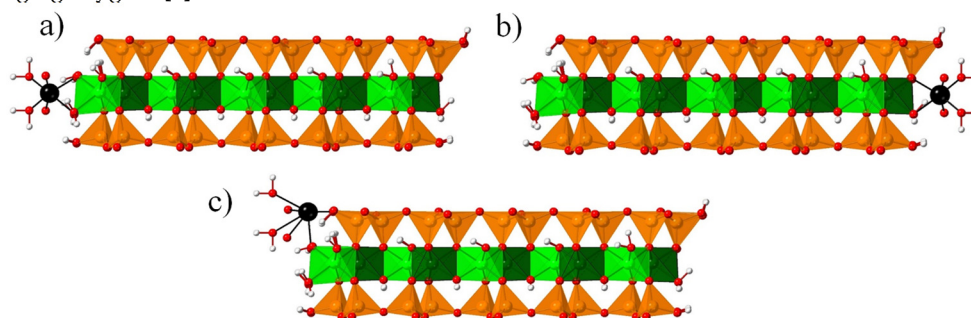


Figure 1: Relaxed structures of the most stable inner-sphere binuclear uranyl complexes. In panels a and b, the uranyl ion binds to the octahedral sheet, while in panel c, one of the bridging oxygens is in the octahedral, the other is in the tetrahedral sheet. Alumina octahedra are shown in green, silica tetrahedra are orange, uranium is marked with black colour, while red and grey colours correspond to oxygen and hydrogen atoms, respectively. The different octahedral occupational sites can be distinguished by the different relative position of hydroxyl (OH^-) groups (the *cis*-site is marked with lighter, while the *trans*-site is shown with the darker green colours).

Transferability of sorption from diluted (crushed) to compacted (thin sections) systems was tested through comparison of R_d values resulting from macroscopic (TXRF) and microscopic (μ -XRF) measurements. Promising results were obtained in the high concentration region. The concentration dependence of R_d values of both macroscopic and microscopic measurements are in agreement with the Ni^{2+} sorption isotherm previously measured using radiotracer on crushed BCF samples.

Related publications

- [1] A. Kéri, R. Dähn, M. Marques Fernandes, A. Scheinost, M. Krack, S. V. Churakov: *Iron Adsorption on Clays Inferred from Atomistic Simulations and X-ray Absorption Spectroscopy*, Environ. Sci. Technol. **54**, **19**, 11886–11893 (2020)
- [2] A. Kéri, R. Dähn, M. Krack, S.V. Churakov: *Uranyl adsorption on montmorillonite edge surfaces*. Clay and Clay Minerals, will be submitted

THE EFFECT OF CHEMICAL COMPOSITION OF CONCRETE ON ITS LONG-TERM PERFORMANCE IN AN IRRADIATED ENVIRONMENT (V4-KOREA RADCON)

K. Gméling, V. Szilágyi, I. Harsányi, L. Szentmiklósi

Objective

During the construction of the new nuclear power plant units for Paks II, the concrete structures will be made preferably from domestic raw materials. For this reason, we have to be prepared with suitable recipes for radiation-resistant, durable concretes with low activation susceptibility. The key to achieve that goal is the careful selection of the raw materials (gravel and sand) based upon the compositional data obtained by analytical and petrological methods. Analysis of the chemical composition of the concrete surrounding the reactor vessel is important because they are exposed to high flux radiation, so their constituents might be substantially activated. Due to the neutron radiation, the high-neutron-capture-cross-section nuclides with short and long half-life become highly radioactive during the reactor operation time, while isotopes with long half-lives remain radioactive in the years following the reactor shutdown.

Results

(1) Prediction of the neutron-induced concrete activity: We calculated the expected radionuclide inventories following neutron irradiation. Since all concretes contain oxides as major components, most of the long lived activity comes from the β -decay of ^{14}C created from ^{17}O via the (n,α) reaction. Unlike the gamma dose rate which can be measured and can be minimized by the proper choice of ingredients, this is hard to measure, and hence more practical to calculate. Elemental compositions of three concrete types, considered in the European Spallation Source European Research Infrastructure Consortium (ESS ERIC), Sweden, were determined via XRF, PGAA, and NAA [1]. Realistic MCNP material input cards were created and validated against measured data of neutron-irradiation experiments.

(2) Neutron flux calculations via MCNP6: The radioisotope production calculation also requires the energy and spatial distribution of the neutrons. This can be obtained via MCNP6 simulations. A detailed MCNP6 model of the Budapest Research Reactor was constructed and preliminary flux values were calculated at relevant positions inside the reactor. This will be used to better plan the in-core activation of samples and to experimentally validate the radioisotope inventory. At the RAD facility, where new biological shielding is being designed, detailed MCNP6 calculations were made for neutron and gamma attenuation features of various shielding options, in which composition, density and thickness were all varied.

(3) Material characterization: A comprehensive petrographic [2] and composition data library of raw materials is being compiled to feed into the radionuclide inventory simulation codes. We continued the geochemical characterization of domestic aggregate additives and of cement samples provided by our collaborators, using NAA and PGAA. Four cements, four clays, two limestones, four slag samples, one ore powder and ore slag, one gypsum, and three clinkers were analysed to assess their applicability as gamma-ray shielding around the active zone of the reactor. A standard and a heavy concrete from NuviaTech, several experimental concretes from Oxydtron Company Ltd. and ÉMI Non-Profit LLC for Quality Control and Innovation in Building were analysed for composition and their linear attenuation coefficients were measured against X-rays and neutrons. In synergy with the K124068 OTKA grant, the PGAA methodology was extended for bulky pieces of concretes and whole rocks [3], by properly correcting for the neutron self-shielding and gamma self-absorption effects.

(4) Chemical characterization study on scrap rock recycling: Red andesite samples from the scrap dump of the andesite rock mine at Gyöngyössolymos (NE Hungary) were investigated. Elevated hydrogen and iron content, higher than the average of fresh andesite, was found. Due to its favourable chemical characteristics, this material can be recycled as a heavy-weight (due to the presence of iron-rich minerals like limonite or hematite) and hydrogenous (with high neutron capture cross-section, like serpentinite) aggregate in neutron or gamma shielding concretes.

A BSc thesis was prepared and submitted to the Eszterházy Károly University by Alexandra Juhász [6].

Related publications

- [1] D. Hajdú, E. Dian, K. Gméling, E. Klinkby, C. P. Cooper-Jensen, J. Osán, P. Zagyvai: *Experimental study of concrete activation compared to MCNP simulations for safety of neutron sources*. (Accepted) Applied Radiation and Isotopes (2021)
- [2] V. Szilágyi, K. Gméling, S. Józsa, I. Harsányi, L. Szentmiklósi (2021): *Oligomictic alluvial aggregates: evaluation of sandy gravel formations on the middle course of the Danube (Hungary) for construction industry applications*. Submitted to Bulletin of Engineering Geology and the Environment
- [3] L. Szentmiklósi, Z. Kis, B. Maróti, L.Z. Horváth: *Correction for neutron self-shielding and gamma-ray self-absorption in prompt-gamma activation analysis for large and irregularly shaped samples*, J. of Anal. Atomic Spectr. **36**, 103 – 110 (2021)
- [4] J. Dragomirová, M.T. Palou, E. Kuzielová, M. Žemlička, R. Novotný, K. Gméling: *Optimization of cementitious composite for heavyweight concrete preparation using conduction calorimetry*, J. of Thermal Anal and Calorimetry **142**, 255–266 (2020)
- [5] D. Józwiak-Niedźwiedzka, A. Antolik, K. Dziedzic, K. Gméling, K. Bogusz: *Laboratory investigations on fine aggregates used for concrete pavements due to the risk of ASR*, Road Materials and Pavement Design (2020)

<https://doi.org/10.1080/14680629.2020.1796767>

- [6] A. Juhász: *Északnyugat magyarországi homokminták nehézasványainak nyomelem-összetétel vizsgálata Neutronaktivációs Analitikai (NAA) módszerrel.*, Eszterházy Károly Egyetem, Eger. (2020)

ELIMINATION OF OXACILLIN, ITS DEGRADATION PRODUCTS, THEIR TOXICITY AND ANTIBACTERIAL ACTIVITY BY USING IONIZING RADIATION

Tünde Tóth, Erzsébet Takács, László Wojnárovits, Renáta Homlok, Krisztina Kovács

Objective

The objective was to obtain information about the chemical changes caused by electron beam and γ irradiations and the biochemical characteristics of degradation products of oxacillin, a frequently used antibiotic. The research was carried out in the frame of a National Office for Research and Development through the Hungarian-Chinese Industrial Research and Development Cooperation Project (No. 2017-2.3.6.-TÉT-CN-2018-00003).

Methods

Pulse radiolysis experiments were carried out using 800 ns pulses of electrons accelerated to 4 MeV energy and applying ~ 20 Gy/pulse absorbed dose. The chemical oxygen demand (COD) values were measured according to ISO Standard 6060:1989 using a Behrotest TRS 200 system. In total organic carbon (TOC) content measurements a Shimadzu TOC-L CSH/CSN analyser was used. Biochemical Oxygen Demand (BOD) experiments were performed by using OxiTop® Control BOD Respirometer System according to DIN EN 1899-1 (1998). For the measurement of oxygen uptake rate (OUR) activated sludge respiration inhibition tests were applied according to ISO 8192:1986 (1986) standard over 180 min at 20 ± 2 °C, with continuous stirring. Acute toxicity to *Vibrio fischeri* bioluminescent bacterium was determined by Microtox® tests according to DIN EN ISO 11348-2 (1999). *Staphylococcus aureus* strains (*S. aureus*, B.01755) were used in the agar diffusion microbiological tests (Collection code in the American Type Culture Collection: ATCC1 6538PTM).

Results

Oxacillin is a poorly biodegradable antibiotic, although it does not exert toxicity to *Vibrio* fishery luminescent bacterium and it is non-toxic to the mixed microbial community of a biodegradation unit in a wastewater treatment plant. However, the microbes cannot use it as nutrient source that is they are not able to decompose it. When the oxacillin containing solution was γ -irradiated with relatively small absorbed dose (0.5 – 1 kGy) the degradation products were utilized by the microbes. During irradiation of aerated aqueous solutions, the main reactants, the hydroxyl radicals predominantly attack the β -lactam part of oxacillin and induce the degradation of this chromophore responsive for the antibiotic effect. Oxacillin and cloxacillin have the same lactam part, the difference between the two antibiotics is at the benzene ring: cloxacillin has a Cl atom on this ring. Because the reaction mainly takes place on the β -lactam part, and not at the aromatic ring, the degradation characteristics of the two antibiotics are highly similar. Under anaerobic conditions the hydrated electrons attack the carbonyl groups in both oxacillin and cloxacillin. This reaction may also induce the degradation of the β -lactam double ring system.

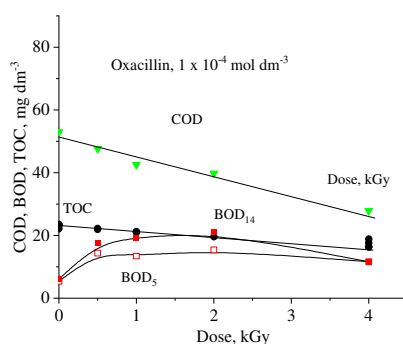


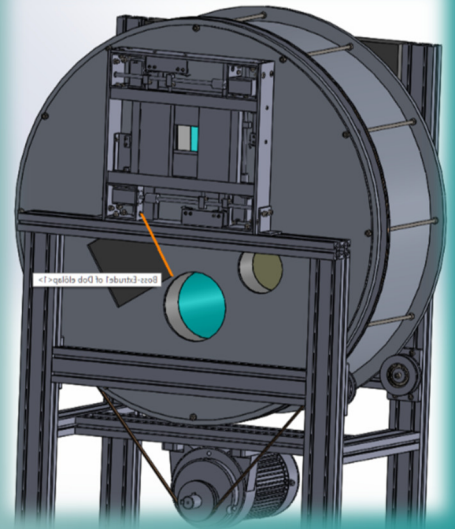
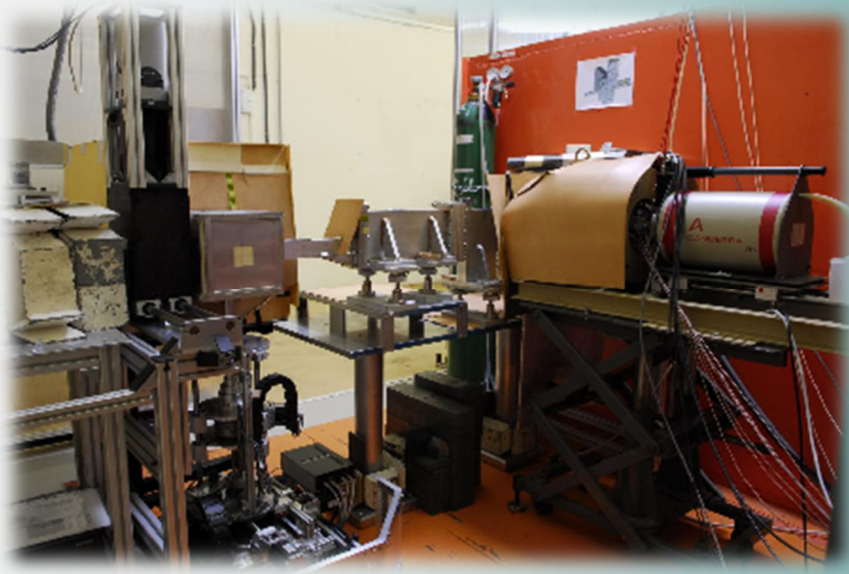
Figure 1: Chemical oxygen demand (COD), biochemical oxygen demand (BOD) and total organic carbon content (TOC) values as a function of the dose in the 0 - 4 kGy range measured in aerated 1.0×10^{-4} mol dm⁻³ oxacillin solution.

Remaining work

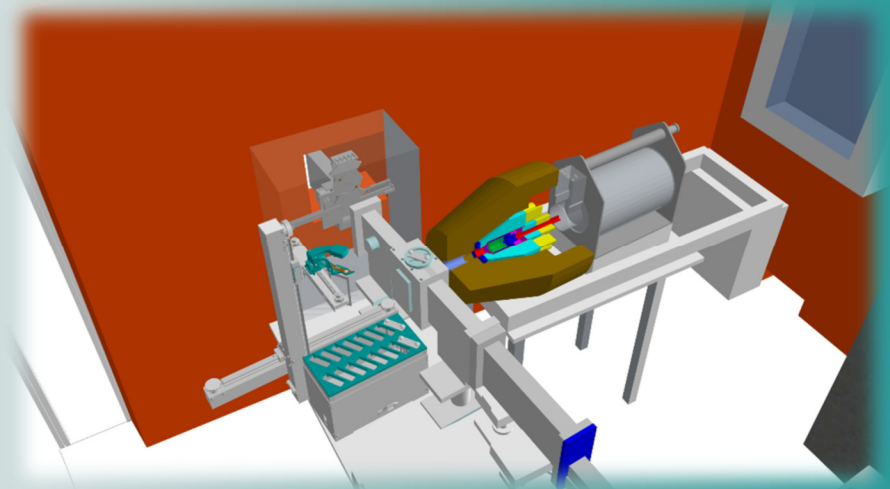
Using these methods we plan following the radiation induced degradation of various antibiotics.

Related publications

- [1] L. Wojnárovits, T. Tóth, E. Takács: Rate constants of carbonate radical anion reactions with molecules of environmental interest in aqueous solution: a review, *Science of the Total Environment* **717**, 137219 (2020)
- [2] J. Wang, L. Chu, L. Wojnárovits, E. Takács: Occurrence and fate of antibiotics, antimicrobial resistant genes (ARGs) and bacteria (ARB) in municipal wastewater treatment plant: An overview, *Science of the Total Environment* **744**, 140997 (2020)



V. NUCLEAR ANALYSIS AND CHEMISTRY



NEUTRON SCATTERING STUDIES ON POROUS MATERIALS, STEELS, COORDINATION COMPLEXES, EXTRACELLULAR VESICLES AND THIN FILMS

László Almásy, Zoltán Dudás, Adél Len, Dániel Géza Merkel

Objective

Small Angle Neutron Scattering (SANS) has been used to characterize the nanostructure of porous systems such as silica aerogels, xerogels and polyurethane, used as drug delivery systems. Mesoporous silica particles were prepared by the sol-gel method to investigate their applicability for low temperature hydrogen storage. The structure of colloidal silica nanoparticles near an isolated planar silica-water interface was studied by specular neutron reflectivity. The effect of three different CaCO_3 polymorphs on hydration of ordinary Portland cement has been investigated. The effect of rolling with shear on the nanostructure of low carbon steels, and the nanostructure of the transition metal coordination complexes at various temperatures has been studied by neutron scattering and by several other complementary methods.

Results

Silica-casein and silica-gelatin hybrid aerogels were prepared by the sol-gel method [1, 2]. By variation of the organic component, different composites were obtained. The primary building blocks of the hybrid aerogels were spheres, interconnecting into mesoporous networks, as shown by scanning electron microscopy (SEM), SANS and nitrogen porosimetry. Contrast-variation SANS experiments showed that the silica and organic components form homogeneous nanocomposite backbones. Even when fully saturated with water, the hybrid silica aerogels retain their original, highly permeable, open mesoporous structures that formed under supercritical drying. Silica-gelatin hybrid aerogels, impregnated with hydrophobic active agents (ibuprofen, ketoprofen), served as drug delivery systems. Importantly, both fast and retarded drug release could be achieved, and the kinetics of drug release was governed by the gelatin content of the carrier. For the first time, a molecular level explanation was given for the strong correlation between the composition and the functionality of a family of aerogel-based drug delivery systems. Characterization of the wet aerogels by SANS and by NMR diffusometry, cryoporometry and relaxometry revealed that the different hydration mechanisms of the aerogels are responsible for the broad range of release kinetics [2].

Methyl substituted silica xerogels have been synthesized by the sol-gel technique, using different tetraethylorthosilicate (TEOS) and methyltriethoxysilane (MTES) molar ratios and two different synthesis pH values. With the increase of the MTES amount, significant skeletal variations were revealed, suggesting a strong influence of MTES in the inorganic silica matrix and the presence of three different structural regimes in the explored MTES substitution ranges as revealed by the various structural characterization methods used. The possibility to "tune" the structural parameters, by varying the MTES content, represents a key point for the design of organic hybrid materials showing enhanced performances compared to those prepared with TEOS only. These could be particularly useful in various potential applications such as medicine and nanotechnology. [3]

A facile low-temperature sol-gel route has been used to synthesize hybrid silica-PVA-iron oxide nanocomposites. An in-vitro cytotoxicity assay was done by monitoring the cell viability (MTT assay) to qualify the materials as MRI contrast agents or as drug carriers. Two cell lines were considered: the HaCaT (human keratinocyte) and the A375 tumour cell line of human melanoma. The results indicate that the concentrations of 100 $\mu\text{g}/\text{mL}$ and 200 $\mu\text{g}/\text{mL}$ of the nanocomposite in DMSO (dimethylsulfoxid) induced a slight decrease in the HaCaT cell viability. The PBS (phosphate saline buffer) based in-vitro assay showed that the nanocomposite did not present toxicity on the HaCaT cells, even at high doses (200 $\mu\text{g}/\text{mL}$ agent). [4]

Mesoporous silica particles were designed and tested for low temperature hydrogen storage. Short chain cationic surfactants were used as a template, and a partially ordered pore structure was obtained. The small pore size is theoretically advantageous as it favours higher specific hydrogen bonding. The ordering of the pores became rather weak and no clear trends could be identified between the synthesis parameters and the pore morphology. Hydrogen adsorption capacity showed values ranging from 2 to 3 wt%, typical for silica-based sorbent materials, and were clearly higher for the samples prepared using the longer tetradecyltrimethylammonium bromide surfactant. [5]

Structuring of aqueous suspensions of colloidal silica nanoparticles near an isolated planar silica-water interface was studied by specular neutron reflectivity. The reflectivity data clearly showed that the suspensions developed a damped, oscillatory concentration profile in the direction perpendicular to the interface. The wavelengths of these oscillations agree well with those independently determined by direct force measurements. The reflectivity data further demonstrate that the oscillatory structure persists over several layers and that the first particle layer is separated from the interface by a particle-free region [6]

Due to their effect of vasodilatation, isosorbide nitrates represent one of the most important and most used medications for angina pectoris. Unfortunately, these compounds have multiple dose-related adverse drug reactions. Chitosan-based polyurethane (PU) structures were obtained with and without isosorbide nitrates and were characterized using a large variety of

methods. Multipopulational structures with an increased tendency to form clusters and a high resistance to heat (up to 280°C), were obtained. The study presented an alternative possibility of administration of isosorbide derivatives based on a PU carrier with a high biocompatibility and a prolonged release. [7]

The hydration of ordinary Portland cement blended with CaCO₃ polymorphs has been investigated. Commercial calcite and laboratory produced polymorphs (aragonite and vaterite) were employed. The hydration process, as well as the mechanical properties were assessed. Heat of hydration has been measured for seven days with isothermal calorimetry. Cylindrical specimens were prepared using eight different binders. SANS measurements have been performed after 28 days, along with compressive strength tests. Fractions generated from the latter were powdered for investigating them with a combination of analytical techniques (XRPD analysis, TA, NMR). Additional samples were used for assessing the phase assemblage after seven-day hydration. The evaluation of the data and publication of the results is under progress. Sadly, the work has been delayed due to the COVID-19 pandemic.

Structural Insights on Fusion Mechanisms of Extracellular Vesicles with a Model Plasma Membrane.

Extracellular vesicles (EVs) represent a potent intercellular communication system. Due to their specific biological functions, they have been proposed as biomarkers for various diseases and as optimal candidates for therapeutic applications. We revealed structure-function correlations, using a multiscale investigation platform based on Atomic Force Microscopy, Small Angle X-ray Scattering, Small Angle Neutron Scattering and Neutron Reflectometry techniques, of purified EVs through the analysis of their interaction with model membrane systems, in the form of both supported lipid bilayers and suspended unilamellar vesicles of variably complex composition. The analysis revealed a strong interaction of EVs with the model membranes and preferentially with liquid ordered raft-like lipid domains. [8]

Reversible control of magnetism in FeRh thin films.

An FeRh thin film deposited at 200 °C is primarily of paramagnetic phase and is fully converted to the magnetic phase by annealing at 300 °C for 60 min. We observed that subsequent irradiation by 120 keV Ne⁺ ions returned the thin film completely to the paramagnetic phase. Repeated annealing at 300°C for 60 min results in a 100% magnetic phase, i.e., this is a phase transition process that appears to be reversible at least twice. [9]

SANS has been used to study steel produced by rolling with shear (RS) technology and compared to similar results from samples produced by standard technology (ST). The scattering in a small scattering vector region showed anisotropy, attributed to the elongation of the pores. The results of the SANS measurements were in accordance with the electrical conductivity measurements made on the specimens. SANS showed smaller and less anisotropic average sizes of the cracks and nanopores for the RS samples than for the ST rods. This confirms the dynamic healing of the nanosized defects during the cold drawing which follows the rolling with shear. These results show that during severe plastic deformation, a cyclic process of nucleation and healing of the nanovoids took place. [10]

The specific class of transition metal coordination complexes with the ability to self-assemble in water into ordered supramolecular architectures is used to obtain advanced dynamic functional materials for applications in medicine or electro-optics. SANS measurements revealed the hexagonal ordering of columns formed by Rh-bipyridine between 25 °C and 55°C, and the disappearance of the ordering above 55°C. The columns formed by Rh-phenantroline complexes were maintained in solution with lamellar ordering. As the temperature increased, the distance between the lamellae decreased. At 45 °C the explicit peaks corresponding to well-ordered structures disappeared, the long-range order vanished. The publication of the results is in progress.

Despite the COVID pandemic, remote user measurements have also been performed on various topics, and two of these topics have been published so far: Silica-coated magnetic nanocomposites for Pb²⁺ removal from aqueous solution nanocomposites [11], The choice of temperature to synthesize SiO₂ aerogels [12].

Remaining work

In several topics, the finalization of measurements and publishing of the results is in progress. Most of the topics presented here are promising and the continuation of the research work is planned.

Related publications

- [1] I. Lázár, A. Forgács, A. Horváth, G. Király, G. Nagy, A. Len, Z. Dudás, V. Papp, Z. Balogh, K. Moldován, L. Juhász, Cs. Cserhádi, Zs. Szántó, I. Fábián, J. Kalmár: *Mechanism of hydration of biocompatible silica-casein aerogels probed by NMR and SANS reveal backbone rigidity*, Appl. Surf. Sci. **531**, 147232 (2020)
- [2] M. Kéri, A. Forgács, V. Papp, I. Bányai, P. Veres, A. Len, Z. Dudás, I. Fábián, J. Kalmár: *Gelatin content governs hydration induced structural changes in silica-gelatin hybrid aerogels – Implications in drug delivery*, Acta Biomater. **105**, 131–145 (2020)
- [3] Z. Dudás, A. Len, C. Ianăși, G. Paladini: *Structural modifications caused by the increasing MTES amount in hybrid MTES/TEOS-based silica xerogels*, Mater. Charact. **167**, 110519 (2020)
- [4] A.-M. Putz, C. Ianăși, Z. Dudás, D. Coricovac, C. (Farcas) Watz, A. Len, L. Almásy, L. Sacarescu, C. Dehelean: *SiO₂-PVA-Fe(acac)₃ Hybrid Based Superparamagnetic Nanocomposites for Nanomedicine: Morpho-textural Evaluation and In Vitro Cytotoxicity Assay*, Molecules **25**, 653 (2020)

- [5] A. Policicchio, G. Conte, S. Stelitano, C.P. Bonaventura, A.-M. Putz, C. Ianăși, L. Almásy, Z.E. Horváth, R.G. Agostino: *Hydrogen storage performances for mesoporous silica synthesized with mixed tetraethoxysilane and methyltriethoxysilane precursors in acidic condition*, *Colloids Surf. Physicochem. Eng. Asp.* **601**, 125040 (2020)
- [6] P. Maroni, M. Gvaramia, D. Kosior, D., K. Kubiak, L. Scarratt, A.M. Smith, D.G. Merkel, L. Bottyán, M. Borkovec: *Structuring of colloidal silica nanoparticle suspensions near water–silica interfaces probed by specular neutron reflectivity*, *Phys. Chem. Chem. Phys.* **22**, 6449–6456 (2020)
- [7] F. Borcan, A. Len, D. Bordejevic, Z. Dudás, M.C. Tomescu, A.N. Valeanu: *Obtaining and Characterization of a Polydisperse System Used as a Transmembrane Carrier for Isosorbide Derivatives*, *Front. Chem.* **8**, (2020)
- [8] F. Perissinotto, V. Rondelli, B. Senigagliaesi, P. Brocca, L. Almásy, L. Bottyan, D.G. Merkel, H. Amenitsch, B. Sartori, K. Pachler, M. Mayr, M. Gimona, E. Rohde, L. Casalis, P. Parisse, *Structural Insights on Fusion Mechanisms of Extracellular Vesicles with Model Plasma Membrane*, *bioRxiv* 2020.05.25.110601 (2020)
- [9] D.G. Merkel, A. Lengyel, D.L. Nagy, A. Németh, Z.E. Horváth, C. Bogdán, M.A. Gracheva, G. Hegedűs, S. Sajti, G.Z. Radnóczy, E. Szilágyi, *Reversible control of magnetism in FeRh thin films*, *Sci. Rep.* **10**, 13923 (2020)
- [10] Zavdoveev, A., Len, A., Pashinska, E., *Small Angle Neutron Scattering Study of Nanoscale Structure of Low-Carbon Steel After Rolling with Shear Followed by Cold Drawing*, *Met. Mater. Int.* (2020)
- [11] R. Nicola, O. Costișor, M. Ciopec, A. Negrea, R. Lazău, C. Ianăși, E.-M. Picioruș, A. Len, L. Almásy, E.I. Szerb, A.-M. Putz, *Silica-Coated Magnetic Nanocomposites for Pb²⁺ Removal from Aqueous Solution*, *Appl. Sci.* **10**, 2726 (2020)
- [12] S.A. Lermontov, A.E. Baranchikov, N.A. Sipyagina, A.N. Malkova, G.P. Kopitsa, Kh.E. Yorov, O.S. Ivanova, A. Len, V.K. Ivanov, *Is Supercritical So Critical? The Choice of Temperature to Synthesize SiO₂ Aerogels*, *Russ. J. Inorg. Chem.* **65**, 255–262 (2020)

NEUTRON OPTICS

Márton Markó, Alex Szakál, Péter Kárpáti, László Bottyán, Gyula Török, László Rosta

Objective

Our neutron optics research and development project involves the basic development of neutron optical devices, including the design, optimization, further development and upgrade of the neutron sources and guides and the neutron scattering instruments at the Budapest Neutron Centre (BNC) and at the other neutron centres and companies collaborating with the Neutron Spectroscopy Department. The work includes hardware (e.g. electronics) / software upgrades as well.

Methods

During our work we have used basic optical considerations to determine the optimal geometries using analytical focusing geometries (parabola and ellipse), defined a differential equation for transforming a non-rectangular 2D phase space (direction-position space), solved it numerically and have performed MonteCarlo calculations using the McStas software package [1].

Results

To study the transport efficiency of the neutron guide system – especially for the long neutron guides – we have made an analytical model to describe the alignment conditions of the neutron guide segments i.e. the misalignment. We also developed a McStas component dealing with this effect in McStas MonteCarlo ray-tracing software. The two different models give similar results (see fig.1), and show that for long neutron guides the misalignment has a large effect.

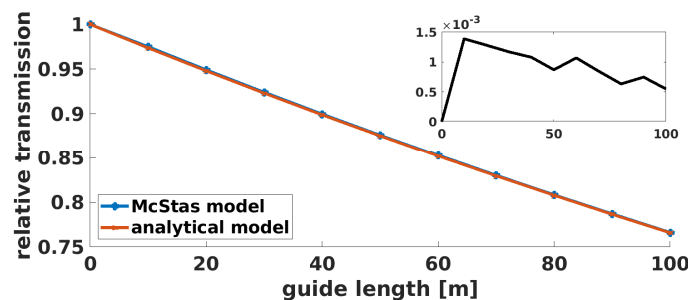


Figure 5: The relative decrease of the transmission as a function of the guide length. The cross section of the beam guide is $3 \times 3 \text{ cm}^2$. The alignment tolerance is $30 \mu\text{m}$ for each 50 cm section. The inset graph shows the relative difference between the two models.

After passing through a curved neutron guide, the divergence distribution, as a function of the position, i.e. the phase space, is highly asymmetric. To expand a beam the generally used geometry is a linearly diverging guide. That system produces an inhomogeneous phase-space distribution resulting in decreased brilliance transfer at the sample position. We have calculated a new geometry that transforms the part of the phase space filled with neutrons into a rectangular homogeneous phase space. The analytical calculations were validated with McStas modelling. The new geometry is applied for the NMX (neutron macromolecular single-crystal diffractometer) instrument at the European Spallation Source (ESS).

The instrument suite of BNC is continuously developing. In addition to the electronic and software upgrades (at the Athos cold triple axis and Yellow Submarine SANS instruments), in the short term we will replace the REF vertical reflectometer by the V14 horizontal polarized reflectometer that was previously installed at HZB Berlin, and will be reinstalled at BNC. In the future, the upgrade of the existing so-called “volume” cold neutron source by a quasi 1 dimensional “pencil” source is planned. The new source will have three times higher brilliance compared to that of the present one. To achieve the optimal beam extraction from the new source, the upgrade of the present neutron guide system is essential. The planned instrument suite will not differ too much from the present one: a cold diffractometer, two PGAA stations, a cold neutron radiography, two SANS and two reflectometers (a horizontal and a vertical one), and a so-called direct time-of-flight spectrometer that will be installed after the reconstruction. We determined the optimal beam parameters at the sample position of each instrument. The results show that, apart from the crystal monochromator based instruments, each instrument can have a dedicated beamline providing the optimal beam conditions. The crystal monochromator instruments are planned to be on one beamline. The diffractometer will be at the end of one guide, and the beams for the reflectometers will be “peeled off” from the side and the top of the beam introducing negligible effect on the beam downstream since the beam size needed by a reflectometer perpendicular to the reflection direction is a maximum of 1 mm. The calculation of the exact optimal guide system geometry is ongoing.

Remaining work

We continue the work in two directions: The first one is the basic research on neutron optics including further investigations

of neutron mirrors, the robustness of the guide systems and development of analytic geometries for optimal beam extraction and focusing. The second one is the applied research: the final design of neutron guide systems for BNC (upgrade of the neutron transport system), participation in European projects like CREMLIN II (building a test station for new neutron cold sources and designing a beam extraction system), ESS, EasiStress, and to design neutron optical systems for other neutron centres through industrial contracts with neutron guide producers.

Related publications

- [1] P. Willendrup, and K. Lefmann: *McStas (i): Introduction, use, and basic principles for ray-tracing simulations*, Journal of Neutron Research, **22(1)**, 1-16 (2020)
- [2] https://www.helmholtz-berlin.de/pubbin/igama_output?modus=einzel&sprache=en&gid=1712&typoid=

TUNGSTEN-CARBIDE-RICH PROTECTIVE COATINGS PRODUCED BY NOBLE-GAS IRRADIATION MIXING

Adél Rácz, Zsolt Kerner, Zsolt Fogarassy, Miklós Menyhárd

Objective

Tungsten-carbide (WC) is known for its exceptional mechanical properties and good chemical resistance. We proposed to apply ion beam mixing to produce WC layered coatings at room temperature. The applicability of ion irradiation to produce tungsten-carbide-rich nano coatings by irradiating various C/W multilayer structures with noble gases in a wide range of fluences and energies has been demonstrated. We show that the quantity previously introduced for the irradiated C/Si system, the effective areal density, enables the tailoring of the chemical resistance of the ion irradiated C/W system as well.

Methods

The samples, four different C/W multilayer systems, were produced by magnetron sputtering in the Jozef Stefan Institute, Ljubljana. The systems differed in the thickness (10-30 nm) and the order of layers. The actual structure of the initial samples has been determined by cross-sectional transmission electron microscopy (XTEM). The layer systems were irradiated with argon and xenon ions. In the case of argon ions, the ion energy was 40 - 110 keV and the fluence was $0.25 - 6 \times 10^{16} \text{ Ar}^+/\text{cm}^2$, while in the case of xenon ions the energy was 40 - 120 keV and the fluence was $0.07 - 3 \times 10^{16} \text{ Xe}^+/\text{cm}^2$. The irradiation took place in the Helmholtz Zentrum Rossendorf in Dresden in the framework of the RADIATE beam time project. Auger electron spectroscopy (AES) identified WC production due to the irradiation. For investigating the chemical resistance of the irradiated layer, a potentiodynamic corrosion test in 3.5 wt% NaCl solution has been performed. It was attempted to describe the mixing process using the TRIDYN simulation algorithm.

Results

The AES depth profiling done on the irradiated samples has shown that the in-depth distribution of the WC that is formed can be tuned by changing the irradiation parameters (fluence, energy) and the original C/W multilayer structure. Figure 1a shows the profile of a 3C + 2W layer structure irradiated by $6 \times 10^{16} \text{ Ar}^+/\text{cm}^2$, at 110 keV energy. Due to the irradiation, serious changes occurred in the sample; namely, an intermixing of W and C and WC compound formation took place. We note that the intermixing of the C/W system is much more intense than that of the (previously investigated) C/Si system. The corrosion test has shown that the corrosion resistance of the mixed layers produced is orders of magnitude better than that of a WC cermet. We found that the previously introduced quantity, the effective areal density, can be used to predict the corrosion resistance of the ion mixed layer. Figure 1b shows the current density of the potentiodynamic test vs. effective areal density for all measured data obtained from all layered structures which were irradiated by various ions, energies and fluences. It can be seen that they are in good correlation even though the WC areal densities vary over an extremely large range. This finding enables the tailoring of the chemical resistance of the system.

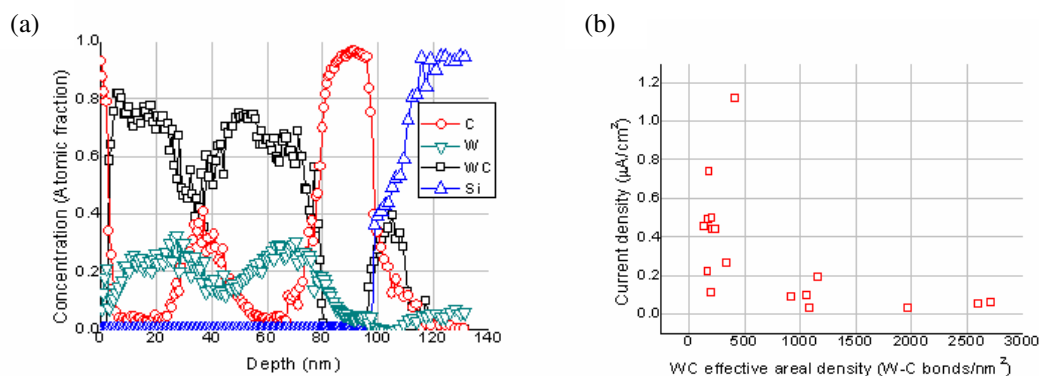


Figure 1: a) AES depth profile of a sample irradiated by $6 \times 10^{16} \text{ Ar}^+/\text{cm}^2$, 110 keV; the initial, non-irradiated structure was C (20 nm)/W (20 nm)/C (20 nm)/W (20 nm)/C (20 nm)//Si substrate b) Current density vs effective areal density of WC for the variously irradiated different layer structures.

According to common knowledge, the mechanism of the ion irradiation induced mixing depends on the average atomic number, which is different for the C/Si and C/W systems. It was shown that for the C/Si system the ballistic model described the mixing, as is expected. Surprisingly in the present case the ballistic model, with some parametrization, unexpectedly describes the main features of the mixing, and can be used for estimation of the process. More work is necessary to understand this finding.

Remaining work

We would like to perform additional irradiations and investigate the chemical protectivity of the system, and check the validity of the TRIDYN simulation. Additionally, the mechanical properties of this system would be extremely interesting as its thickness is below 100 nm.

APPLICATIONS OF NUCLEAR ANALYTICAL TECHNIQUES

*Zsolt Kasztovszky, László Szentmiklósi, Ildikó Harsányi, Zoltán Kis, Veronika Szilágyi,
Katalin Gméling, Boglárka Maróti*

Objective

We determined the elemental compositions of various kinds of samples using PGAA, PGAI, NAA and portable XRF methods. The data obtained are very useful in studies in catalysis, material science, geochemistry, palaeontology and heritage science.

Methods

- Prompt Gamma Activation Analysis (PGAA) – to determine the bulk elemental composition, mostly for major components, and for some trace elements with high neutron absorption cross-section
- Neutron Activation Analysis (NAA) – to determine the elemental composition of a sample taken from a larger object, mostly for trace elements
- Portable X-ray Fluorescence instrument (pXRF) – to determine the elemental composition of a near-surface region of an object

Results

- We predicted the neutron-induced sample activity, based on the elemental compositions of three concrete types considered for use in the construction of the European Spallation Source (ERIC, Sweden). Compositions were determined via XRF, PGAA, and NAA [1].
- Radionuclide inventories (gamma dose rates) following neutron irradiation were calculated for domestic raw materials. A comprehensive petrographic [2] and composition data library of raw materials is being compiled to use as input to the radionuclide inventory simulation codes. We continued the geochemical characterization of domestic additives and cement samples provided by our collaborators, using NAA and PGAA. Realistic MCNP material cards were created and validated against the measured data of neutron-irradiation experiments.
- A detailed MCNP6 model of the Budapest Research Reactor was established and preliminary neutron flux values were calculated at relevant positions to better plan the in-core activation of samples. At the RAD facility, where new biological shielding is being designed, detailed MCNP6 calculations were made for neutron and gamma attenuation features of various shielding options, for various shielding compositions, densities and thicknesses.
- A standard and a heavy concrete from NuviaTech, several experimental concretes from Oxydtron Company Ltd. and ÉMI Non-Profit LLC for Quality Control and Innovation in Building were analysed for their composition, and their linear attenuation coefficients for X-rays and neutrons were measured.
- Major, minor, and trace element content of heavy mineral separata from concrete aggregate raw materials was quantified by nuclear analytical techniques. The results for the NW Hungarian mines were presented in a BSc thesis [6].
- Compositional data on heavy-weight concrete constituents designed by the Slovakian RADCON partners were determined [3] to support the optimization of the composition: blended cements (Portland cement CEM I 42.5 R was replaced by different portions of supplementary cementitious materials, i.e. blast furnace slag, metakaolin, silica fume/limestone), mixture of two high-density aggregates (barite and magnetite). The different designs were controlled and qualified by thermophysical (thermal conductivity, volumetric specific heat, thermal diffusivity) and other physical investigations (volume expansion, shrinkage). Another study focused on the alkali-silica reaction (ASR) [4]. A complex analytical protocol was proposed to select fine aggregates for concrete production with the possible least ASR [5]. The protocol involves PGAA, digital image procedure (DIP) and mortar bar test to determine the chemical composition of aggregate and the related ASR risk. A strong correlation of sand origin and its susceptibility to ASR is observed. Our data provided a basis for recommendations on the disposal of cement-based composites as radioactive waste after the decommissioning of nuclear power plants.
- Red andesite samples from the barren dump of the andesite rock mine at Gyöngyössolymos (NE Hungary) were investigated. Elevated hydrogen and iron content, higher than the average of fresh andesite, was found. Due to the favourable chemical characteristics, this material can be recycled as heavy-weight (due to the presence of iron-rich minerals like limonite or hematite) and hydrogenous (with high neutron capture cross-section, like serpentinite) aggregate in neutron or gamma shielding concretes.
- In co-operation with ATOMKI, in the frame of the IAEA “Enhancing Nuclear Analytical Techniques to Meet the Needs of Forensic Sciences” CRP, the elemental composition of 20 forensic glass samples originated from the windshields of various car brands were measured by PGAA and pXRF. The aim of the study was to see whether we can differentiate between the brands, based on their composition. PGAA and XRF data will be complemented by Inductively Coupled Plasma Mass Spectrometry (ICP-MS) data and evaluated by statistical tools.
- In co-operation with the Hungarian National Museum, and also within the frame of the K-131814 NKFIH (OTKA) project, PGAA, NAA and pXRF were used on chipped and polished stone archaeological objects from Neolithic sites (Polgár-Csőszhalom, Lengyel, etc) and on geological reference samples. Based on the composition, the possible raw material

sources can be determined. The evaluation of data is in progress.

- To complete the datasets published in [8] by Szilágyi et al, additional PGAA measurements have been done on geological references of Balkan flint from the Lithoteka of the Hungarian National Museum.
- In a previous IPERION CH project, Late-Copper-Age ceramic bowls were studied by micro-CT and PGAA to decide if they were local products in Slovenia or long distance imported. A similar study was done on 3rd millennium BC ceramics from a UNESCO heritage site in Oman. The results suggest that most of the vessels were locally produced, except a black slipped jar which was imported from today's Pakistan [11, 12].
- The user access within the new IPERION HS TNA project, started on 1st April 2020, was hindered by the COVID-19 pandemic.
- Following the inquiry of the Museum of Ethnography, we took part in the multi-technique study of an Aztec ritual mask. The aim was to identify the mineral grains covering the mask. To determine their elemental composition, handheld XRF was applied. To identify the provenance, further reference data needed.
- The editorial works of a section titled Large Facilities and Cultural Heritage in the Handbook of Cultural Heritage Analysis by Springer are almost finished. It is planned to publish in 2021.
- The noble-metal content of alumina-based supported catalysts were measured, and the results were published [13]

Remaining work

Applications of PGAA and other elemental compositional measurements will be continued according to the current applications from various groups of users and ongoing projects.

Related publications

- [1] D. Hajdú, E. Dian, K. Gméling, E. Klinkby, C. P. Cooper-Jensen, J. Osán, P. Zagyvai: *Experimental study of concrete activation compared to MCNP simulations for safety of neutron sources*, Applied Radiation and Isotopes, Submitted (2020)
- [2] V. Szilágyi, K. Gméling, S. Józsa, I. Harsányi, L. Szentmiklósi: *Oligomictic alluvial aggregates: evaluation of sandy gravel formations on the middle course of the Danube (Hungary) for construction industry applications*. Bulletin of Engineering Geology and the Environment. Under review (2020)
- [3] J. Dragomirová, M. T. Palou, E. Kuzielová, M. Žemlička, R. Novotný, K. Gméling: *Optimization of cementitious composite for heavyweight concrete preparation using conduction calorimetry*, Journal of Thermal Analysis and Calorimetry **142**, 255–266 (2020) <https://doi.org/10.1007/s10973-020-09530-0>
- [4] D. Jóźwiak-Niedźwiedzka, A. Antolik, K. Dziedzic, K. Gméling, K. Bogusz: *Laboratory investigations on fine aggregates used for concrete pavements due to the risk of ASR*, Road Materials and Pavement Design, (2020) <https://doi.org/10.1080/14680629.2020.1796767>
- [5] D. Jóźwiak-Niedźwiedzka, K. Gméling, I. Harsányi, K. Dziedzic, M. A. Glinicki: *Assessment of long-lived residual radioisotopes in cement induced by neutron radiation*. Construction and Building Materials. (Under review) MATBUD 2020 MATEC Web conferences 322 01019 (2020) <https://doi.org/10.1051/mateconf/202032201019>
- [6] A. Juhász: *Északnyugat magyarországi homokminták nehézasványainak nyomelem-összetétel vizsgálata Neutronaktivációs Analitikai (NAA) módszerrel*, BSc Thesis, Eszterházy Károly Egyetem, Eger. (2020)
- [7] E. Kereskényi, Gy. Szakmány, B. Fehér, I. Harsányi, V. Szilágyi, Zs. Kasztovszky, T. M. Tóth: *Archaeometrical results related to Neolithic amphibolite stone implements from Northeast Hungary*, Journal of Archaeological Science: Reports, **32**, 102437 (2020)
- [8] V. T. Szilágyi, K. Biró, M. Brandl, I. Harsányi, B. Maróti & Zs. Kasztovszky: *A kárpát-medencei radiolarit nyersanyagok szöveti típusai és geokémiai jellegei*, Archeometriai Műhely, XVII.1. 1-30. (2020)
- [9] B. Maróti, V. Szilágyi, I. Harsányi, Zs. Kasztovszky, Zs. L. Szentmiklósi: *Régészeti kőeszközök és bronztárgyak vizsgálata hordozható készülékekkel*, Archeometriai Műhely, XVII.3. 243-252. (2020)
- [10] Zs. Kasztovszky, L. Szentmiklósi, Z. Kis, V. Szilágyi, B. Maróti, I. Harsányi, T. Belgya, K. Gméling, K. Bajnok, A. Len, Gy. Káli, I. Kovács, Z. Szőkefalvi-Nagy, L. Rosta: *A Budapesti Neutron Centrum részvétele az Európai örökségtudományi kutatásokban / Participation of the Budapest Neutron Centre in the European Heritage Science Projects*, Archeometriai Műhely 2020/XVII./1. 87-92
- [11] E. Leghissa, Z. Kasztovszky, V. Szilágyi, I. Harsányi, A. De Min, F. Princivale, MM. Kokelj, F. Bernardini: *Late-Copper-Age decorated bowls from the Trieste Karst (north-eastern Italy): What can typology, technology and non-destructive chemical analyses tell us on local vs. foreign production, exchange systems and human mobility patterns?* Quat. Int. 539, 92–104. (2020) <https://doi.org/10.1016/j.quaint.2020.02.008>
- [12] Bernardini, F., Vinci, G., Prokop, D., Savonuzzi, L. B., De Min, A., Lenaz, D., Princivale, F., Cocca, E., Kasztovszky, Zs., Szilágyi, V., Harsányi, I., Tuniz, C., Cattani, M., *A multi-analytical study of Bronze Age pottery from the UNESCO site of Al-Khutm (Bat, Oman)*, Archaeological and Anthropolog. Sci. (2020) 12: 163. <https://doi.org/10.1007/s12520-020-01099-x>
- [13] Nagy G, Gál T, Srankó DF, Sáfrán G, Maróti B., Sajó IE, Schmidt FP, Beck A: 2020. *Selective aerobic oxidation of benzyl alcohol*

on alumina supported Au-Ru and Au-Ir catalysts. Mol. Catal. 492, 110917.

<https://doi.org/10.1016/j.mcat.2020.110917>

- [14] Šmit, Maróti, B., Kasztovszky, Z., Šemrov, A., Kos, P., 2020. *Analysis of Celtic small silver coins from Slovenia by PIXE and PGAA*. Archaeol. Anthropol. Sci. 12. <https://doi.org/10.1007/s12520-020-01124-z>

DEVELOPMENT OF NUCLEAR ANALYTICAL TECHNIQUES, NUCLEAR DATA MEASUREMENTS

Tamás Belgya, László Szentmiklósi

Objective

To develop our analytical capabilities and know-how in the Prompt Gamma Activation Analysis (PGAA) technique, to accurately determine nuclear data using PGAA.

Methods

(n,γ) measurements, evaluation of nuclear data and comparison to literature, computer programming, geant4 simulations.

Results

After successfully concluding the data analysis of the γ - γ -coincidence experiment made at the PGAA facility for neutron capture on a natural Nb target, intensities of the two-step gamma cascades in the compound nucleus ^{94}Nb to those final levels with excitation energies below 400 keV were derived from the experimental spectra. The intensities and energies of primary and secondary transitions of 216 energy-resolved cascades as well as the energies of the intermediate cascade levels were determined. A significant part of the level scheme of ^{94}Nb was obtained from analysing the spectral intensity of the strongest cascades. The results were compared to the existing data on ^{94}Nb in the ENSDF database. 27 primary transitions, 29 intermediate cascade energy levels, and 183 secondary transitions were recommended as new nuclear data.

The results of geant4 Monte Carlo simulations carried out for the Budapest PGAA detector were finalized and published. A complete set of detector response functions, i.e. the gamma spectra corresponding to incremental gamma-ray energies up to 12 MeV, were obtained by simulations (Fig. 1) and used to unfold the experimental gamma spectra of ^{60}Co (Figs. 2-3) and ^{152}Eu . The unfolding successfully removed the continuous Compton-background and the escape peaks related to a full-energy peak but preserved the shape and area of the full-energy peak itself. We finally demonstrated the applicability of this approach in determining the total radiative neutron capture cross-sections of the $^{14}\text{N}(n,\gamma)$ reaction, where an excellent agreement with literature data was found.

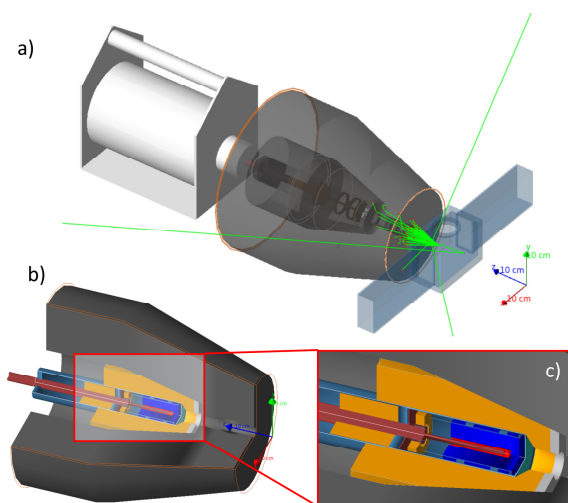


Fig. 1: a) The definition of the Budapest PGAA detector's geometry as used in geant4 and an event shower from a 2.223 MeV gamma-ray of $\text{H}(n,\gamma)$. b) and c) Cutaway views of the detector model. The dark grey colour represents the outer lead shielding, orange is the main and catcher guard BGO detectors for Compton-suppression, blue is the HPGe crystal, light grey is the aluminum, red is the copper cold-finger, while green is the epoxy end-window.

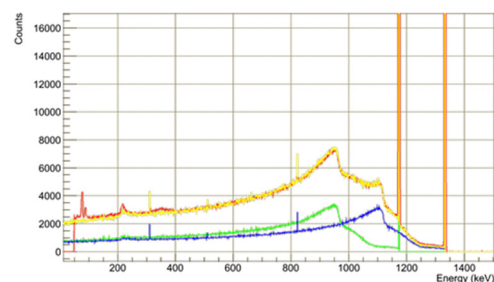


Fig. 2: Green and blue curves are the simulated response functions for the 1173-keV and 1332-keV peaks of ^{60}Co . The yellow curve is their weighted sum, while the red line is the measured spectrum.

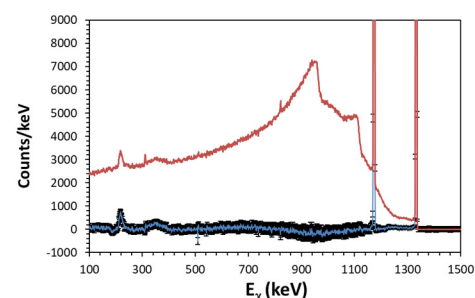


Fig. 3: The successful removal of the continuous background via unfolding. The measured spectrum is plotted in red, the unfolded spectrum in blue, the calculated error bars are shaded in black.

Related publications

- [1] D. Knezevic, et al.: Study of gamma transitions and level scheme of ^{94}Nb using the $^{93}\text{Nb}(n,2\gamma)$ reaction, Nucl. Phys. A **993**, 121645 (2020) <https://doi.org/10.1016/j.nuclphysa.2019.121645>
- [2] T. Belgya, L. Szentmiklósi: Monte-Carlo calculated detector response functions to unfold radiative neutron capture spectra, Nucl. Instr. Meth. A **165018**. (2021) <https://doi.org/10.1016/j.nima.2021.165018>

NANOCOMPOSITES, THIN IRON FILMS AND NANOPARTICLES STUDIED BY MÖSSBAUER SPECTROSCOPY AND OTHER METHODS

Sándor Stichleutner, Zoltán Klencsár, Károly Lázár

Objective

Iron is an important constituent in various systems and the identification of its phases and valence states is essential for interpreting the observed properties. Recently, prednisolone loaded mesoporous silica nanocomposites with different amounts of maghemite core, suitable for drug administration in a magnetic field, swift heavy ion irradiated 100 Å thick ^{57}Fe thin films, and magnetic nanoparticles were studied by ^{57}Fe Mössbauer spectroscopy and other methods.

Methods

^{57}Fe transmission and conversion electron Mössbauer spectroscopy was mainly used, along with other appropriate techniques.

Results

Prednisolone loaded mesoporous silica nanocomposites with different amounts of maghemite core were synthesized to obtain a drug delivery system suitable for drug administration in a magnetic field. ^{57}Fe Mössbauer spectroscopic results, obtained at room and low temperatures, proved the presence of small maghemite nanoparticles exhibiting superparamagnetic behaviour inside the silica structure. X-ray Diffraction (XRD), Fourier-transform infrared spectroscopy (FT-IR) and Raman spectroscopic measurements revealed the polymorphic transformation of the parent Form I prednisolone to the Form II polymorph by the prednisolone loading method, which was used. The spectroscopic data suggest weak bonding between silanol groups of the mesoporous silica nanoparticles and the prednisolone molecules. An *in vitro* release process performed at pH = 7 showed lower solubility of the polymorphic Form II compared to Form I, resulting in a slower, sustained release of prednisolone by silica loaded formulations, reaching its total release amount in 10 h. The effect of prednisolone polymorphs loaded in a silica carrier on its pharmacokinetic properties was studied for the first time [1].

^{57}Fe conversion electron Mössbauer spectroscopy was used to study the effect of swift heavy ion irradiation on 100 Å thick ^{57}Fe thin films vacuum deposited onto Si wafers. The irradiation was performed with 160 MeV ^{132}Xe ions with a fluence of 10^{13} ions/cm² at the IC-100 heavy ion accelerator of the Flerov Laboratory of Nuclear Reactions, Joint Institute for Nuclear Research, Dubna, Russia. The room temperature Mössbauer spectra of the irradiated samples show the formation of a number of new Fe⁰, Fe^{II} and Fe^{III} containing phases. To study the superparamagnetic nature of the new phases, a series of low temperature conversion electron Mössbauer spectroscopic measurements were performed over a wide temperature range, between room temperature and 17 K. Additional magnetic measurements are in progress in order to facilitate the identification of the newly formed phases.

Industrial-level applications of nanoparticles requires the development of nanoparticle preparation methods with which large-scale synthesis of nanoparticles with sufficient compositional, structural and morphological homogeneity becomes feasible. Achieving homogeneity of nanoparticle material properties on a mass scale exceeding the typical laboratory-level production scales of 100-1000 mg by 3 or more orders of magnitude is a considerable challenge, and also requires applied research techniques for the monitoring and improving of the homogeneity and quality of the nanoparticle products. By using the methods of ^{57}Fe Mössbauer spectroscopy and powder X-ray diffractometry, we have investigated two different magnetic nanoparticle products of (Fe^{II},Fe^{III})-oxide and Fe^{III}-oxide, which were prepared at the mass scales of ca. 1/2 kg and ca. 1 kg, respectively. The room temperature ^{57}Fe Mössbauer spectrum of the (Fe^{II},Fe^{III})-oxide revealed the sample to be composed of spinel oxide (magnetite, partly oxidized magnetite or maghemite), and reflected the powder's nanoparticle nature via line broadening caused by magnetic relaxation effects. The associated powder X-ray diffractogram corroborated this result, and revealed a cubic lattice parameter of $a \approx 8.35$ Å, and a crystallite size of ~16 nm. On the basis of the lattice parameter, the sample can be characterized as oxidized magnetite or maghemite spinel oxide. Neither the Mössbauer spectrum nor the powder X-ray diffractogram detected any secondary phases, signalling the rather high level of phase purity of the sample. The room temperature ^{57}Fe Mössbauer spectrum of the Fe^{III}-oxide powder revealed the sample to be composed of hematite and goethite along with a doublet component presumably associated with a superparamagnetic oxide or oxide-hydroxide. The powder's nanoparticle nature was also reflected in a hyperfine magnetic field distribution of the two magnetic phases. The corresponding powder X-ray diffractogram established that the sample is composed exclusively of hematite and goethite particles, with an approximately equal crystallite size of ~12 nm.

Related publications

- [1] Á. Szegedi, I. Trendafilova, J. Mihály, K. Lázár, P. Németh, G. Momekov, D. Momekova, L. Marinov, I. Nikolova, M. Popova: *New insight on prednisolone polymorphs in silica/maghemite nanocomposites*, Journal of Drug Delivery Science and Technology **60**, 102092 (2020)
- [2] E. Kuzmann, Z. Homonnay, Z. Klencsár, R. Szalay: *Néhány fém-organikus vegyület molekuláris mágnességének vizsgálata Mössbauer-spektroszkópiával*, Magyar Kémiai Folyóirat **126**, 54-64 (2020)
- [3] M. Popova, S. Boycheva, H. Lazarova, D. Zgureva, K. Lázár, Á. Szegedi: *VOC oxidation and CO₂ adsorption on dual adsorption/catalytic system based on fly ash zeolites*, Catalysis Today **357**, 518-525 (2020)

CHARACTERIZATION OF NANOPARTICLE SYSTEMS

Zoltán Klencsár, Sándor Stichleutner, Viktória Kovácsné Kis

Objective

Characterization of different nanoparticle systems, in part to be used in studies investigating the metal uptake and iron metabolism of plants.

Methods

Samples were prepared via wet-chemical synthesis processes by Gy. Tolnai. The samples were investigated via ^{57}Fe Mössbauer spectroscopy, transmission electron microscopy (TEM), selected area electron diffraction (SAED), energy-dispersive X-ray spectroscopy (EDX) and powder X-ray diffractometry (PXRD). The PXRD experiments were performed in cooperation with L.K. Varga at the Wigner Research Centre for Physics (Wigner FK).

Results

The investigation of the structure of the nominally ZnFe_2O_4 nanoparticle powder samples "ZF5" and "ZF6", prepared via a coprecipitation process, was continued by PXRD and TEM measurements on both of the samples. TEM and PXRD measurements confirmed that ZF5 consists of cubic spinel nanoparticles having a close to nominal elemental composition with the characteristic particle size being below ca. 10 nm and the mean crystallite size being ca. 5 nm. In contrast, in ZF6 the main constituent phase was found to have a structure akin to that of beta-FeO(OH), forming needle-like anisometric particles with a characteristic size of 2-300 nm x 10-20 nm. In addition, in the latter sample the possible presence of Zn oxide is also reflected in both the TEM and PXRD results, with the corresponding crystal structure being (on the basis of PXRD results) hexagonal with lattice parameters ($a \approx 0.3$ nm, $c \approx 0.51$ nm) similar to those of ZnO. The structural differences between the samples can be associated with the different preparation conditions. The sample ZF5 was prepared via fast precipitation at pH=13 which was set via the admixture of KOH solution, whereas ZF6 was prepared via slower precipitation at pH=7 which was set via the addition of carbamide. The formation of the spinel structure is clearly preferred in the former case.

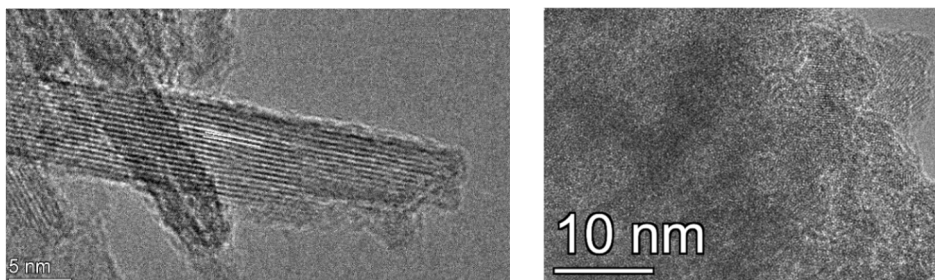


Figure 1: (left) High resolution transmission electron microscopy image of nanometric goethite in "VSK04" and (right) ordered domains extending only over the scale of a few nanometers in "HMT010"

Due to its advantageous adsorption properties towards various toxic ions and chemicals, synthetic goethite, $\alpha\text{-FeO(OH)}$, is considered as a promising substance to be used in the field of environmental protection and remediation, e.g., as an adsorbent in waste water treatment and detoxification procedures. From the point of view of these applications, the nanometric form of goethite can be especially advantageous on account of its high specific surface area available for adsorption processes. We have investigated two different iron-oxide-hydroxide nanoparticle powders (referred to below as „HMT010” and „VSK04”) synthesized by a reverse precipitation method. The room temperature ^{57}Fe Mössbauer spectra exhibited a doublet feature for both samples, due to the paramagnetic or superparamagnetic state of the materials. Somewhat higher quadrupole splitting and slightly broader absorption peaks were observed for "HMT010", contributing to a moderate difference between the Mössbauer spectra of the two materials. PXRD measurements of "VSK04" revealed an orthorhombic crystal structure with lattice parameters ($a \approx 0.46$ nm, $b \approx 0.996$ nm, $c \approx 0.3$ nm) akin to those of goethite, along with broad reflections due to a mean crystallite size of ~ 7 nm. In contrast, the X-ray diffractogram of "HMT010" displayed even broader reflections, suggesting a crystallite size in the order of 1-2 nm. While the assumption of nanocrystalline orthorhombic goethite also provided an acceptable fit to the diffractogram in this case, due to the very broad reflections the crystal structure of "HMT010" could not be derived unambiguously on the basis of the PXRD measurement. For the sample "VSK04", TEM measurements confirmed the presence of goethite in the form of several times 10 nm wide and 50-200 nm long aggregates of crystallites, with an Fe:O ratio close to the expected 1:2 as revealed by the EDX analysis. As reflected by the HRTEM images (Figure 1 left), the individual goethite nanocrystals are ca. 4-8 nm wide and few tens of nanometers long. The characteristic lattice periodicity of goethite, $d(100) = 0.42$ nm can be observed as well. In contrast, in the case of „HMT010", HRTEM (Figure 1 right) and SAED reflects a very poorly crystalline Fe-oxide, with composition approaching Fe:O = 1:2 ratio, and with the ordered domains extending over the scale of only a few nanometers.

In conclusion, the reverse precipitation preparation methods used resulted in iron-oxide-hydroxide nanopowder samples

with a remarkable difference in their crystallinity. While the main phase of the sample "VSK04", having the higher level of crystallinity, could clearly be identified as goethite, the low-crystallinity nature of the „HMT010" sample hinders the unambiguous association of a definite crystal structure with this sample.

Related publications

- [1] I.V. Alenkina, V.K. Kis, I. Felner, E. Kuzmann, Z. Klencsár, M.I. Oshtrakh: *Structural and magnetic study of the iron cores in iron(III)-polymaltose pharmaceutical ferritin analogue Ferrifol®*. J. Inorg. Biochem. 111202 (2020) <https://doi.org/10.1016/j.jinorgbio.2020.111202>
- [2] Z. Klencsár, J. Wang, R. Ge, W. Zhou, D. Liu, A.I. Rykov, T. Zhang: Further development of the database of the Mössbauer Effect Data Center. *Hyperfine Interact.* **241**, 1–6. (2020) <https://doi.org/10.1007/s10751-019-1660-1>

SELF-ASSEMBLY AND REVERSIBLE REORGANIZATIONS OF GRANA - REVEALED BY SMALL-ANGLE NEUTRON SCATTERING

Renáta Ünnepe

Objective

Photosynthesis is the energetic basis of virtually all life on Earth. The light reactions of oxygenic photosynthesis occur in the thylakoid membranes, flattened closed lipid vesicles, which are densely packed with proteins. In green plants, these membranes are differentiated into stacked grana and unstacked stroma regions. The cylindrical grana stacks are interconnected by stroma membranes. These thylakoids enclose a single, contiguous inner aqueous phase and form a highly organized continuum membrane, which, despite its robustness, appears to possess high structural flexibility. The molecular and physical mechanism of the self-assembly of this membrane system and the role of its structural dynamics in different regulatory mechanisms are not well understood. Here, we carried out small-angle neutron scattering (SANS) measurements with the aims (i) to clarify the role of hydration forces in stabilizing the stacking interactions in grana - we investigated the effects of Hofmeister salts on the periodic organization of isolated thylakoid membranes; and (ii) to establish correlation between the most important photoprotective mechanism, the non-photochemical quenching (NPQ), and the ultrastructural changes in excess light - we monitored the light-induced, dark reversible reorganizations of grana in correlation with NPQ in live leaf segments. NPQ safely dissipated the excess excitation energy as heat to protect the photosynthetic complexes.

Methods

Small-angle neutron scattering is a non-invasive technique, which is capable of providing unique, spatially and statistically averaged information under physiologically relevant conditions on the ultrastructure of multilamellar membrane systems and their temporal variations on the time scale of seconds to tens of minutes. SANS measurements were performed on (i) freshly isolated thylakoid membranes, which were treated with different concentrations of kosmotropic, neutral and chaotropic Hofmeister salts; and (ii) on leaf segments of the evergreen plant, *Monstera deliciosa* possessing very large multilamellar grana in the vertical direction and showing intense NPQ in excess light.

Results

The Hofmeister series of salts ranks the cations and anions, which have different effects on the aggregation, structure, dynamics and crystallization properties of proteins. The ultrastructural changes in the presence of a relatively low concentration of NaCl and NaSCN are predominantly induced by the cationic effect, suggested by the similar effect of NaCl and NaSCN (chaotrop) on the repeat distance and periodic order of grana membranes. While the periodic order of the thylakoid membranes was basically retained with 1.5 M NaCl, it was largely and rapidly diminished with 0.5-1.5 M NaSCN. These SANS results contribute to the better understanding of the mechanisms of Hofmeister salts on different levels of structural complexity. The main steps of the disassembly of grana in the presence of chaotropes in terms of their timescale from faster to slower ones are (1) diminishment of long-range periodic order, (2) gradual loss of stacked membrane pairs (3) disappearance of the long-range chiral order of the protein complexes (as concluded from complementary circular dichroism measurements). These results corroborate that the hydration forces have primary importance in the stabilization of grana thylakoid membranes. [1]

We have shown that NPQ-inducing illumination causes a strong decrease in the periodic order and a slight decrease in the repeat distance of grana thylakoid membranes. These dark-reversible ultrastructural changes occur on the time scale of minutes, following similar kinetic patterns as the build-up and relaxation of the NPQ. Furthermore, these changes accelerate upon repeated illumination, similar to the NPQ. These results would suggest a close correlation between ultrastructural changes and NPQ, but the effect of the photosystem II electron transport inhibitor diuron is different on NPQ and on the ultrastructural changes. Diuron impedes only the relaxation of the structural changes and not their formation, whereas the NPQ is suppressed by diuron. This suggests that the structural changes do not cause, but enable, NPQ. We have also shown that the changes of the SANS peak do not originate from light-induced redistribution and reorientation of chloroplasts. [2]

Remaining work

We could not use our SANS beamtime at the Laue Langevin Institute on green algae due to the COVID-19 pandemic situation. These measurements will be performed after the lifting of travel restrictions. We have made progress on the *Arabidopsis thaliana* (higher plant) project, but some measurements are to be repeated and conclusions have yet to be drawn.

Related publications

- [1] O. Zsiros, R. Ünnepe, G. Nagy, L. Almásy, R. Patai, N. K. Székely, J. Kohlbrecher, G. Garab, A. Dér, L. Kovács: *Role of Protein-Water Interface in the Stacking Interactions of Granum Thylakoid Membranes-As Revealed by the Effects of Hofmeister Salts*, *Frontiers in Plant Science*, **11**: 1257 (2020) doi: 10.3389/fpls.2020.01257
- [2] R. Ünnepe, S. Paul, O. Zsiros, L. Kovács, N.K. Székely, G. Steinbach, M.-S. Appavou, L. Porcar, A.R. Holzwarth, G. Garab, G. Nagy: *Thylakoid membrane reorganizations revealed by small-angle neutron scattering of *Monstera deliciosa* leaves associated with non-photochemical quenching*, *Open Biology*, **10**:200144 (2020) <http://dx.doi.org/10.1098/rsob.200144>

NEUTRON AND X-RAY RADIOGRAPHY AND TOMOGRAPHY AT BRR

Zoltán Kis, László Horváth, László Szentmiklósi

Objective:

To develop and apply imaging instrumentation and methodology at the Budapest Research Reactor (BRR).

Methods

Thermal and cold neutron, as well as X-ray imaging in 2D and 3D, tomographic reconstruction, volume rendering

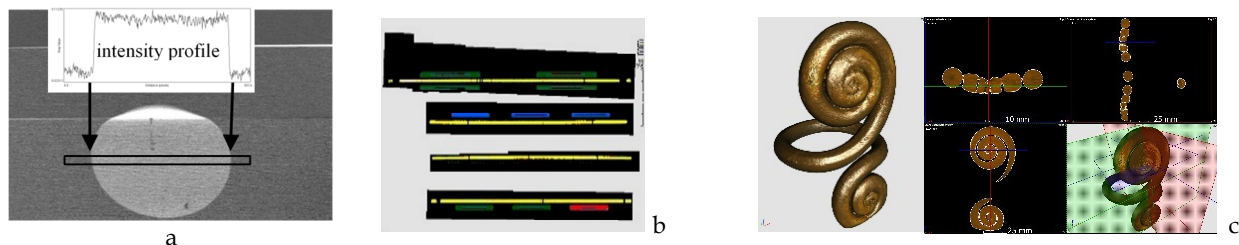
Results

Neutron imaging:

- Pilot dynamical neutron radiography experiments were carried out at the RAD station to prove the feasibility of an inspection, which will follow both the temporal and spatial movement of a **fluid hydrocarbon material** in a shock absorber (motion damper) used in the automotive industry. It was shown that the hydrogen content of the fluid provides enough contrast even when used behind several cm thick metal layers and with seconds-long exposure time (*Fig.1 a*).
- The lack of recycling leads to the loss of valuable resources, as many components of *electronic waste*, such as gold, copper, rare earth elements could be extracted economically. To determine the overall elemental composition of electronic waste by non-destructive nuclear analysis methods, we exploited the in-beam activation of elements during neutron tomography (NT). After having completed an NT scan, the object was measured by gamma-ray spectroscopy in a low-level chamber. In this way its composition was determined according to the principles of neutron activation analysis. In *Fig.1 b*, one can see different types of memory cards.
- Within the *cultural heritage* field, in the framework of a Lendület project, we carried out the NT of an emblematic bronze spiral from Tiszafüred-Majoroshalom dated in the Late Bronze Age. (*Fig. 1 c*). According to the structural analysis we concluded it was produced using the lost-wax technique. Later Time-of-Flight measurements supported this first idea.

X-ray imaging:

- *Nuclear forensics* helps to identify the origin and history of nuclear and other radioactive materials not under regulatory control. Specific sealed sources (e.g. neutron sources) are now in focus, because finding the original producer and licensee of an unknown source is essential. Characteristic parameters (e.g. internal structure) helps to identify the production technology and the producer. As a non-destructive and safe analytical technique, X-ray radiography was used to examine the internal structure of several Cf-252- and Cm-244-based sources. The similarities and differences (internal capsules, double-capsulizing, wall-thickness of the inner capsules, form and distribution of source material in the inner capsule between different sources) are informative about the producer. In *Fig.1 d* one can see two different Cf-252 sources. A database will help the inspector's work in the future.
- We tested the idea of *dual-energy X-ray imaging* in a joint project with neutron, ion beam, synchrotron and X-ray measurements on a purposely-made piece of Sevres ceramics, which was decorated on its surface. The thin painted layers are hard to visualize in normal X-ray radiography, however, the pointwise ratio of the images taken at lower and higher X-ray energy beams allowed to enhance the contrast (*Fig.1 e*).
- Quantitative X-ray radiography was carried out for an HPGe gamma-ray detector to provide real, otherwise inaccessible, geometrical *data for MCNP simulations*. The measured dimensions and angles will be used in the optimisation process of a low-level chamber design (*Fig.1 f*).



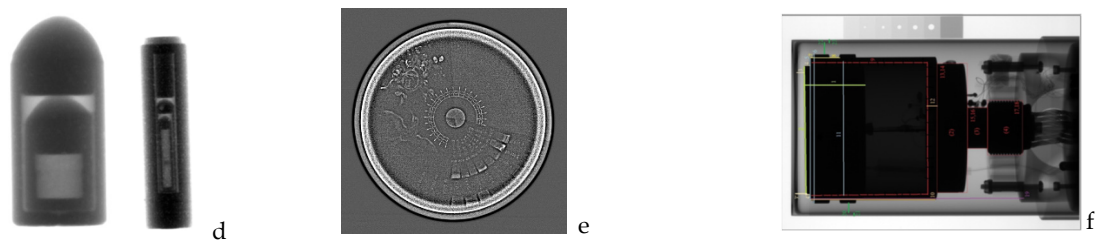


Figure 1: Neutron and X-ray imaging results: see text for further information

Related publications

- [1] R. Zboray, C. Greer, A. Rattner, R. Adams, Z. Kis: *Fast Neutron Imaging at a Reactor Beam Line*. Mater. Res. Proc. **15**, 180–184 (2020)
- [2] Roncsolásmentes anyagvizsgálat neutronokkal, Innotéka Magazin, Issue May 2020 14-16, in Hungarian (2020)

EXAMINING TECHNOLOGY AND PROVENANCE OF ARCHAEOLOGICAL CERAMICS

Katalin Bajnok, Adél Len

Objective

Pottery constitutes one of the most common and enduring physical remains of ancient human societies, consequently forms a major area of interest within archaeological research as a proxy of the history and transmission of technology, and as a witness to the social, economic and cultural factors that influenced such technology. Our research focuses on three main subtopics: investigating the application of Small Angle Neutron Scattering (SANS) to the identification of ancient pottery forming techniques, further developing the methodology of assessing maximum firing temperature of archaeological ceramics using SANS and applying this method to late Roman-early medieval ceramic wares, and examining the provenance of early mediaeval pottery from Western Hungary with ceramic petrography and elemental analysis (SEM-EDS).

Results

Within the overall pottery production sequence, forming technology represents a critical stage. The adequacy of SANS method for the differentiation of pottery forming techniques by reference to two series of modern fine-ware vessels made under controlled conditions has been proved. In the present study it is assumed that pores and other scattering objects become preferentially aligned according to the forces applied during forming, reflecting the different forming techniques used, within and below the clay-sized ($< 2 \mu\text{m}$) fraction. Repeated measurements were made on samples taken from a series of vessels prepared using a range of historical forming techniques: coil building, wheel-shaping and wheel-throwing. Results have shown that a clear differentiation between the wheel-shaping and wheel-throwing techniques can be made based on SANS scattering patterns (**Figure 1**), which, besides of proving to be reliable, is also a non-destructive technique. The development of the HWXY two-dimensional SANS data evaluation software towards a quantitative presentation of the results has also been done.

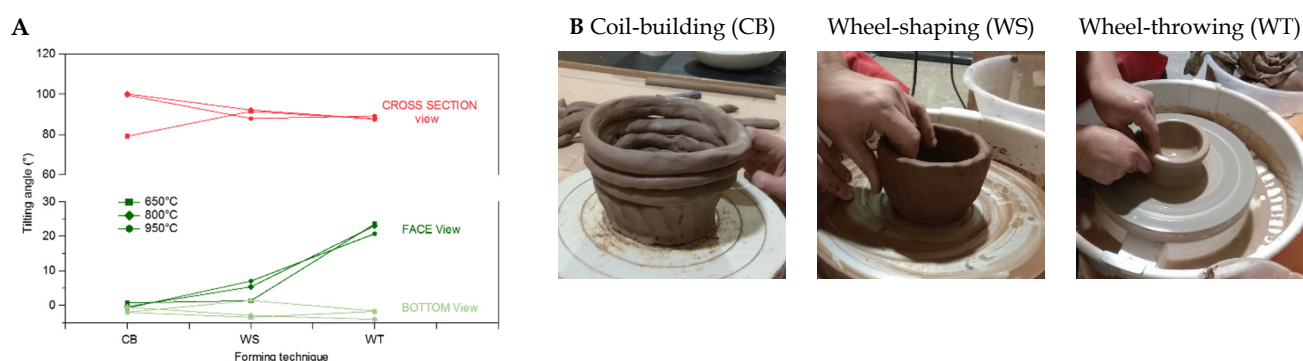


Figure 1: A: Representation of the tilting angles measured on the scattering pattern for face, cross-sectional and bottom views for all three forming techniques. Wheel-thrown samples can be distinguished by their characteristic $\sim 22\text{-}25^\circ$ tilting angle in face view. B: The making of the experimental vessels, displaying the three historical techniques

A SANS-based methodology was further developed for estimating maximum firing temperature of ceramic wares. The previously established method is based on the linear dependence of the exponent p on maximum firing temperature, however, with that method accurate results can only be obtained if the geological source of the clay is known, and control series of this raw material is used to calibrate the results. For archaeological ceramics, in many cases the exact geological source of the clay is not known. A new approach combined with various combinations of heating and tempering treatments was tested on four experimental control clay series to explore how to determine maximum firing temperature when the original raw material cannot be identified. Subsequently, 16 ceramic sherds from the late Roman fortress of Keszthely-Fenékpuszta (4–6th c. context) were analysed and the value for maximum firing temperature was obtained. These results assist to better understand the technological changes in the socio-economic transformation that followed the collapse of Western Roman Empire. Our results are summarised in an already accepted manuscript that was delayed to be published in the second half of 2021.

The origin of a distinct pottery assemblage from the early medieval period (6–7th century AD, Early Avar Age) was examined by ceramic petrography (polarising light optical microscopy) and SEM-EDS. Based on their mineralogical and elemental composition, most of the analysed samples indicate that they were produced locally, while some are connected to distant territories. Our results show that this group of vessels reflect the migration of a craftsman, or a group of craftsmen, from northern Italy or western Germany to the territory of the Avar Empire [1].

Related publication

- [1] K. Bajnok, Gy. Szakmány and Zs. Bendő: *Petrographic contribution to the origin of Early Avar Age 'Csákberény group' ceramics*, Journal of Archaeological Science: Reports **32**, 102411 (2020)

NON-DESTRUCTIVE, SPATIALLY-RESOLVED ELEMENT ANALYSIS OF STRUCTURED SAMPLES

László Szentmiklósi, Boglárka Maróti, Zoltán Kis

Objective

To develop Prompt-Gamma Activation Imaging (PGAI), and use it to study non-homogeneous and irregularly-shaped samples

Methods

Linear attenuation coefficient measurements via neutron imaging, composition measurements by PGAI-NT (Neutron Tomography), computer programming, Monte Carlo modelling.

Results

Within the project K124068 funded by the NKFIH, we worked out a comprehensive correction method, applicable to voluminous and/or complex-shaped samples, to handle the negative matrix effects of PGAA related to the neutron self-shielding and gamma self-absorption [1]. It relies on the detailed geometrical data obtained by 3D optical scanning. The scanning results were used for the MCNP input simulation model of the NIPS-NORMA facility, thus implementing the real experimental sample geometry. Neutrons with known energy- and directional distributions were propagated with MCNP through the object and the neutron field, as well as the capture rate of selected elements, were mapped with 3D mesh tallies. In a second step, these were used to define a distributed source of the emerging capture gamma rays with characteristic energies and to simulate their attenuations as they propagated towards the HPGe detector. The method was applied to a whole-rock geological sample of about 1 kg mass, to determine the spatial distribution of its representative elemental compositions non-destructively. After correction, good general consistency was found between the several measurement positions, as well as with the destructively obtained powder samples analysed with our validated standard procedure. A book chapter has been finalized on the heritage-science applications of the PGAI-NT technique [2].

We developed a state-of-the-art combination of three-dimensional surface and volumetric digital imaging techniques, as well as position-resolved element composition analysis by PGAI, and used it on fossils of the *Parascutella gibbercula* species to scrutinize their shapes and internal structures [3]. The study opens new perspectives in the understanding of the sedimentation conditions of the rocks.

In collaboration with the AGLAE PIXE facility at Museum Louvre, Paris, the coupling of 3D scanned non-planar geometries and the sample positioning was elaborated and published [4].

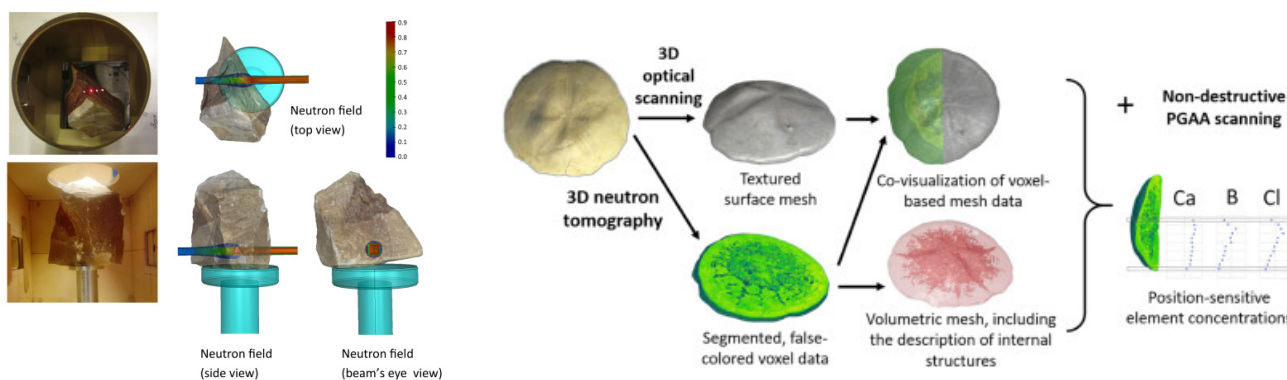


Fig.1: Photos of a bulk geological stone object (left top and bottom), its 3D scanned model, and the MCNP6-calculated neutron field overlaid (right top and bottom).

Fig.2: The false-coloured 3D neutron tomography data co-visualized with the photorealistic surface mesh from the 3D optical scanning. Radial profiles of Ca, B and Cl, relative to the calcite, the major constituent of the shell, are shown on the right side.

Related publications

- [1] L. Szentmiklósi, Z. Kis, B. Maróti, L. Z. Horváth: *Correction for Neutron Self-Shielding and Gamma-Ray Self-Absorption in Prompt-Gamma Activation Analysis for Large and Irregularly-Shaped Samples*. J. Anal. At. Spectrom. 36, 103–110. (2021)
- [2] L. Szentmiklósi, B. Maróti, Z. Kis, Z. Kasztovszky: *Integration of neutron-based elemental analysis and imaging methods and applications to cultural heritage research*, in Springer Handbook of Cultural Heritage Analysis, (2021) ISBN 978-3-030-60015-0
- [3] B. Maróti, B. Polonkai, V. Szilágyi, Z. Kis, Z. Kasztovszky, L. Szentmiklósi, B. Székely: *Joint application of structured-light optical scanning, neutron tomography and position-sensitive prompt gamma activation analysis for the non-destructive structural and compositional characterization of fossil echinoids*. NDT & E Int. 115. (2020), 102295

- [4] T. Calligaro, L. Arean, C. Pacheco, Q. Lemasson, L. Pichon, B. Moignard, C. Boust, L. Bertrand, S. Schoeder, M. Thoury, L. Rosta, L. Szentmiklósi, J. Füzi, Z. László, V. Heirich: *A new 3D positioner for the analytical mapping of non-flat objects under accelerator beams*. Nucl. Inst. Methods **B 467**, 65–72 (2020)

LARGE FACILITY ANALYTICAL STUDIES OF POLISHED AND GROUND STONE ARTEFACTS

Zsolt Kasztovszky¹, Bálint Péterdi², Katalin T. Biró³, György Szakmány⁴, Veronika Szilágyi¹, Katalin Gméling¹, Kata Szilágyi⁵, Ildikó Harsányi¹, Dóra Miklós⁴, Erika Kereskényi⁶, Tamás Sági⁴, Levente Illés¹

¹Centre for Energy Research, ²Mining and Geological Survey of Hungary, ³Hungarian National Museum, ⁴Eötvös Loránd University, Department of Petrology and Geochemistry, ⁵Móra Ferenc Museum, ⁶Herman Ottó Museum

Objective

The project aims to identify the raw material sources of polished and ground stone artefacts in Hungary, delimiting the potential source areas as precisely as possible. Based on our former results, potential sources of some raw material types are located outside Hungary, even outside the Carpathian Basin. The research focuses on a systematic study of finds and raw materials that were not or only partly studied so far, completing former results by application of new methods. We pay special attention to source collected reference materials from the potential raw material sources.

Methods

The irreplaceable archaeological finds will be analysed mostly by non-destructive methods Prompt-gamma Activation Analysis (PGAA) and “Original Surface” Scanning Electron Microscopy with Energy Dispersive X-Ray microanalyses (OS-SEM-EDX) for major components, while Neutron Activation Analysis (NAA) is used to measure the trace elements.

Results

Critical and systematic organization of the previous data

During previous projects related to polished stone tools, data from around 1000 PGAA measurements were collected. Eighty % of these records has been checked, however the names and categories of the rocks need to be reviewed in some cases. With this, we started to prepare for the planned data base. The IT framework is planned to be constructed by an external IT expert, on the model of previous data bases (e.g. “Miss Marble”). On the server of the EK, an ftp storage place is reserved for raw data. Besides our own experimental data, we plan to provide literature data as well.

Selection of archaeological objects to study from Hungarian museums

Due to COVID19, almost all the tasks connected to travel (i.e. museum visits, field trips within or outside the Hungarian border, conferences) were cancelled. In February, Katalin T. Biró visited the Jósza András Museum in Nyíregyháza and observed their collection of stone tools.

PGAA, NAA and SEM-EDX experiments

We started to analyse the following stone tool (polished axes) collections, which were easily available:

Objects from the Prehistoric collection of the Hungarian National Museum, from the “Lengyel” collection (21), from Bakonyszűcs (1), from Kup-Egyes (1), from field trips in Cserhát region (Péntek Attila’s collection, 23), from an excavation in Polgár-Csőszhalom (3), Deszk-Ordos (1, Móra Ferenc Museum) – altogether 50 pieces.

Non-destructive PGAA was done on them. From 13 objects, it was allowed to prepare thin sections (at ELTE Dept. of Petrology and Geochemistry). On 30 axes, OS SEM-EDX studies were done at the Nanosensors Lab of the EK. Further complementary SEM-EDX measurements are planned at ELTE.

49 sandstone samples (mostly powdered + some fragments) connected to other stone utensils were measured by PGAA, and 18 by NAA at the Budapest Neutron Centre of the EK. NAA of another 28 sandstones are postponed to 2021, due to the renovation of the NAA lab. Heavy minerals separation was done on 13 samples. These works are connected to the PhD study of Dóra Miklós.

The evaluation of the PGAA, NAA and SEM-EDX experimental data is in progress. We started to select the objects for the 2021 experiments.

Remaining work

We have started to preselect the objects from museums and fieldworks for the 2021 analytical studies and also to organize the structure of the Polished Stone Tools Atlas, according to the research plan.

Related publications

- [1] K. Szilágyi, K.T. Biró, Gy. Szakmány, B. Péterdi, V. Szilágyi, Zs. Kasztovszky: *Provenance study of polished and ground stone artefacts in the Carpathian Basin and its surrounding from an archaeological perspective*, EAA2020, 26-30 August, 2020,

Budapest, on-line.

- [2] Zs. Kasztovszky, KT. Biró: *Application of neutron-based methods in provenance research of lithic archaeological material* (poster), EAA2020, 26-30 August, 2020, Budapest, on-line.
- [3] E. Kereskényi, B. Fehér, F. Kristály, I. Harsányi, Zs. Kasztovszky, Gy. Szakmány: *Minek nevezzetek? Archeometriai szemelvény egy sadaganait-tartalmú kőbaltáról* (in Hungarian). In: J. Füri, E. Király (szerk): *Átalakulások*. 11. Közettani és Geokémiai Vándorgyűlés; Magyarhoni Földtani Társulat, Budapest, p. 38. ISBN: 978-963-671-320-1 (2020)
- [4] E. Kereskényi, Gy. Szakmány, B. Fehér, I. Harsányi, Zs. Kasztovszky: *Kékpala-zöldpala átmeneti fáciesű csiszolt kőeszközök a Herman Ottó Múzeumból* (in Hungarian). In: J. Füri, E. Király (szerk): *Átalakulások*. 11. Közettani és Geokémiai Vándorgyűlés; Magyarhoni Földtani Társulat, Budapest, pp. 39-41. ISBN: 978-963-671-320-1 (2020)
- [5] D.G. Miklós, Gy. Szakmány, S. Józsa, F. Horváth: *A gorzsai késő neolit vörös homokkő anyagú szerszámkövek petrográfiai alapú rendszere* (in Hungarian). In: J. Füri, E. Király (szerk): *Átalakulások*. 11. Közettani és Geokémiai Vándorgyűlés; Magyarhoni Földtani Társulat, Budapest, pp. 59-62. ISBN: 978-963-671-320-1 (2020)
- [6] E. Kereskényi, Gy. Szakmány, B. Fehér, I. Harsányi, V. Szilágyi, Zs. Kasztovszky, M. T. Tóth: *Archaeometrical results related to Neolithic amphibolite stone implements from Northeast Hungary*, *Journal of Archaeological Science: Reports* **32**, 102437 (2020)

INVESTIGATION OF SURFACE REACTIVITY ON STEEL/CEMENT AND STEEL/CLAY SYSTEMS

Margit Fábrián, János Osán, Ottó Czömpöly, Zsolt Kerner

Objective

Long-term exposure of materials in a radioactive waste repository could result in significant alterations in materials during the service life. The planned work is an attempt to investigate the corrosion intensity through laboratory tests modelling in-situ conditions. The corrosion of metals (steel) in clay/concrete is a huge problem which can affect the performance of long term disposal. Most of the planned and potential disposal environments are saturated with moisture. In addition to designing the experiments to measure corrosion behaviour, we must also develop statistical methods to evaluate the data collected during these experiments. The aim of the planned experiments is to characterize the steel/clay and steel/concrete interfaces evolved under different conditions (temperature, ground water) using different methods. These data will help us to understand the strengths and weaknesses of the system model, allowing us to optimize it.

Methods

Two laboratory experiments were set up to gain information on corrosion intensity at the interfaces between carbon steel and cement and carbon steel and clay. The experiments were set up in parallel, for steel/cement and for steel/clay, using a double walled closed-reactor system kept at a constant temperature of 80°C. It comprises 3 steel/clay and 3 steel/cement experimental units, which are planned to be taken out after 3, 7 and 12 months and will be running until June 2021. An internal Teflon cylinder contains a carbon steel cylinder embedded in concrete/clay. There is an external Teflon cylinder filled with the simulated groundwater to keep the degree of water saturation close to 100 %. Holes of 0.7 mm in diameter in the inner Teflon cylinder walls ensures the connection with the groundwater in the outer Teflon cylinder. Synthetic groundwater of the Boda Claystone and cementitious water are used for saturating the clay and cement, respectively, as realistic environmental conditions. The physical and chemical properties of the Boda synthetic groundwater and conditioned cementitious water have been compiled to further define the initial states of the reactive transport model. During the experiment an online monitoring of the corrosion potential will be done. The first cycle (3 months) finished on 30 September 2020. We took out the first containers from the incubator, and started to perform characterization of the steel/clay and steel/cement interfaces using different methods.

Results

On the interface of steel/cement, Scanning Electron Microscopy (SEM) imaging and energy dispersive X-ray spectroscopy (EDS) were performed, and now we are preparing for X-ray diffraction measurements.

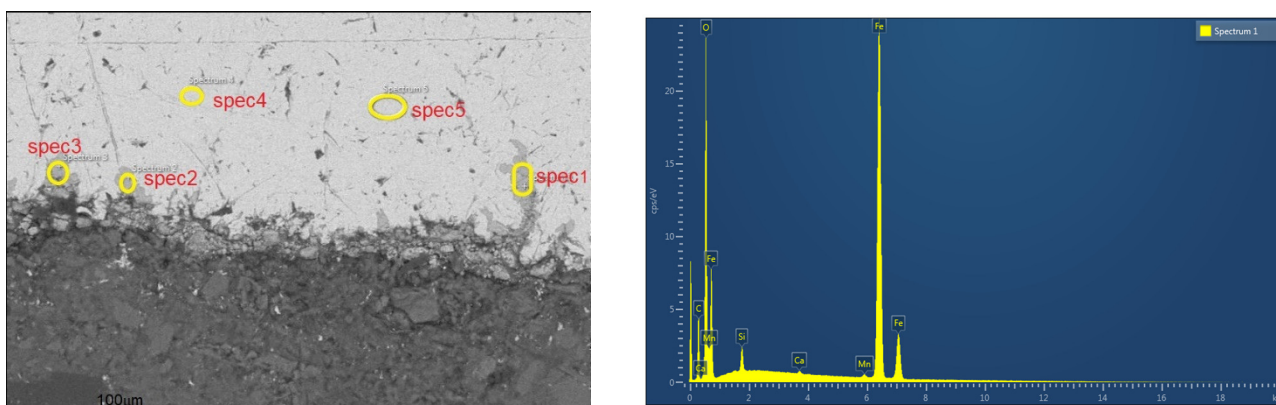


Figure 1: SEM image of the steel/cement interface and the EDS spectrum in a characteristic interface position.

On the steel/cement interface the appearance of Fe-oxide could be identified in the SEM image as a corrosion product, and the x-ray results in Table 1 also show that the corrosion product is present along the interface.

Table 1: Elemental compositions of the signed area from Fig 1 (in weight %).

Spectrum Label	Spectrum 1	Spectrum 2	Spectrum 3	Spectrum 4	Spectrum 5
O	20.59	18.42	20.76		
Si	1.28	0.13	0.36	0.33	0.49
Ca	0.17	0.16	0.12		
Mn	0.55	0.40	0.32	0.58	0.60
Fe	77.42	80.90	78.45	99.08	98.91

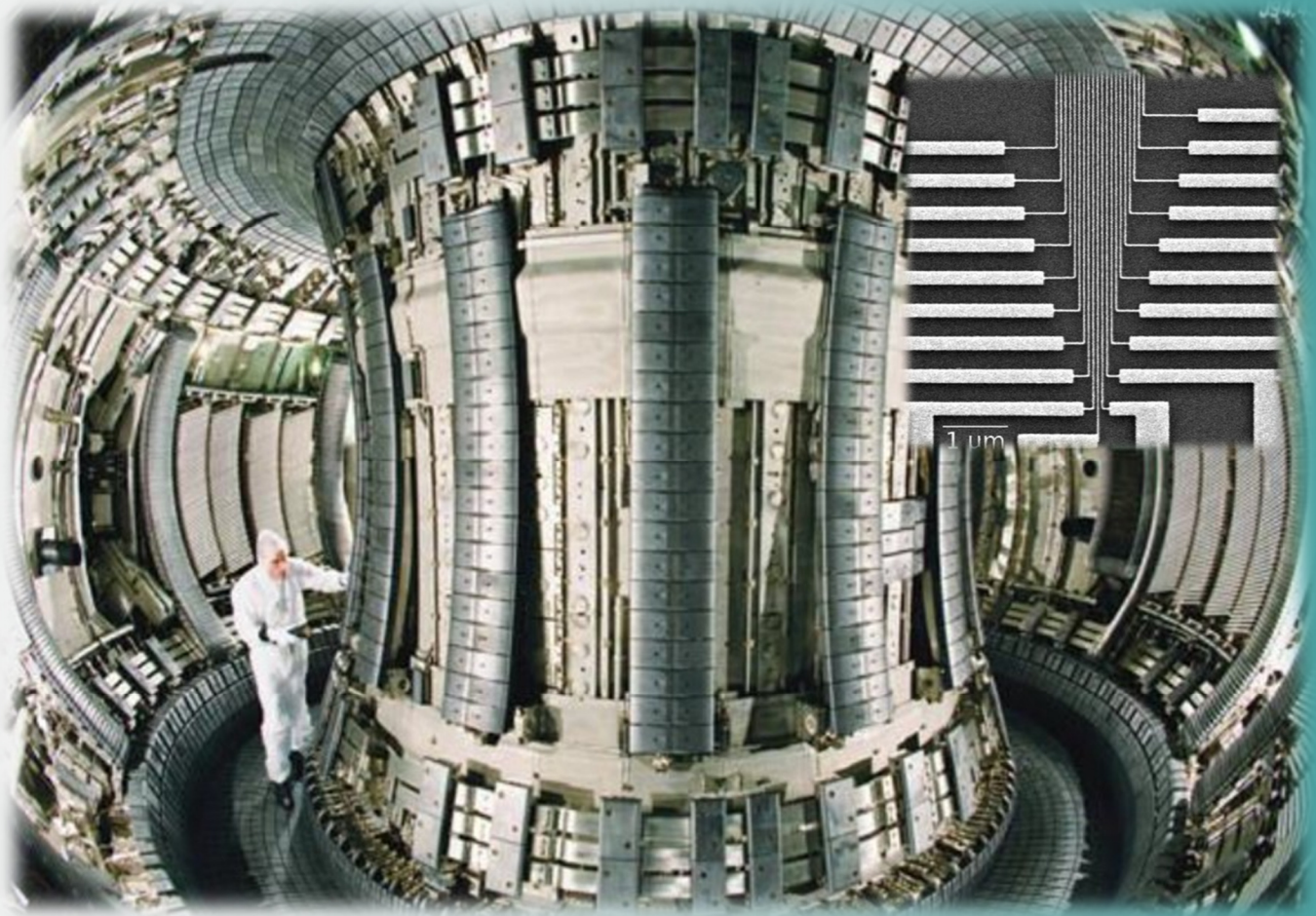
Total	100.00	100.00	100.00	100.00	100.00
-------	--------	--------	--------	--------	--------

The evaluation of the chemical-physical and corrosion properties are in progress for the samples which were taken out after 3 months, for both type of experiments. We expect that results from these experiments will serve as data for modelling and serve for a better understanding of the planned concept. The modelling applied to these tests will be carried out by SCK CEN (Centre d'Étude de l'énergie Nucléaire) after the acquisition of the experimental results and when the modelling approach is defined in a later stage of the project.

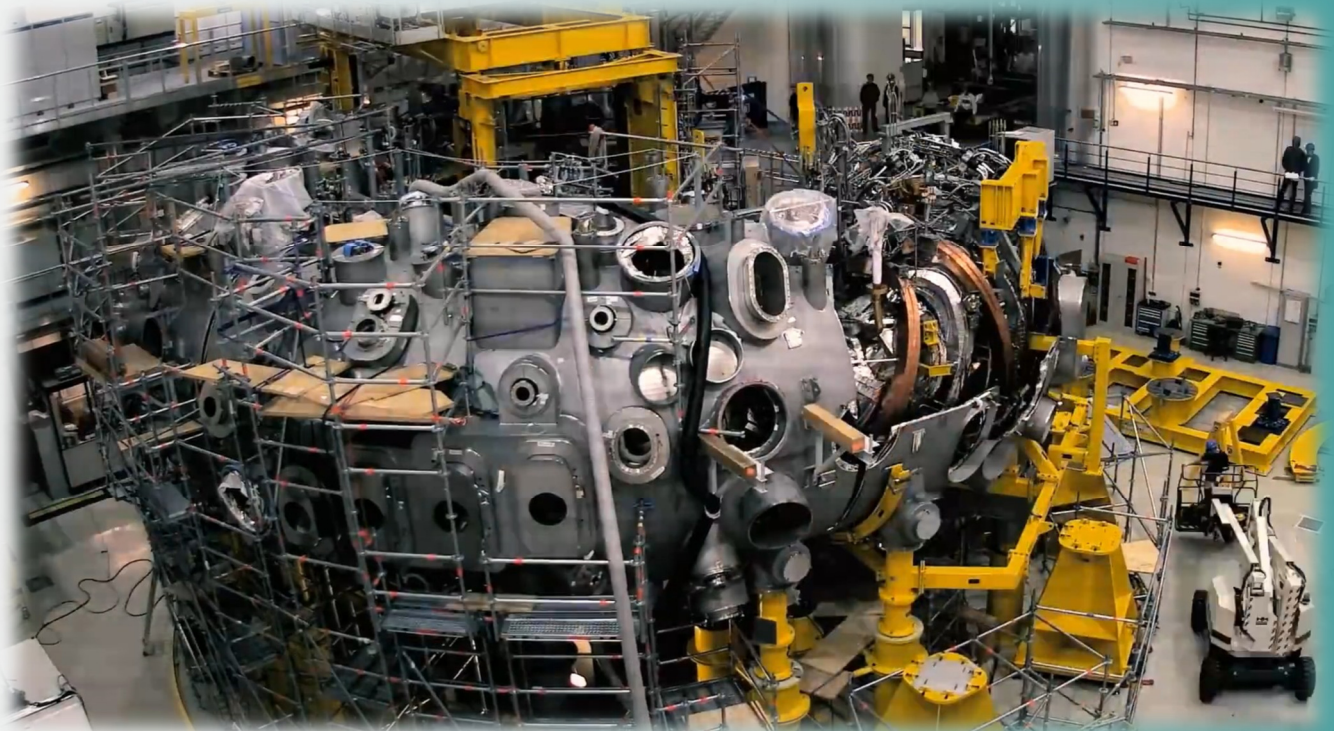
This work was partly supported by the H-2020 European Joint Program on Radioactive Waste Management (EURAD) -847593.

Remaining work

Intense research efforts are underway to understand the corrosion activity on the steel/cement and steel/clay interfaces.



VI. NULEAR FUSION RESEARCH



PARTICIPATION IN THE EUROFUSION PROGRAMME

Overview

Eurofusion is a European consortium coordinating fusion energy research in the European Union. Each Member State nominated a participant in the consortium, which coordinates the national research activities. Eurofusion is partially supported by the Horizon 2020 research programme at a maximum rate of 55%; the rest is provided by national funds. For Hungary, the Wigner Research Centre for Physics was originally the nominated member of the Consortium. During the reorganization of the Hungarian Academy of Science research network starting in January 2020, the fusion research activities of Wigner RCP were moved to the Centre for Energy Research. Here three departments are involved in Eurofusion. The Fusion Plasma Physics Department builds and operates plasma diagnostic equipment for major European and worldwide fusion experiments, performs engineering design for various facilities and does numerical and analytical calculations for understanding the physics of high temperature plasmas. The Fusion Technology Department is involved in engineering design activities, while the Fuel and Reactor Materials Department performs analysis and irradiation studies of materials used in fusion devices. The sections below describe their most important activities in 2020.

IDENTITY OF THE JET M-MODE AND THE ASDEX UPGRADE I-PHASE PHENOMENA

Dániel Imre Réfy, Sándor Zoletnik, Dániel Dunai, Örs Asztalos

Objective

A high confinement mode (H-mode) plasma state close to the low to high confinement transition with clear density and temperature pedestal has been observed both at the Joint European Torus (JET) and at the ASDEX Upgrade (AUG) tokamaks usually identified by a low frequency (1–2 kHz) oscillation of the magnetics and the modulation of pedestal profiles. The regime at JET is referred to as Magnetic mode or M-mode while at AUG as intermediate phase or I-phase. This contribution aims at a comparative analysis of these phenomena in terms of the density and temperature pedestal properties, the magnetic oscillations and symmetries.

Methods

The investigation of the density profile dynamics during these phenomena became possible with the upgraded Lithium Beam Emission Spectroscopy (Li-BES) at both machines, as the diagnostics are capable of density profile measurements up to the pedestal top with 0.5–1 cm spatial and 50–100 μ s temporal resolution. The Li-BES technique is a routinely used diagnostic for electron density profile measurement at several plasma experiments.

Results

The M-mode and the I-phase related density profile modulation is analysed in terms of coherence spectra of the turbulence amplitude and the electron density at different radial locations along the Li-BES beam path. Figure 1 shows the density profile behaviour of the M-mode on the left, I-phase on the right: the (a) and (b) figures show the coherence, the (c) and the (d) the average density profile while (e) and (f) the phase profile relative to the turbulence power modulation. The beam is propagating from right to left. The top and the bottom of the pedestal is mostly modulated, as indicated by the two maxima in the coherence at these positions at the M-mode/I-phase frequency. The relative phase between the top and bottom of the pedestal fluctuation is π , while the middle of the pedestal is less affected, which indicates that the gradient is modulated. The phase of the pedestal bottom density relative to the turbulence power modulation of the magnetics is $+0.3\pi$ which means that the flattening of the pedestal is preceded by the turbulence power pulse in the magnetics by 120 μ s. The negative (-0.7π) phase at the pedestal top represents the same: the minima of the pedestal top density during the flattening of the pedestal is preceded by the turbulence power activity maxima by 0.3 π . A radially outward propagating density perturbation in the SOL is also related to the phenomena, indicated by the clear phase delay outwards in the SOL. These results, as well as all other observations in reference [1] are fairly similar for the M-mode and the I-phase which lead to the conclusion that their physical background is the same.

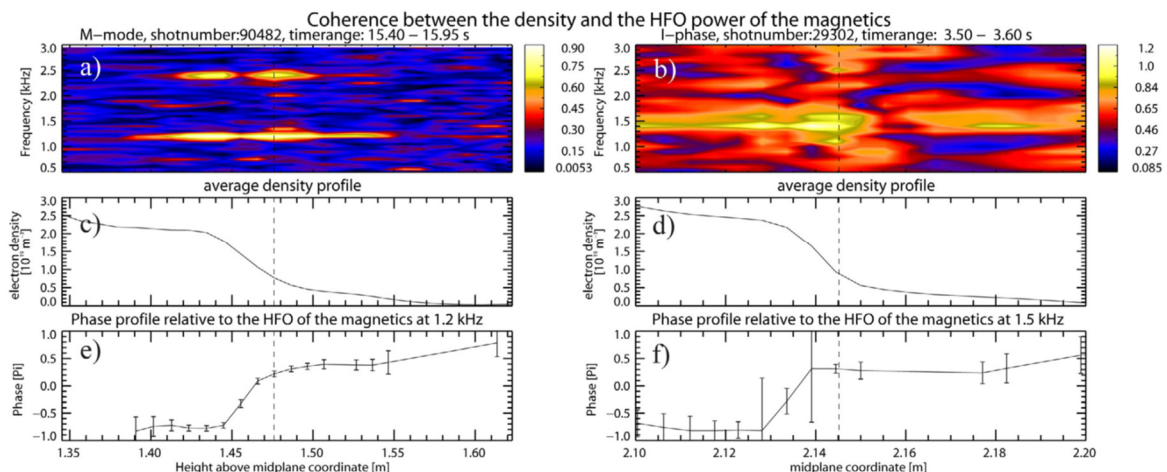


Figure 1: M-mode (a) and I-phase (b) coherence of the turbulence amplitude of the magnetics and the low frequency oscillation of the electron density; M-mode (c) and I-phase (d) averaged density profile; M-mode (e) and I-phase (f) phase profile at the relevant frequency range relative to the turbulence amplitude modulation of the magnetics.

Remaining work

This project has been completed however there are several opened questions which can be found in reference [1].

Related publication

[1] D.I. Réfy et al: *Identity of the JET M-mode and the ASDEX Upgrade I-phase phenomena* Nucl. Fusion **60**, 056004 (2020)

INVESTIGATION OF THE EDGE PLASMA ON THE WENDELSTEIN 7-X STELLARATOR

Gábor Kocsis, Gábor Anda, Gábor Cseh, Dániel Dunai, Tamás Szepesi, Miklós Vécsei, Sándor Zoletnik, Lilla Zsuga

Objective

In 2020 the investigation of the edge plasma on the Wendelstein 7-X stellarator covered the following topics: analysis of video diagnostics data to study hot-spots, small stable plasmas and turbulent filaments, edge and upstream island density profile evaluation during long pulse discharges, analysis of video diagnostics and alkali beam data for turbulence in the edge plasma and island, and exploring the 3D structure of filaments by correlation analysis.

Methods

The data of video and alkali metal beam diagnostics were analysed with various methods such as cross correlation and conditional averaging. Several software tools were developed or upgraded: a video data visualization software (EDVIS), a statistical analysis library (FLAP) to explore multidimensional data and a new and swift code to reconstruct the density for the alkali beam spectroscopy. To address the hot-spot problem in a more general manner, the development of a universal detection algorithm was started. This algorithm will be able to detect multiple hot-spots in an image, and determine their characteristics, such as location and size.

Results

During plasma operation in W7-X, several examples of “small plasmas” were observed, where the plasma size was significantly smaller than the nominal plasma size, down to 50% or less. These plasmas had absolutely no contact with plasma facing components and were stable for many confinement times. Significant toroidal asymmetry can be observed in the radiation pattern of the plasma, being different in each module on the video camera images [1].

The data analysis code for obtaining density profiles from the Alkali Beam Emission Spectroscopy (ABES) has been completed and utilized for the reconstruction of density data for several plasma discharges, with a time resolution up to 20 μ s. A manuscript detailing the method has been completed [2]. Several works using the diagnostic data has been published in 2020 [3-6].

After hydrogen pellet injection, an improved plasma confinement was found in the previous experimental campaign. Although the turbulence drive changes in the core, a significant effect in the edge turbulence is also observed. It was found that in this improved plasma confinement regime the turbulence is significantly changed, since a clear suppression is observed in the power spectra in the 1-10 kHz range. When the core temperature drops, the edge density increases as well as the edge turbulence.

A conditional averaging program package was developed to investigate filament behaviour such as fluctuation amplitude, poloidal distribution, poloidal rotation speed, etc. A few discharges with high camera frame rate (90 kHz) were analysed in detail. Among others, it was concluded that more significant filament activity and larger filament amplitudes were observed at those poloidal locations where more positive events can be found.

A multi-diagnostic study [6] was conducted to reveal the 3D structure and dynamics of the edge filaments. Filaments are seen to be born at the edge and, at least in some cases, seen to extend to up to four toroidal turns. After moving radially out a few cm, they enter the edge island. Here they disappear and about 200 microseconds later reappear on the outboard side of the island.

Remaining work

Most of the studies presented here are ongoing and therefore will be continued in the next years.

Related publications

- [1] T. S. Pedersen et al: 62nd Annual Meeting of the APS Division of Plasma Physics (2020)
- [2] M. Vécsei et al: *Swift evaluation of electron density profiles obtained by the Alkali Beam Emission Spectroscopy technique using linearized reconstruction*, submitted to Plasma Physics and Controlled Fusion
- [3] A. Tancetti et al: *Experimental investigation of parametric decay instability in Wendelstein 7-X*, Bulletin of the American Physical Society (2020)
- [4] A. Krämer-Flecken et al: *Investigation of turbulence rotation in the SOL and plasma edge of W7-X for different magnetic configurations*, Plasma Science and Technology **22.6**, 064004 (2020)
- [5] X Han et al: *Validation of the elliptic approximation model for the edge turbulence perpendicular velocity measurement via the poloidal correlation reflectometer in Wendelstein 7-X*, submitted to Nuclear Fusion
- [6] S Zoletnik, et al: Plasma Phys. Control. Fusion **62**, 014017 (2020)

INSTALLATION AND COMMISSIONING OF THE EDICAM VIDEO DIAGNOSTIC SYSTEM AT JT-60SA

Tamás Szepesi, Gábor Cseh, Gábor Kocsis, Tamás Szabolics, Sándor Zoletnik

Objective

Visible video diagnostics is one of the key systems in present-day magnetic confinement fusion experiments, as they offer a wide range of applications from machine safety to scientific analysis. The Event Detection Intelligent Camera (EDICAM), developed especially for fusion experiments, is equipped with a special CMOS sensor to be able to fulfil these two tasks by a single device. It can produce full resolution overview movies at lower frame rates (for operational and safety purposes), while additional movie streams can be produced at reduced resolution and increased frame rate (for scientific analysis). A video diagnostic system, based on the EDICAM camera, was designed, built and delivered for the Japanese JT-60SA tokamak experiment in the last few years [1], with the main task for 2020 being the installation and commissioning.

Methods

Following the delivery of the system, it was found on-site that the accessibility of the camera's surrounding is poor, risking safe installation. Therefore, an additional unit, the so-called 'docking aid' was designed, built and delivered to Japan, where it served two purposes: a) when attached to the entrance of the observation port, it serves as a shelf, carrying the significant weight (11.5 kg) of the camera system; b) during the docking process (when the camera is moved to the measurement location, its position is set by locaters) it helps the person to exert the necessary force.

The commissioning of the camera system has two phases. In phase 1 the camera's data acquisition and control (DAQ) system is connected to and tested with the experiment's environment, using a computer network (LAN). During individual linkage tests the experiment control system is only controlling the EDICAM system, checking whether the camera controls can accept all possible operational command scenarios, as well as the proper production of data. In subsequent integrated linkage tests the EDICAM is running along with several other systems, simulating complete experiment cycles.

In phase 2 the camera system is operated in real plasma experiments, that is, this commissioning phase coincides – at least for some time – with the actual making of measurement. The aim in this final phase is to find optimal camera settings that fit to the (constantly changing) status of the experiment, in order to achieve the highest quality images.

Results

The installation and docking of the diagnostic system were successfully completed. This was verified by producing images with the camera of the interior of the empty vacuum vessel of the experiment – where proper docking is proved by the good quality of the imaging (see Figure 1, right).

During individual and integrated linkage tests the EDICAM system worked as expected: the camera DAQ software reacted to control signals as planned, while the data production was flawless, exhibiting the highest possible transfer speed (see Figure 1, left).

	Standard	Low framing
Frame rate	100 Hz	10 Hz
Measurement time	60 s	60 s
Total frames	6000	600
Time for processing	140 s	10 s
Unprocessed data size	15,7 GB	1,6 GB
Data server upload time	135 s	14 s
Processed data size	488 MB	48 MB
Data server upload time	5 s	1 s
PC2 → PC1 transfer	135 s	14 s



Figure 1: Left: EDICAM image recording test results. Right: First camera image from the JT-60SA plasma vessel.

Remaining work

Minor modifications to the control software were requested, which add more features, such as the recording/discarding of technical discharges. Plasma operation in JT-60SA was shifted to 2021. Therefore phase 2 of the commissioning will be conducted next year.

Related publication

[1] T. Szepesi et al: *Wide-angle visible video diagnostics for JT-60SA utilizing EDICAM*, Fus. Eng. Des. **153**, 111505 (2020)

ENGINEERING DESIGN CONTRIBUTIONS TO THE DONES PROJECT

András Zsákai, Mátyás Tóth, Imre Katona, Tamás Dézsi

Objective

An accelerator-based neutron source called DONES (Demo-Oriented early NEutron Source) is being designed as a dedicated irradiation facility for testing candidate materials for the DEMO (DEMONstration Power Station) fusion reactor. Almost twenty Research Units around Europe, as well as industry Third Parties, are involved working on different aspects of the DONES project.

Our laboratory is mainly involved in the engineering design of the Material Test Cell of DONES, which is the heart of the DONES facility, because the material testing will take place inside it. Our other contribution is the implementation of the Systems Engineering Approach to the whole project and the identification and management of the overall facility's interfaces.

An industry contribution is also involved, mainly focusing on the engineering design of the Lithium Loops, the Test Cell liner, the design of the HFTM (High flux test module), which will contain the material specimens, the alignment support mechanism and Remote Handling related aspects.

Methods

The engineering design of the Test Cell includes the design of the model using CATIA, the definition of the Design Description Document of the subsystem and the identification of interfaces and requirements connected to the Test Cell.

The System Engineering work mainly focused on the implementation of a useful and comprehensible interface identification approach. A previously developed (spell out php) (php) based software is used as a basis, but it was tailored to the needs of DONES. After this, the main focus was to identify and maintain the interfaces of the system.

The industry contribution work mainly focused on the engineering design of the Lithium Loop hydraulic system and on the thermal calculations of the Test Cell atmosphere considering also the nuclear heat provided by the beam. Work also has been done on the design of the HFTM positioning.

Results

Previously, a monolithic concept was used for the Test Cell, but this was deemed inappropriate, and a maintainable test cell concept had to be developed. A useful and appropriate design was submitted to the project leaders and was approved, changing the fixed concrete structure of the Test Cell into movable blocks and changing the fixed Test Cell liner to a removable liner concept.

The Test Cell design description document has been updated taking into account the previously provided documents, e.g. remote handling of the sample in the Test Cell, safety aspects, beam impact on the test cell and many more. The applicable requirements (around 250) and interfaces (around 50) have been identified and defined in the appropriate software.

The implementation of the interface approach has resulted in an appropriate methodology to identify the boundaries (main connecting points) of the system and then going into more detail by defining the interfaces of the system. Around a thousand interfaces have been identified and defined so far.

The engineering design of the Lithium Loop hydraulic system mainly yielded the result that a revision was needed to change the outline of the room to acquire more space and also to have a more compact outline of the system. Two concepts have been worked out for the support and alignment of the HFTM, but the decision has not yet been made to use either one. A CFD analysis on the maintainable test cell atmosphere has been conducted which provided thermal field results on the Test Cell liner that was used to determine the efficiency of the cooling layout.

Remaining work

The project is ongoing for several years under the EUROfusion Consortium, and the industrial contribution work is also ongoing.

Related publications

- [1] A. Zsákai et al.: *DONES Systems Identification and requirements allocation*, Abstract submission (2021)
- [2] A. Zsákai et al.: *Requirements engineering in interface management of IFMIF-DONES facility*, Abstract submission (2021)
- [3] I. Katona, A. Zsákai, M. Tóth, A. Dézsi et al.: *Preliminary Finite Element Analysis of the Stainless- steel Liner of the Maintainable Test Cell Concept of IFMIF-DONES*, Abstract Submission (2021)

IRRADIATION OF EUROFER MATERIAL FOR EUROFUSION WPMAT PROJECT

*Ildikó Szenthe, Márta Horváth,
Ferenc Gillemot, Levente Tatár, Dániel Antok*

Objective

In fusion reactors, the materials of the components should resist high neutron radiation, so the effect of radiation-induced aging should be investigated. Until the planned IFMIF-DONES irradiation device (high flux neutron source for future fusion material testing with appropriate spectrum) will be built, the neutron aging embrittlement will be studied in the available fission environment. As part of this task, EK started irradiating Eurofer steel fracture-toughness-testing specimens in the Research Reactor of the Budapest Neutron Center. The purpose is to irradiate the specimens at 300 and 350°C up to 0.5 dpa fluence. This task required the development of the BAGIRA (Budapest Advanced Gas-cooled Irradiation Rig with Aluminium structure) rig for controlling at two different temperatures during more than 1000 hours' irradiation time.

Methods

Prior to irradiation, the hardness measurements required by the standard for comparison to results from later post-irradiation material testing and the pre-fatigue of the samples were performed. Irradiation to 0.5 dpa (Fe) at two temperatures: 300 and -350 °C was started in the second half of 2020.

After the elaboration of the research plan, the target holder and the capsules were designed and manufactured. Based on the fabrication plan the Eurofer block arrived from the Karlsruhe Institute of Technology (KIT) from which the 24 pieces of CT (compact tension) specimens were fabricated and coded. The specimens were notched using 0.12 mm molybdenum wire electrical discharge machining and pre-fatigued according to the ASTM E-1921 standard. The final specimen geometry was checked. Vickers hardness measurements were also performed, and all data were collected into a database. The irradiation was performed in an inert gas (Helium-nitrogen mix) atmosphere. Each capsule temperature during irradiation was measured by separate thermocouples and controlled by auxiliary electric heating. The PC controlled automatic system regulated the heating and collected the temperature-time data. Dosimetry monitors were used to measure the fluence. Six specimens were irradiated at 300°C and another six one were irradiated at 350°C, while the remaining 12 specimens are stored for higher temperature irradiation.

Results

The first 12 specimen irradiation was started in the third quarter of 2020. The irradiation temperature (except for the starting periods) was successfully controlled within a ± 10 °C range.



Figure 1: BAGIRA irradiation rig in the reactor, linked to gas and electrical connections

Remaining work

The start of the irradiation was delayed due to the COVID-19 pandemic and will be finished in the first quarter of 2021. The irradiated specimens will be withdrawn and prepared for testing and the dosimetry foils will be evaluated in 2021. The higher temperature irradiation is delayed and is planned to be performed in 2021.

PARTICIPATION IN EUROFUSION WPMAT PROJECT - DATABASE AND MATERIAL PROPERTY HANDBOOK

*Ildikó Szenthe, Ferenc Gillemot,
Szilvia Móricz, Kristóf Andor Csikós*

Objective

Research reports are generally scientific. Individual reports generally have only a few results. Several research reports together can contain the sum of new knowledge required by the designers of the future fusion devices. The purpose of the Material Properties Handbooks (MPH) is to collect all relevant material properties and provide them to the designers in a user-friendly format. Centre for Energy Research (EK) collects the relevant data into a database developed in the proper format of other MPH-s within the EUROFUSION WPMAT project. Earlier the database for the Materials Property Handbook for Eurofer steel, Cu-Cr-Zr alloy was prepared in co-operation with KIT (Karlsruhe Institute of Technology). In 2020, our task was to collect and put into the Functional Materials MPH the new data on irradiated optical and dielectrical materials.

Methods

In order to produce a useful, easy-to-understand handbook for designers, it is essential to evaluate the research results provided in different forms. The relevant results are digitized and stored in the database. The aged properties (mainly after neutron and gamma irradiation) were compiled from reports of the EUROfusion WPMAT research group. The collected data have been evaluated together. The data provided in diagram format have been re-digitized and stored in Excel sheets, which easily can be transferred into other forms of materials database storage.

Results

Both in the database of functional materials and in the Material Property Handbook, a large amount of data has been processed. In the database, the number of records exceeds 15,000. The three types of data collected were: optical, physical, and mechanical properties of the optical and dielectrical materials. The most important properties are the electrical resistance, electrical conductivity, permittivity, dissipation factor, dielectric loss, optical transmission, absorption and reflection.

In 2020, mainly aged data were collected, uploaded and used for the Functional Material MPH. The database was used for elaboration of the FM MPH. As an example, Figure 1 summarizes the neutron irradiation effect on Sapphire.

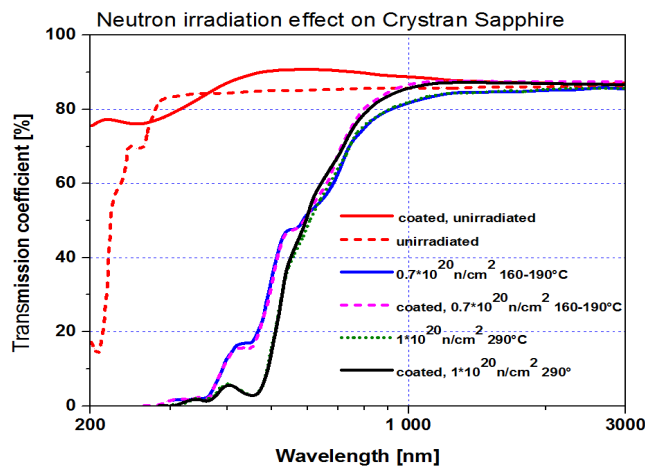


Figure 1: Figure from Functional Material MPH: Transmission coefficient of coated and uncoated sapphire manufactured by Crystran as a function of wavelength after neutron irradiation at different fluxes and temperatures

Remaining work

The development of structural and functional materials for future fusion devices (mainly for the energy generating “DEMO” fusion reactor) are continuing in the frame of WPMAT project. The database and MPH-s have to follow the research and continuously have to be upgraded. EK together with other European institutes is expected to participate in this task.

Related publication

- [1] M. Gorley, E. Diegele, E. Gaganidze, F. Gillemot, G. Pintsuk, F. Schoofs, I. Szenthe: *The EUROfusion material property handbook for DEMO-in vessel components- Status and the challenge to improve confidence level for engineering data* Fusion Engineering and Design September 2020P.

ENGINEERING SERVICES FOR ITER'S LOWER-PORTS

Miklós Palánkai, Jenő Kádi, László Poszovecz, Gábor Veres

Objective

The objective of the International Thermonuclear Experimental Reactor (ITER) Lower Port Services Engineering taskforce is to support the ITER Diagnostics team in the establishment and evaluation of diagnostics systems, providing mechanical engineering design, modelling, analysis and development of mock-ups and prototypes required for design validation, and also input to construction work descriptions.

This work concerns development of remote handling equipment and port integration services for the ITER fusion experiment.

These systems are present in 3 lower ports of the ITER machine. The key component of these systems are the diagnostic racks (DR), which are 10.5 ton steel structures housing various diagnostic tenant apparatuses and they also contribute to the nuclear shielding performance of the ITER machine. These DRs need to be fed with water and gas pipes and electrical cables to actuate subsystems and observe plasma parameters. Being inside the vacuum vessel, these racks are fully Remote Handling (RH) compatible, since human presence is not allowed in this environment.

Port integration is also a highly complex work because the different diagnostic systems hosted by the ports are typically developed and manufactured in different ITER partner countries. For example, in the second lower port, the diagnostic system is manufactured in Japan, but the rack holding the whole system is from Russia. Insuring that these two subsystems are compatible with each other is the port integrators job.

Methods

During the evaluation of the Lower Port Services Engineering task, three key computer programs have been used:

- CATIA V5-6R
- ANSYS 2019
- 3D Experience

To be able to properly execute the tasks, besides the three programs, access to the ITER ENOVIA database is also mandatory. All the designs which have been created needed to be implemented into the ITER's own database.

Results

In order to service the DR systems, it is necessary to cut some of the supply piping and move it out of the way. After finishing the service, the pipes are reinstalled and rewelded.

Until now, several industrial methods for pipe welding and cutting have been checked and, with modifications, the most suitable ones have been implemented into all three ports. As the cutting and welding tools are heavy equipment, support structures needed to be developed in order to be able to position and hold them during their operation. The cutting tool on the support during operation can be seen in Figure 1/a. Because there is very limited space for such big tools (e.g. orbital pipe cutting and welding tools), to be able to solve the removal of the DRs, after cutting, the wall mounted pipes need to be remotely moved out of the way of the DRs. For this purpose, the manipulator that can be seen in Figure 1/b, has been developed.

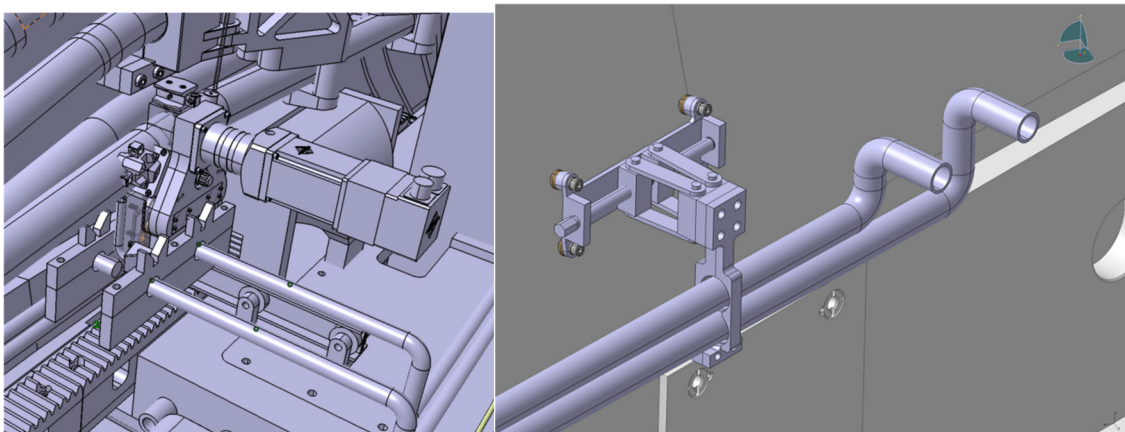


Figure 1: a: Orbital pipe Cutter with the movable support structure; b: Pipe manipulator

To make sure the supports/manipulators are structurally proper and will work as planned, several analyses have been performed on them. This design is made for the preliminary design review of the remote handling ports.

Remaining work

The project is still running. Remote handling methods, materials, design need to be finalized.

DIFFUSION BONDING EXPERIMENTS OF 316L SPECIMENS IN A GLEEBLE 3800 THERMOMECHANICAL SIMULATOR

Tétény Baross, Péter Bereczki, László Jánosi, Miklós Palánkai, Botond Sánta and Gábor Veres

Objective

Diffusion bonding methods as a candidate solution for Plasma Facing Components in fusion reactors involved significant investigations over the last decades. In 2019-2020 diffusion bonding and reference heat affected zone tests of the 316L specimens were performed in a Gleeble 3800 GTC physical simulator and a 1D numerical simulation code was developed for these diffusion bonding processes.

Methods

For diffusion bonding the 1D numerical simulation code was written which took into account the material properties, Joule-heating in function of temperature and altering cross-section and the axial force as it was controlled by Gleeble 3800 thermomechanical simulator. The creep deformation was modelled on the specimens with the uneven temperature distribution and with altering cross-sections. The contact electrical resistance between the bonded surfaces was approximated by an exponential decreasing function, as a function of time. The numerical simulations were able to model the stroke differences as they occurred during the physical tests between the heat affected zone tests and the diffusion bonding tests at same conditions. The code was written in MATLAB with the help of Excel sheets.

The code with the R_{surf} function approximated well with the measurement results as it is visible on Fig.2. a. Further studies shall be required in future to specify the axial stroke via a more precise plasticity model, since the creep stress exponent can be the function of the temperature above 650–700 °C. For Joule-heating by the Gleeble system used AC current the DC current was modelled. However, they have the same linear increasing tendency as it was expected, but the value of the exact Power Angle of the Gleeble system and the simulated DC current could not be associated exactly to each other.

Results

One of the main observations of the experiments was that the diffusion bonded specimens' axial strokes were lower than the HAZ specimens with the same bonding conditions, where the applied pressure and temperature were: DG7/RG7: 1055 °C, 30 MPa, DG3/RG3: 1000 °C/30MPa. These phenomena could be explained and modelled by the contact electrical resistance at the bonded surfaces as it is visible on Fig.2. b. Since the modelling of the diffusion bonding surface has many uncertainties (oxides, contaminations), this kind of estimation of the contact electrical resistivity by measurements can give an important information for larger scale joining processes.

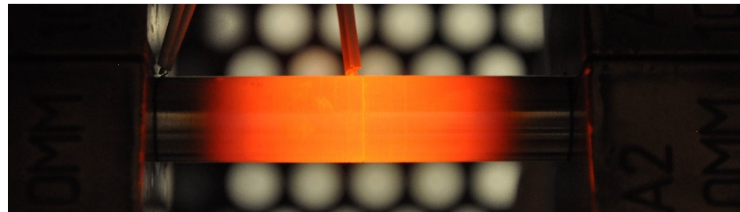


Figure 1: a.) 1.4404 Diffusion bonding specimen in Gleeble 3800, University of Dunaújváros [1]

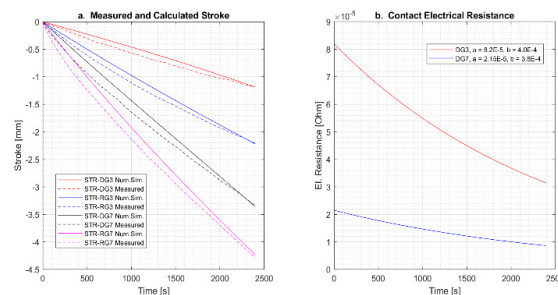


Figure 2: a.) The measured and the numerical results for the stroke functions of DG3, RG3, DG7, RG7 tests during the 2400 s period
b.) The functions of surface contact electrical resistance during bonding in numerical simulations, the a , b parameters for DG3, DG7 are visible on the image, the equation: $R_{surf} = a \cdot e^{-b \cdot t}$ [1]

Related publication

- [1] T. Baross, P. Bereczki, L. Jánosi, M. Palánkai, B. Sánta, G. Veres: Diffusion bonding experiments of 316L steels in a Gleeble 3800 thermomechanical simulator for investigation of non-destructive inspection methods, Fusion Engineering and Design, 160 111768 (2020)

ABBREVIATIONS

2D	Two-dimensional
8YSZ	8mol% Yttria-stabilized Zirconia
ACP	Amorphous Calcium Phosphate
ACTOF	Accident Tolerant Fuels
AEKI	Institute for Atomic Energy Research
AER	Atomic Energy Research
AES	Auger Electron Spectroscopy
AFM	Atomic Force Microscopy
a-Ge	Amorphized Ge
AMTD	Activity Median Thermodynamic Diameter
ANOVA	Analysis of Variance
ANP	Analytical Network Process
AQ	Amodiaquine
ALD	Atomic Layer Deposition
ALLEGRO	Experimental Helium Gas Cooled Fast Reactor Developed by the European V4G4
ATLAS+	Advanced Structural Integrity Assessment Tools for Safe Long Term Operation
ATOMKI	MTA Institute for Nuclear Research
BAGIRA	New Irradiation Device at the Budapest Research Reactor
BC	Black Carbon
BCA	Bicinchoninic Acid
BCC	Body Centred Cubic
BCS	Boron Coated Straw
BDD	Boron Doped Diamond
BEMA	Bruggeman Effective Medium Approximation
BF	Bright Field
BITS	Bin Type Statistical Simulation
BME	Budapest University of Technology and Economics
BNC	Budapest Neutron Centre
BRR	Budapest Research Reactor
BSA	Bovine Serum Albumin
BzO	Benzaldehyde (C ₆ H ₅ CHO)
BzOH	Benzyl alcohol (C ₆ H ₅ CH ₂ OH)
BZN	Bay Zoltán Nonprofit Ltd. for Applied Research
CAD	Computer-Aided Design
CAK	Zirconium Material Studies
CCMP	Computer Controlled Micropipette
CDS	Ceramic Dispersion Strengthened
CEFR	China Experimental Fast Reactor
CERIC	Central European Research Infrastructure Consortium
CERN	Centre Européen pour la Recherche Nucléaire (French name of the European Organization for Nuclear Research)
CFD	Computational Fluid Dynamics
CL	Cody-Lorentz
CNA	Complex Network Analysis
CNS	Cold Neutron Source
CNT	Carbon Nanotube
CMA	Cylindrical Mirror Analyser
CMD	Classical Molecular Dynamics, Carboxymethyl dextran
CMUT	Capacitive Micromachined Ultrasonic Transducer

COD	Chemical Oxygen Demand
COF	Friction Coefficient
CONCERT	EU H2020 Project for the Integration of Radiation Protection Research
CONFIDENCE	Consortia of an European Joint Programme (COPing with uNcertainties For Improved modelling and DEcision making in Nuclear emergenCIes)
COPD	Chronic Obstructive Pulmonary Disease
CPE	Controlled Potential Electrolysis
CRP	IAEA Coordinated Research Project
CPL	Coplanar Transmission Line
CV	Cyclic Voltammetry
CVD	Chemical Vapour Deposition
D&D	Decommissioning and Dismantling
DBA	Design Basis Accident
DBC	Double-bent-crystal
DBTT	Ductile-to-brittle Transition Temperature
D3S	Distributed Space Weather Sensor System
DFT	Density Functional Theory
DFT-LSDA	Density Functional Theory with the Local Spin-density Approximation
DGA	Diglycol Amide
DLD	Deterministic Lateral Displacement
DLR	German Aerospace Centre
DOPC	Dioleoylphosphatidylcholine
DP	Deposition Precipitation
DRIFTS	Diffuse Reflectance Fourier Transform Infrared Spectroscopy
DRM	Dry Reforming
DSB	Double Strand Break
DSP	Dithiobis(succimidyl propionate)
DUV	Deep Ultraviolet
EB	Electron Beam
EBB	Elegant Breadboard Model
EB GL	Electricity Balancing Guidelines
EBS	Electron Backscatter Diffraction
ECR	Equivalent Cladding Reacted
EDS, EDX	Energy-dispersive X-ray Spectroscopy
EDXRF	Energy-dispersive X-ray Fluorescence
EELS	Electron Energy Loss Spectroscopy
EEW	Electric Explosion of Wires
EGCG	Epigallocatechin-gallate
EMR	Electron Magnetic Resonance
ELTE	Eötvös Loránd University, Budapest
EMA	Effective Medium Approximation
EMR	Electron Magnetic Resonance
E-MRS	European Materials Research Society
EPS	Environmental Protection Service
EQM	Engineering Qualification Model
ERDA	Elastic Recoil Detection Analysis
ESA	European Space Agency
ESD	Electrospray Deposition
ESS	European Spallation Source, Lund
EURADOS	European Radiation Dosimetry Group
EVs	Extracellular Vehicles
EXAFS	Extended X-ray Absorption Fine Structure

FAZ	Fly Ash Zeolites
FC	Field Cooling
FCC	Face Centred Cubic
FEG	Field Emission Gun
FEM	Finite Element Method
FFT	Fast Fourier Transform
FIB	Focused Ion Beam
FluidFM BOT	Specialized Robotic Fluid Force Microscope
FS	Force Spectroscopy
FTO	Fluorine-doped Tin Oxide
GC	Glassy Carbon
GDML	Geometry Description Markup Language
GFR	Gas-Cooled Fast Reactor
GILD	Gas Immersion Laser Doping
GINOP	Economic Development Innovation and Operative Program
GLE	Ground Level Enhancement
GM	Geiger–Müller
GMCS	Graphene Added Multilayer Ceramic Sandwich
GPU	Graphics Processing Unit
GRAS	Geant4 Radiation Analysis for Space
GSTP	General Support Technology Programme
HAADF	High-angle Annular Dark-field
Hap	Hydroxyapatite
HIP	Hot Isostatic Pressing
HLW	High-level Radioactive Waste
HOPG	Highly Oriented Pyrolytic Graphite
HP	Hot Pressing
HPGe	High-purity Germanium
HPT	High Pressure Torsion
HRTEM	High Resolution Transmission Electron Microscopy
HSA	Human Serum Albumin
HV	High Voltage
IAEA	International Atomic Energy Agency
IBM	Ion-beam Mixing
IBMP	Institute for Biomedical Problems, Moscow
ICP-MS	Inductively Coupled Plasma Mass Spectrometry
ICP-OES	Inductively Coupled Plasma Optical Emission Spectrometry
IFFT	Inverse Fast Fourier Transition
ILL	Institut Laue-Langevin
ILW	Intermediate Level Waste
INCLUDING	INnovative CLUster for raDIological and Nuclear emerGencies
INSIDER	Improved Nuclear Site characterisation for waste minimisation In Decommissioning and dismantling operations under constrained EnviRonment
InvOLS	Inverse Optical Lever Sensitivity
IOD	In-Orbit Demonstration
IoT	Internet of Things
IPERION CH	EU Funded Project (Integrated Platform for the European Research Infrastructure ON Cultural Heritage)
IPF	Inverse Pole Figure
IR	Infrared
ISO	International Organization for Standardization
ISS	International Space Station

ITO	Indium Tin Oxide
KFKI	Former Name of the Research Centre, Nowadays the Campus Name
KIKO3DMG	Nodal Reactor Physics Calculation Code Developed in the CER
KIT	Karlsruhe Institute of Technology
KVSZ	Environmental Protection Service (Hungarian acronym)
LDOS	Local Density of States
LEL	Lower Explosion Limit
LET	Linear Energy Transfer
LLW	Low Level Waste
LOC	Lab-on-a-Chip
LOCA	Loss of Coolant Accident
LSC	Liquid Scintillation Counting
LTO	Long Term Operation
MAT	Magnetic Adaptive Testing
MCB	Moiré Commensurate Bilayer
MCBJ	Mechanically Controlled Break Junctions
MCC	Multilayer Ceramic Composite
MCD	Multi-criteria Decision
MCNP	Monte Carlo N-Particle Transport Code
MCNPX	Monte Carlo N-Particle eXtended
MELODI	Multidisciplinary European Low Dose Initiative
MEMS	Microelectromechanical System
MFA	Institute of Technical Physics and Materials Science (Hungarian acronym)
MIC	Minimum Inhibitory Concentration
MLG	Multi-layered Graphene
MOX	Mixed Oxide
MS	Mass Spectrometry or Mössbauer Spectroscopy or Member States
MU	Mock-ups
EK	Centre for Energy Research (Hungarian acronym)
MWCNT	Multiwall Carbon Nanotube
MU	Mock-up
MVM	Hungarian Power Companies
NAA	Neutron Activation Analysis
NAL	Nuclear Analysis and Radiography Department, MTA EK
ND	Neutron Diffraction
NDE	Non Destructive Evaluation
NEAAA	Neutron-based Element Analysis and Activation Assessment
NIPS	Neutron Induced Prompt Gamma-ray Spectroscopy
NIPS-NORMA	Neutron-Induced Prompt Gamma-ray Spectroscopy & Neutron Optics and Radiography for Material Analysis
NIR	Near InfraRed
NKFIH	National Research, Development and Research Office (Hungarian acronym)
NMR	Nuclear Magnetic Resonance
NMX	Neutron Macromolecular Diffraction
NNKP	National Nuclear Research Program (Hungarian acronym)
NOMAD	Non-destructive Evaluation System for the Inspection of Operation-Induced Material Degradation in Nuclear Power Plants (EU H2020 project)
NP	Nanoparticle
NPP	Nuclear Power Plant
NR	Neutron Radiography, Nanorod
NR/NT	Neutron Radiography and Tomography
NS	Nanosphere

NUBIKI	Nuclear Safety Research Institute
O&M	Operation and Maintenance
OAH	Hungarian Atomic Energy Authority (Hungarian acronym)
ODS	Oxide Dispersion Strengthened
OECD	Organisation for Economic Co-operation and Development
OTKA	Hungarian Scientific Research Fund (Hungarian Acronym)
OWLS	Optical Waveguide Light Mode Spectroscopy
Paks NPP	Paks Nuclear Power Plant
PBI	2,2'(2-pyridyl)benzimidazole
PCA	Principal Component Analysis
PCB	Printed Circuit Board
PD	Prisoner's Dilemma
PDMS	Polydimethylsiloxane
PE-ALD	Plasma Enhanced Atomic Layer Deposition
PEG	Polyethylene Glycol
PFM	Protonflight Model
PGAA	Prompt-gamma Neutron Activation Analysis
PGAI	Prompt-gamma Activation Imaging
PGAI-NT	Prompt-gamma Activation Imaging – Neutron Tomography
PL	Power-Law
PLA	Polylactic Acid
PoC	Point of Care
PPKE	Pázmány Péter Catholic University (Hungarian acronym)
PSD	Position Sensitive Detector
PSF	Photon Strength Function
PURAM	Public Limited Company for Radioactive Waste Management
PXRD	Powder X-ray Diffractometry
pXRF	Portable XRF Spectrometer
PWR	Pressurized Water Reactor
RAD	Static/dynamic Thermal-neutron and X-ray Imaging Station at BNC
RADACT	Alpha Particle – Epithelial Cell Interaction Model
RADCUBE	A Joint Mission Name of the ESA
RadMag	Instrument for Measuring Space Radiation and Magnetic Field Parameters
RBC	Red Blood Cell
RBS	Rutherford Backscattering Spectrometry
REXUS/BEXUS	Rocket and Balloon Experiments for University Students
RF	Radio Frequency
RID	Radioisotope Identification Detector
RM	RadMag
RMC Method	Reverse Monte Carlo Method
RMS	Root Mean Square
RPV	Reactor Pressure Vessel
RT	Room Temperature
SAA	South Atlantic Anomaly
SAED	Selected Area Electron Diffraction
SAFEST	EU Funded Project: Severe Accident Facilities for European Safety Targets
SANS	Small Angle Neutron Scattering
SAXS	Small Angle X-ray Scattering
SBO	Station Blackout
SBR	Signal-to-Background Ratio
SCK•CEN	Belgian Nuclear Research Centre
SCFS	Single-Cell Adhesion Forces

SD	Snowdrift Quadrant
SE	Spectroscopic Ellipsometry
SEM	Scanning Electron Microscopy
SERS	Surface Enhanced Raman Spectroscopy (or scattering)
SH	Stag-Hunt
SINE2020	EU Funded Project: Science and Innovation with Neutrons in Europe in 2020
SINAC	Simulator Software for Interactive Consequences of Nuclear Accidents
SLM	Stochastic Lung Model
SMAD	Solvated Metal Atom Deposition
SMPS	Scanning Mobility Particle Sizers
SOD	Superoxide Dismutase
SO GL	System Operational Regulation Guidelines
SOI	Silicon-on-Insulator
SPR	Surface Plasmon Resonance
SPS	Spark Plasma Sintering
SPV	Sulfo-phospho-vanillin
SRA	Strategic Research Agenda
SSNTD	Solid State Nuclear Track Detector
SURET	SUBchannel REactor Thermohydraulics
STEM	Scanning Transmission Electron Microscopy
STEM HAADF	Scanning Transmission Electron Microscope High-Angle Annular Dark-Field
STM	Scanning Tunnelling Microscopy
STS	Scanning Tunnelling Spectroscopy
SWE	Space Weather Service Network
SWV	Square Wave Voltammetry
TDC	Time-to-Digital Conversion
TEM	Transmission Electron Microscopy
TENORM	Technologically Enhanced Naturally Occurring Radioactive Materials
TÉT	Bilateral Research Program (Hungarian acronym)
TG	Thermogravimetric
TL	Thermoluminescent
TLD	Thermoluminescent Dosimeter
TLG	Trilayer Graphene
TMCs	Transition Metal Chalcogenides
TMP	Turbomolecular Pump
TNA	Technology Needs Assessment Project, Transnational Access
TO	Transistor Outline
TOC	Total Organic Carbon
TOF-ND	Time of Flight Neutron Diffraction
TPO	Temperature Programed Oxidation
TPR	Temperature Programmed Reduction
TQCM	Thermoelectric Quartz Crystal Microbalances
T-VAC	Thermal-Vacuum Test
TXRF	Total-reflection X-ray Fluorescence
UHV	Ultra-High Vacuum
UOX	Uranium Oxide
UV-VIS	Ultraviolet-Visible (Spectroscopy)
VERONA	Reactor Core Monitoring and the Reactivity Measurement System for VVER Type NPPs
VOC	Volatile Organic Compounds
VVER	Water-Cooled Water-Moderated Energetic Reactor, Russian acronym
XANES	X-ray Absorption Near Edge Structure

XAS	X-ray Absorption Spectrometry
XAFS	X-ray Absorption Fine Structure
XPS	X-ray Photoelectron Spectroscopy
XRD	X-ray Diffraction
XRF	X-ray Fluorescence Analysis
XTEM	Cross-sectional Transmission Electron Microscopy
WG	Work Group
WI	Wet Impregnation
Wigner FK	Wigner Research Centre for Physics
ZFC	Zero Field Cooling

IMPRINT

Editors

*László Redler
Attila R. Imre*

Lector

*Ferenc Szlávik
Jesse Weil*

Publisher

*Ákos Horváth
Tamás Belgya
Centre for Energy Research
H-1121, Budapest, Konkoly Thege M. út 29-33.
Hungary*

Design

Anikó Jécsai

Picture credits

Centre for Energy Research,

Accessibility

<http://www.energia.mta.hu/>

Contact

*Centre for Energy Research, Hungarian Academy of Sciences
Location: KFKI Campus 29-33 Konkoly-Thege Miklós street 1121 Budapest, Hungary
Mailing address: 1525 Budapest 114., P.O. Box 49., Hungary
Phone: (+36 1) 395 91 59 Fax: (+36 1) 395 92 93
E-mail addresses: info@energia.mta.hu*



